Supporting Information for

High-Concentration Aqueous Synthesis of Salicylate-Based Metal-Organic Frameworks

Zayim M. Jamil,[a] Tristan A. Pitt,[a] Clarisse A. Doligon, Ronald T. Jerozal,[a,b] Phillip J. Milner[a,*]

[a]Department of Chemistry and Chemical Biology, Cornell University, Ithaca, NY, 14850, United States
[b]Department of Chemistry, Hamilton College, Clinton, NY 13323, United States
*pjm347@cornell.edu

Table of Contents.

1. General Procedures.

All reagents were purchased from commercial vendors and used without further purification unless specified otherwise. The solvents ethanol (EtOH, Fisher, ACS Grade), methanol (MeOH, Fisher, ACS Grade), isopropanol (iPrOH, Fisher, ACS Grade), *N*,*N*-dimethylformamide (DMF, Fisher, ACS Grade), hydrochloric acid (HCl, Fisher, ACS Grade), 1,4-dioxane (Oakwood Chemical), hydrobromic acid (HBr, Fisher, 33% in acetic acid), glacial acetic acid (EMD Millipore), and dichloromethane (CH_2Cl_2, Honeywell, 99.5%) were purchased from commercial vendors. The reagents 2,5-dihydroxyterephthalic acid (H_4dobdc, Astatech, 95%), resorcinol (AESAR, 99%), potassium bicarbonate ($KHCO_3$, Oakwood Chemical, 99%), methyl 5-chloro-2-methoxybenzoate (AESAR, 98%), potassium acetate (KOAc, Aldrich, 99%), bis(pinacolato)diboron (Oakwood Chemical, 99%), potassium carbonate (K_2CO_3, Fluka Chemical, anhydrous powder, 325 mesh, 99%), and sodium hydroxide (NaOH, Fisher, pellets) were purchased from commercial vendors. The metal salts $Mg(NO_3)_2{\cdot}6H_2O$ (Beantown, 98%), $Co(NO_3)_2{\cdot}6H_2O$ (Aldrich, 98%), $Ni(NO_3)_2{\cdot}6H_2O$ (Acros, 98%), and $Zn(NO_3)_2{\cdot}6H_2O$ (Lancaster, 99%) were purchased from commercial vendors and stored in desiccators when not in use. XPhos Pd G3 was synthesized according to the literature procedure.[1] Deuterated dimethyl sulfoxide (DMSO-d_6, Cambridge Isotope Laboratories, 99%) and deuterated chloroform ($CDCl_3$, Cambridge Isotope Laboratories, 99.8%) were purchased from commercial vendors. Cylinders of research grade CO_2 (99.999%) and N_2 (Ultra High Purity, 99.999%) were purchased from Airgas.

Powder X-ray diffraction (PXRD) data were collected on a Bruker D8 Advance ECO or Rigaku Smartlab SE diffractometer equipped with Cu K_α sources (λ = 1.5406 Å). Backgrounds were subtracted from PXRD measurements using OriginPro for presentation but were included and modeled in all data analyses. Scanning electron microscopy (SEM) images were taken at 1.0 kV using a Zeiss Gemini 500 scanning electron microscope. The powder samples were immobilized on carbon tape mounted on an aluminum stub. The samples were blown using compressed air to remove excess material not stuck to the tape and then were spin-coated with a Au/Pd layer. Thermogravimetric decomposition profiles were collected on a TA instruments Discovery TGA 550 thermogravimetric analyzer (TGA) using a temperature ramp of 5.00 °C/min from room temperature to 600.00 °C under an atmosphere of N_2 (99.999%). Masses are uncorrected for buoyancy effects. NMR data were collected on Bruker INOVA 500 MHz spectrometers and are referenced to residual solvent. Infrared (IR) spectra were collected on a Bruker Tensor II IR spectrometer equipped with a diamond Attenuated Total Reflectance (ATR) attachment. Surface area data were collected on either a Micromeritics ASAP 2460 or a Micromeritics 3-Flex gas sorption analyzer using ultrapure N_2 (99.999%) and a liquid N_2 bath. Brunauer-Emmett-Teller (BET) surface areas were determined by linear least squares regression analysis using the linearized form of the BET equation. The Rouquerol criteria were used to find the optimal P/P_0 range for calculating BET surface areas. DFT-calculated pore size distributions were determined using a metal oxide surface assuming cylindrical pores.

MOFs were activated with supercritical CO_2 in a Tousimis™ Samdri®-PVT-3D critical point dryer. The dried MOF samples were placed inside the dryer and soaked in iPrOH. The sample chamber was then cooled to at least 0 °C. The chamber was then filled with liquid CO_2. CO_2 was

vented under positive pressure for 5 min. The rate of venting of CO_2 was always kept below the rate of filling to maintain a full drying chamber while keeping the temperature between 0–10 °C. After 5 min, the chamber was filled with CO_2. The chamber was then sealed, and the temperature was raised to at least 31 °C. Once the chamber pressure was at ~1200 psi (above the critical point of CO_2), the chamber was slowly bled until the pressure was around 400 psi, and then the chamber was purged.[2]

X-ray photoelectron spectroscopy (XPS) spectra were collected on a Thermo Scientific Nexsa G2 surface analysis system using a monochromatic Al K_α (1486.6 eV) X-ray source (12 kV, 10 mA). The sample was mounted in a standard Nexsa G2. Survey scan analyses (0–1350 eV) were carried out by using an X-ray beam size of 400 μm and pass energy of 200 eV, dwell time of 10 ms, and energy step size of 1.000 eV.

2. Synthesis of organic linkers.

2.1. Synthesis of H_4(*m*-dobdc).

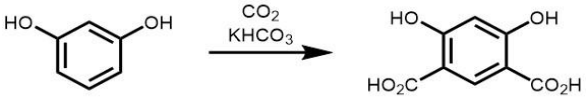

Prepared according to the literature procedure.[3] Resorcinol (5.00 g, 45.2 mmol, 1.00 equiv.) and $KHCO_3$ (10.5 g, 105 mmol, 2.32 equiv.) were pulverized separately using a mortar and pestle and then thoroughly mixed. The combined solids were sealed in a Parr reactor equipped with a pressure gauge. The Parr reactor was pressurized with CO_2 to 25 bar at room temperature and then vented. This process was repeated a total of three times. The Parr reactor was pressurized with CO_2 to 25 bar at room temperature and sealed. The Parr reactor was then heated to 230 °C (as measured by an external thermocouple) in a sand bath for 18 h and then slowly cooled to room temperature. The pressure was vented, and 1 L of H_2O was added. The solid in the suspension was broken up mechanically and then by sonication. The resulting suspension was filtered, and the filtrate was acidified with concentrated HCl until the pH of the solution was less than 1, at which time a white solid precipitated from solution. The product was then collected by filtration and recrystallized from hot H_2O to yield 2,4-dihydroxybenzene-1,5-dicarboxylic acid (H_4*m*-dobdc, 4.19 g, 47%) as a pale-yellow solid. ^{1}H NMR (500 MHz, DMSO-d6): δ 8.30 (s, 1H), 6.42 (s, 1H) ppm (the phenol and carboxylic acid protons could not be observed); ^{13}C NMR (126 MHz, DMSO-d_6): δ 171.59, 167.00, 134.83, 106.46, 103.70 ppm. These spectra are consistent with those reported in the literature.[3]

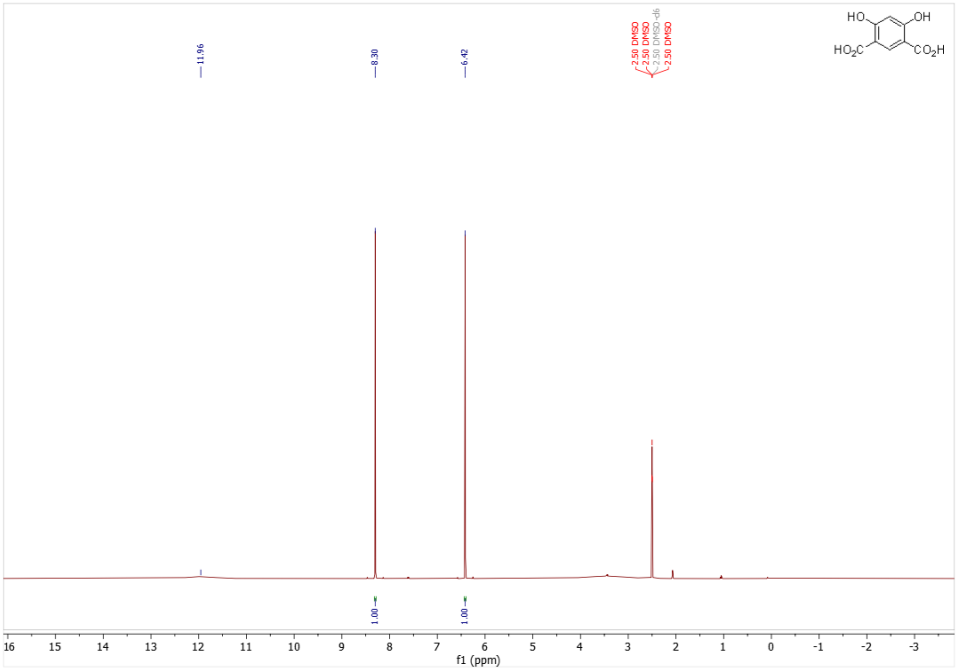

Figure S1. ^{1}H NMR spectrum (500 MHz, DMSO-d_6) of H_4*m*-dobdc.

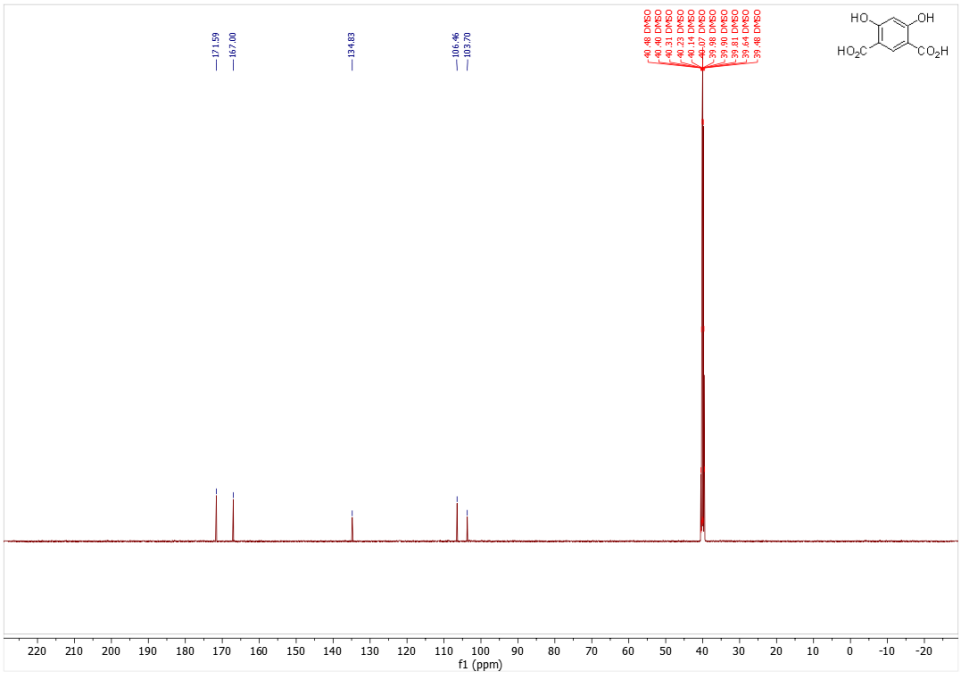

Figure S2. ^{13}C NMR spectrum (126 MHz, DMSO-d_6) of H$_4$*m*-dobdc.

2.2. Synthesis of H$_4$dobpdc.

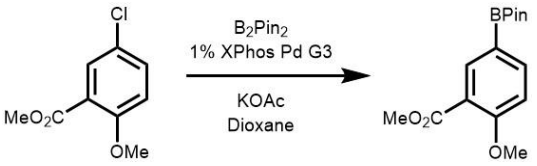

Prepared according to the literature procedure.[4] A 500 mL 3-neck round-bottom flask equipped with a stir bar and reflux condenser was charged with methyl 5-chloro-2-methoxybenzoate (5.44 g, 27.1 mmol, 1.00 equiv.), KOAc (7.981 g, 81.318 mmol, 3.00 equiv.), XPhos Pd G3[3] (229 mg, 0.271 mmol, 1%), and bis(pinacolato)diboron (7.57 g, 29.82 mmol, 1.10 equiv.). The flask was placed under high vacuum and back-filled with N_2. This process was repeated a total of three times. Next, freshly degassed 1,4-dioxane (57 mL) was added, and the reaction mixture was stirred at reflux under N_2 for 24 h. At this time, the reaction mixture was allowed to cool to room temperature and concentrated to yield a black solid. CH_2Cl_2 (200 mL) and H_2O (200 mL) were added, and the mixture was vigorously stirred for 5 min to dissolve all solids. The phases were separated, and the aqueous phase was further extracted with CH_2Cl_2 (2 × 100 mL). The combined organic extracts were washed with brine (100 mL), dried over Mg_2SO_4, and filtered through a short plug of celite, eluting with CH_2Cl_2. The solution was concentrated, and the resulting solid was triturated with hexanes and filtered, yielding methyl 5-(pinacalboryl)-2-methoxybenzoate (6.92 g, 87%) as a fluffy white solid. ^{1}H NMR (500 MHz, $CDCl_3$): δ 8.15 (d, J = 1.7 Hz, 1H), 7.83 (dd, J = 8.4, 1.8 Hz, 1H), 6.89 (d, J = 8.4 Hz, 1H), 3.85 (s, 3H), 3.80 (s, 3H), 1.26 (s, 12H) ppm. This spectrum is consistent with that reported in the literature.[5]

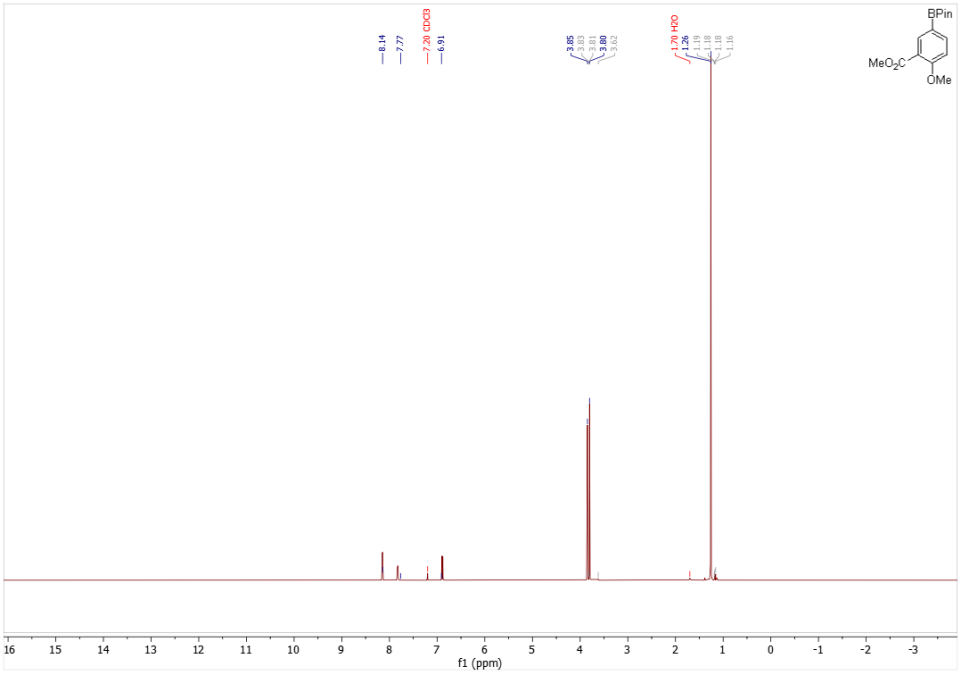

Figure S3. ^{1}H NMR spectrum (500 MHz, $CDCl_3$) of methyl 5-(pinacalboryl)-2-methoxybenzoate.

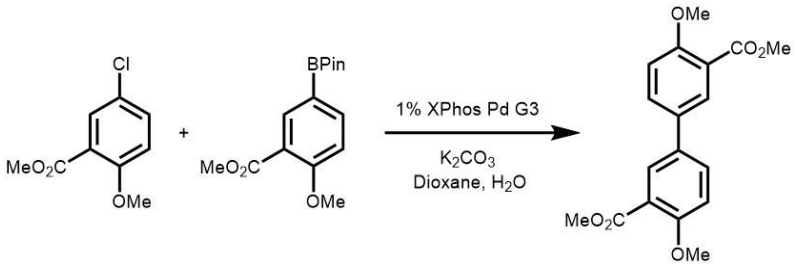

A 500 mL 3-neck round-bottom flask equipped with a stir bar and reflux condenser was charged with methyl 5-chloro-2-methoxybenzoate (4.32 g, 21.5 mmol, 1.00 equiv.), 5-(pinacalboryl)-2-methoxybenzoate (6.92 g, 23.7 mmol, 1.10 equiv.), K_2CO_3 (5.95 g, 43.1 mmol, 2.00 equiv.) and XPhos Pd G3 (182 mg, 0.215 mmol, 1 mol %). The flask was placed under high vacuum and back-filled with N_2. This process was repeated a total of three times. Next, freshly degassed 1,4-dioxane (43.2 mL) and freshly degassed H_2O (21.6 mL) were added, and the reaction mixture was stirred at reflux under N_2 for 24 h. At this time, the reaction mixture cooled to room temperature and poured into H_2O (200 mL), resulting in the precipitation of a gray solid from solution. The heterogeneous mixture was filtered, and the resulting solid was washed thoroughly with H_2O (100 mL). The solid was dissolved in CH_2Cl_2 (250 mL), dried over Mg_2SO_4, and filtered through a short plug of celite, eluting with CH_2Cl_2. The solution was concentrated, and the resulting solid was triturated with MeOH and filtered, yielding dimethyl 4,4'-dimethoxy-[1,1'-biphenyl]-3,3'-dicarboxylate (5.36 g, 75%) as an off-white solid. ^{1}H NMR (500 MHz, DMSO-d_6): δ 7.87 (d, J = 2.5 Hz, 1H), 7.83 (dd, J = 8.7, 2.5 Hz, 1H), 7.24 (d, J = 8.7 Hz, 1H), 3.87 (s, 3H), 3.82 (s, 3H) ppm. This spectrum is consistent with that reported in the literature.[6]

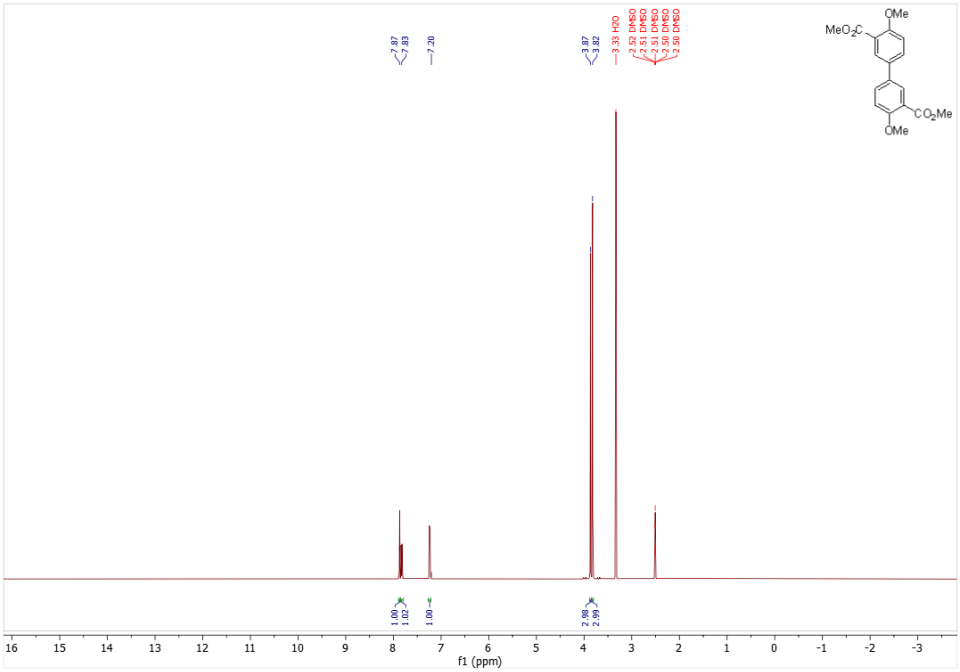

Figure S4. ^{1}H NMR spectrum (500 MHz, DMSO-d_6) of dimethyl 4,4'-dimethoxy-[1,1'-biphenyl]-3,3'-dicarboxylate.

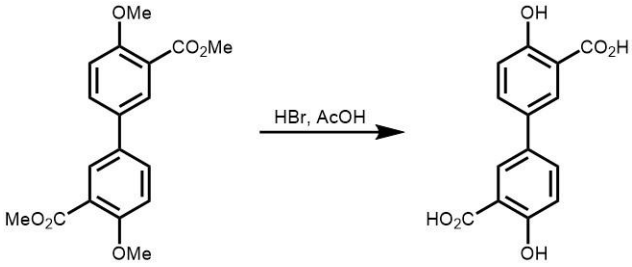

A 500 mL round-bottom flask equipped with a stir bar and reflux condenser was charged with 4,4'-dimethoxy-[1,1'-biphenyl]-3,3'-dicarboxylate (5.36 g, 16.2 mmol, 1.00 equiv.), concentrated HBr (129 mL), and glacial AcOH (129 mL). The reaction mixture was allowed to stir vigorously at reflux for 48 h. At this time, the reaction mixture was allowed to cool to room temperature and poured into H_2O (500 mL), resulting in precipitation of a light-brown solid from solution. The heterogeneous mixture was filtered, and the resulting solid was washed with H_2O (300 mL) and diethyl ether (300 mL), yielding 4,4'-dihydroxy-[1,1'-biphenyl]-3,3'-dicarboxylic acid (H_4dobpdc, 3.02 g, 68%) as a light-brown solid. ^{1}H NMR (500 MHz, DMSO-d_6): δ 7.96 (d, J = 2.5 Hz, 2H), 7.79 (dd, J = 8.6, 2.5 Hz, 2H), 7.04 (d, J = 8.6 Hz, 2H) ppm; ^{13}C NMR (126 MHz, DMSO-d_6): δ 172.17, 160.75, 133.96, 130.71, 127.83, 118.35, 113.84 ppm. These spectra are consistent with those reported in the literature.[7]

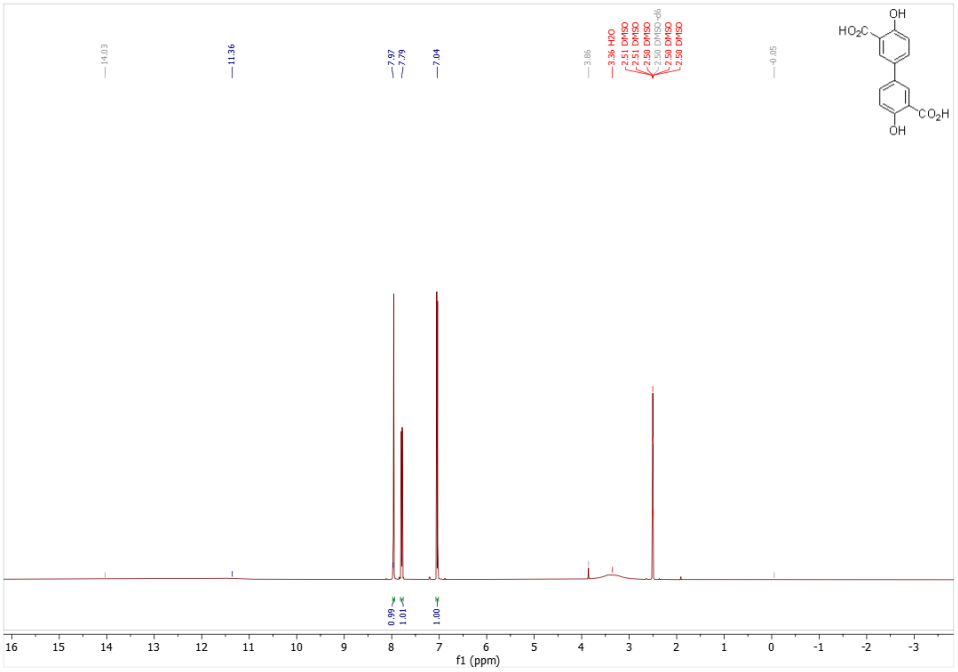

Figure S5. ^{1}H NMR spectrum (500 MHz, DMSO-d_6) of H_4dobpdc.

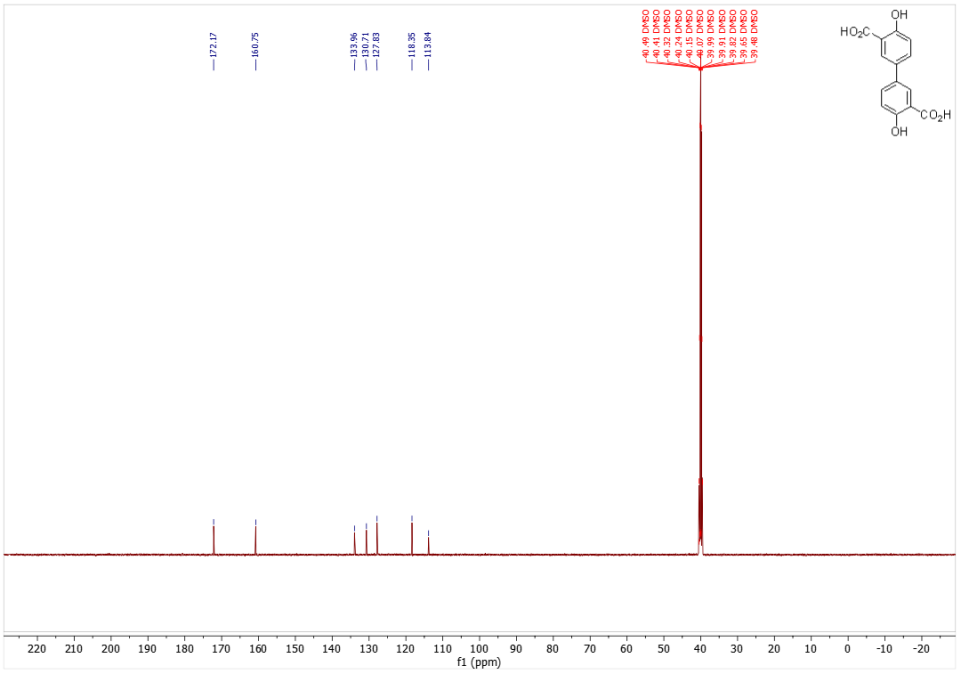

Figure S6. ^{13}C NMR spectrum (126 MHz, DMSO-d_6) of H_4dobpdc.

3. High-concentration aqueous syntheses of M_2(dobdc) MOFs.

3.1. Mg_2(dobdc).

Prepared according to a modified literature procedure.[8] In a 20 mL scintillation vial, $Mg(NO_3)_2$•$6H_2O$ (641 mg, 2.50 mmol, 2.50 equiv.) was dissolved in H_2O (5 mL, 1.0 mL, or 0.5 mL for 0.1 M, 0.5 M, and 1.0 M, respectively). In a separate 20 mL scintillation vial equipped with a stir bar, NaOH (160 mg, 4.00 mmol, 4.00 equiv.), H_4dobdc (198 mg, 1.00 mmol, 1.00 equiv.), and H_2O (5 mL, 1.0 mL, or 0.5 mL for 0.1 M, 0.5 M, and 1.0 M, respectively) were combined. The $Mg(NO_3)_2$•H_2O solution was added all at once to the H_4dobdc solution via a plastic pipette. The mixture was stirred at room temperature for 1 h. The reaction mixture was vacuum-filtered, and the resulting solid was rinsed with MeOH (10–15 mL). The resulting dark-yellow solid was transferred to a new scintillation vial filled with MeOH (10–15 mL). The vial was transferred to an aluminum block on a hot plate that had been pre-heated to 60 °C and was allowed to stand at this temperature for at least 12 h. At this time, the heterogenous mixture was allowed to cool to room temperature, the solvent was decanted, and fresh MeOH (10–15 mL) was added. This process was repeated for a total of six MeOH soaks. After the final soak, the solvent was decanted, and the remaining solid was allowed to dry in air. The sample was then activated using supercritical CO_2 (See Section 1), yielding activated Mg_2(dobdc) (42.7%, 74.6%, and 71.5% yield for 0.1 M, 0.5 M, and 1.0 M, respectively) that was immediately transferred to a glass adsorption tube equipped with a Micromeritics *CheckSeal*. The sample was activated on the SmartVac under high vacuum (<10 μbar), ramping the temperature slowly to 250 °C (0.1 °C/min). The sample was allowed to stand at 250 °C under high vacuum (<10 μbar) for 12 h prior to gas adsorption analysis.

Reaction Temperature Study.

The same procedure as above was followed for the synthesis of Mg_2(dobdc) at each concentration (0.1 M, 0.5 M, and 1.0 M). Meanwhile, a temperature probe was inserted into the H_4dobdc/NaOH scintillation vial before adding any H_2O. The temperature was then measured every minute after adding in H_2O and the $Mg(NO_3)_2$•H_2O solution for 10 min. After that, the temperature was measured every 10 min for a total reaction time of 1 h.

Table S1. Temperature (°C) vs time at different concentration conditions for the synthesis of Mg_2(dobdc).

Time (min)	0.1 M Temp (°C)	0.5 M Temp (°C)	1.0 M Temp (°C)
0	27.4	31.8	34.2
1	26.0	28.5	33.0
2	25.3	26.2	32.1
3	24.9	25.1	30.2
4	24.7	24.2	29.4
5	24.6	23.5	28.8
6	24.4	23.2	28.2
7	24.1	23.0	27.6
8	23.9	22.8	27.1
9	23.8	22.5	26.8
10	23.8	22.3	26.2
20	23.4	22.1	25.0
30	23.2	22.0	24.1
40	23.1	22.0	23.1
50	23.0	22.0	23.1
60	23.0	22.0	23.1

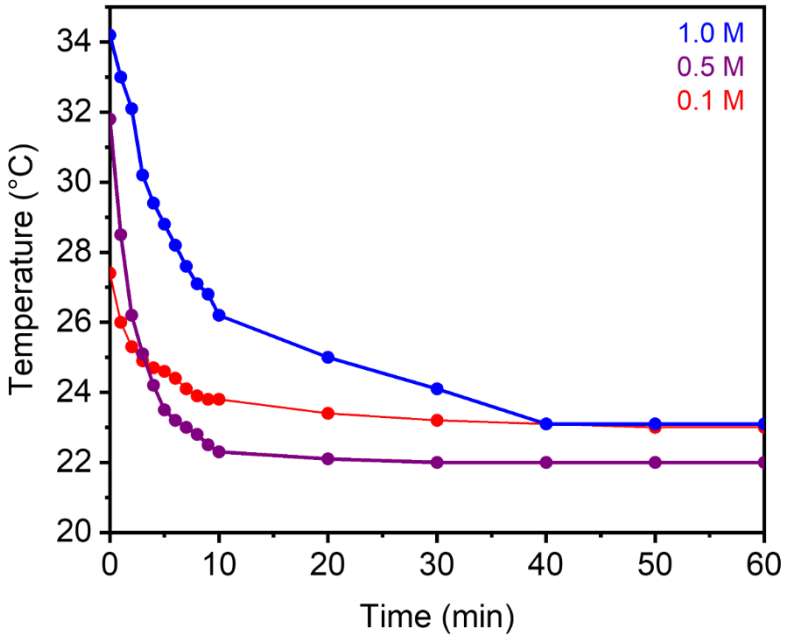

Figure S7. Temperature (°C) vs time for the synthesis of Mg_2(dobdc) at different concentration conditions. The maximum temperature increase upon mixing increases as a function of the reaction concentration.

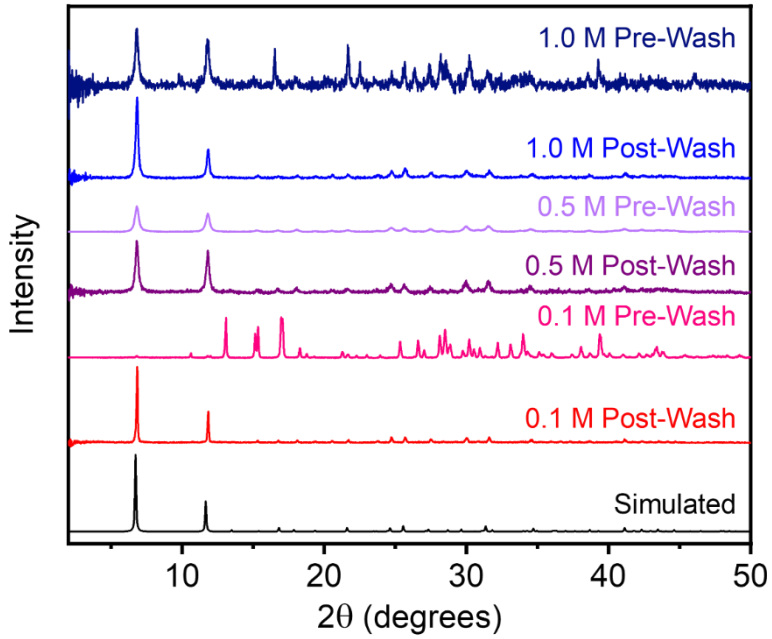

Figure S8. Baseline-corrected PXRD patterns (λ = 1.5406 Å) of Mg_2(dobdc) synthesized at different concentrations before (pre-wash) and after (post-wash) soaking in MeOH. The simulated pattern based on the previously reported SCXRD structure of the isostructural framework Zn_2(dobdc) is included for reference.[9] While the samples prepared at 0.5 M and 1.0 M consist largely of Mg_2(dobdc) before soaking in MeOH, the sample prepared at 0.1 M consists of a different phase or mixture of phases that transforms into phase-pure Mg_2(dobdc) upon soaking in MeOH. The powder pattern of this product was reliably indexed, and refined unit cell parameters were determined through Pawley refinement (Figure S140).

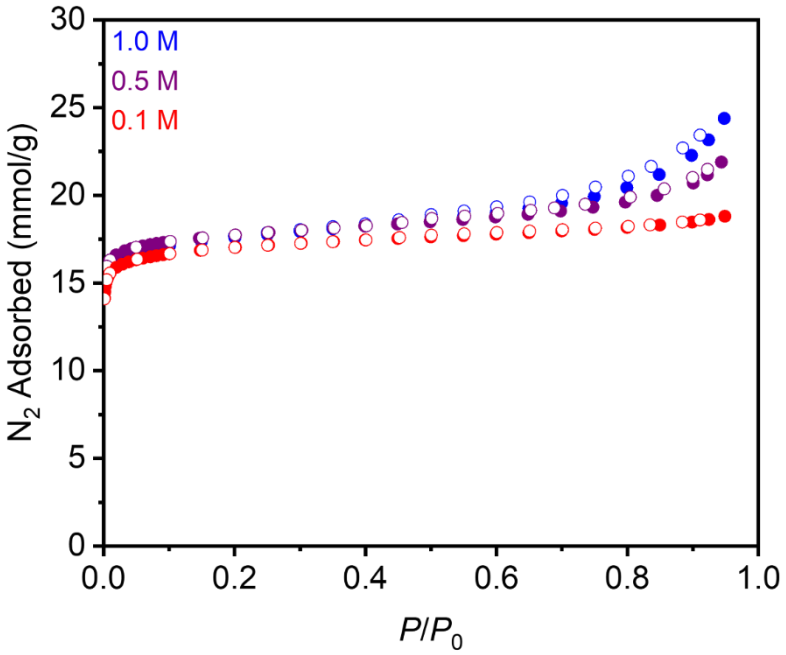

Figure S9. 77 K N_2 adsorption (filled circles) and desorption (open circles) isotherms of activated Mg_2(dobdc) synthesized at different reaction concentrations. The BET surface areas determined from these data are 1532 ± 1 m^2/g (0.1 M), 1597 ± 1 m^2/g (0.5 M), and 1569 ± 1 m^2/g (1.0 M), respectively. The Langmuir surface areas determined from these data are 1792 m^2/g (0.1 M), 1974 m^2/g (0.5 M), and 2092 m^2/g (1.0 M), respectively. The literature BET and Langmuir surface areas of this MOF are 1800 m^2/g and 2060 m_2/g,[7] respectively.

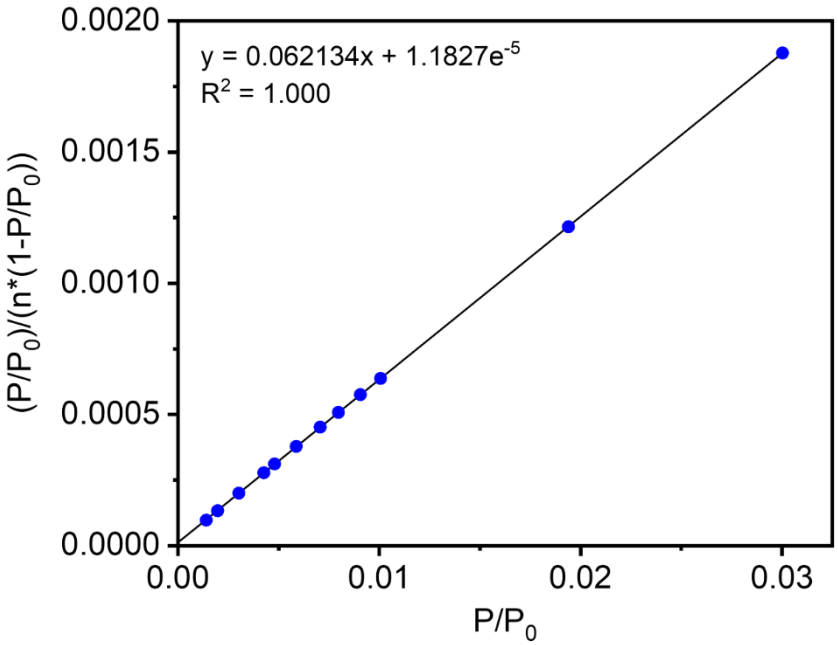

Figure S10. Linearized BET plot for the N_2 adsorption data of Mg_2(dobdc) synthesized at 1.0 M.

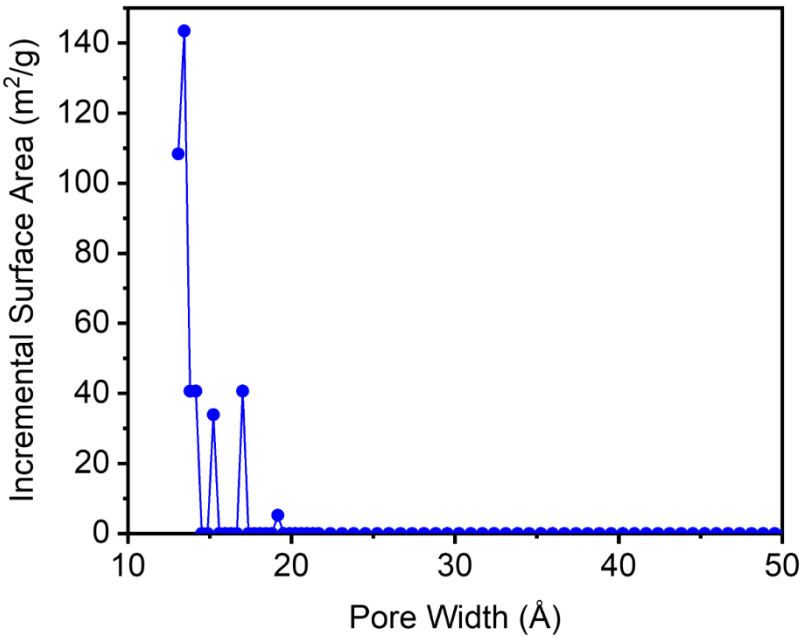

Figure S11. DFT-calculated pore size distribution for Mg_2(dobdc) synthesized at 1.0 M, assuming a cylindrical pore geometry. The primary pore size is below the lower limit of the measurement.

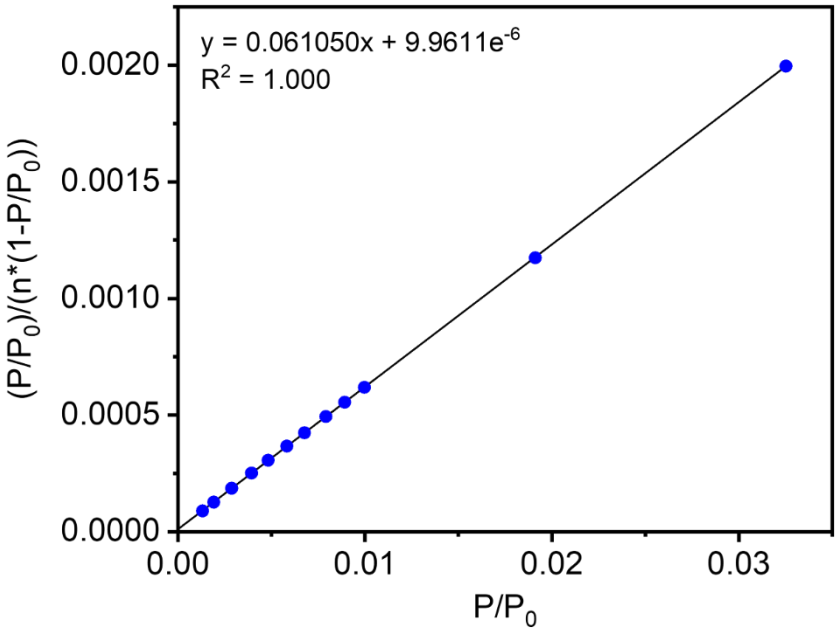

Figure S12. Linearized BET plot for the N_2 adsorption data of Mg_2(dobdc) synthesized at 0.5 M.

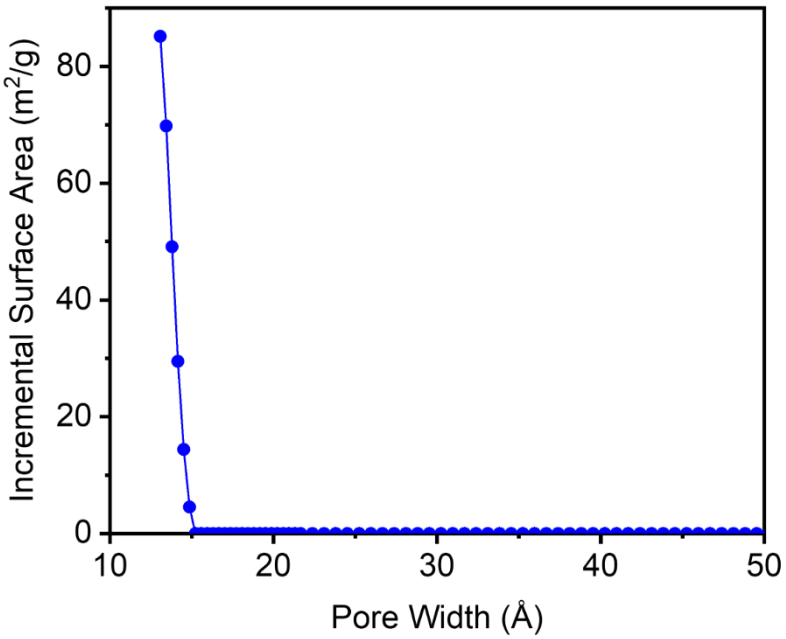

Figure S13. DFT-calculated pore size distribution for Mg_2(dobdc) synthesized at 0.5 M, assuming a cylindrical pore geometry. The primary pore size is below the lower limit of the measurement.

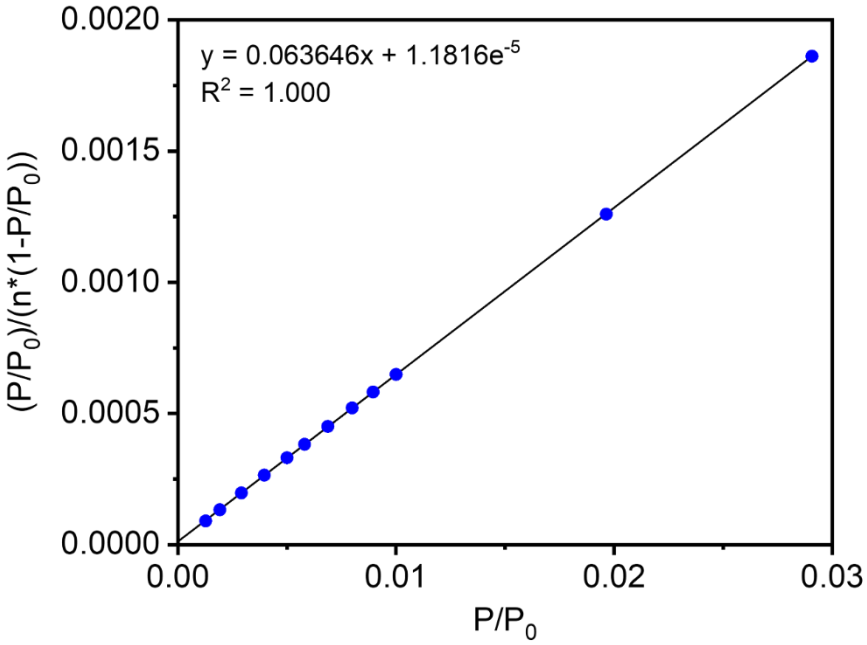

Figure S14. Linearized BET plot for the N_2 adsorption data of Mg_2(dobdc) synthesized at 0.1 M.

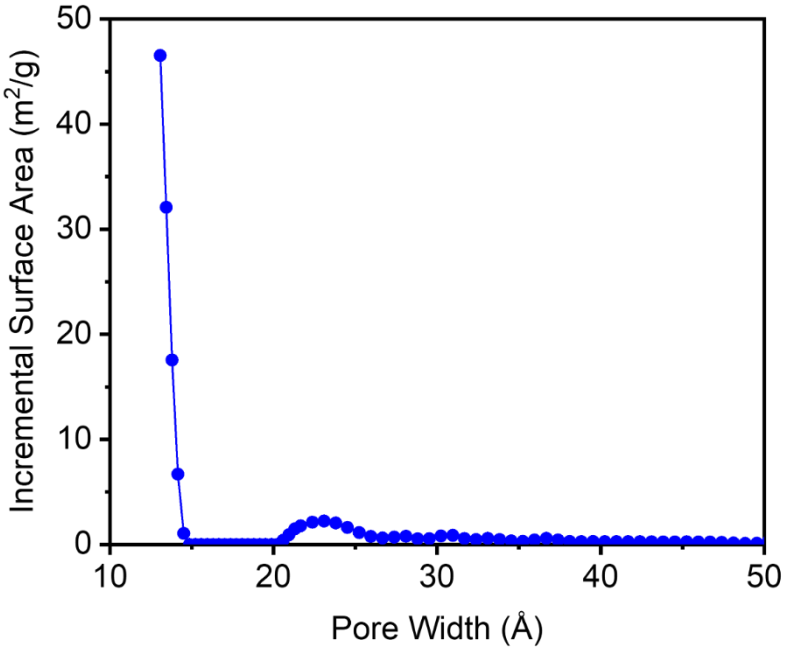

Figure S15. DFT-calculated pore size distribution for Mg_2(dobdc) synthesized at 0.1 M, assuming a cylindrical pore geometry. The primary pore size is below the lower limit of the measurement.

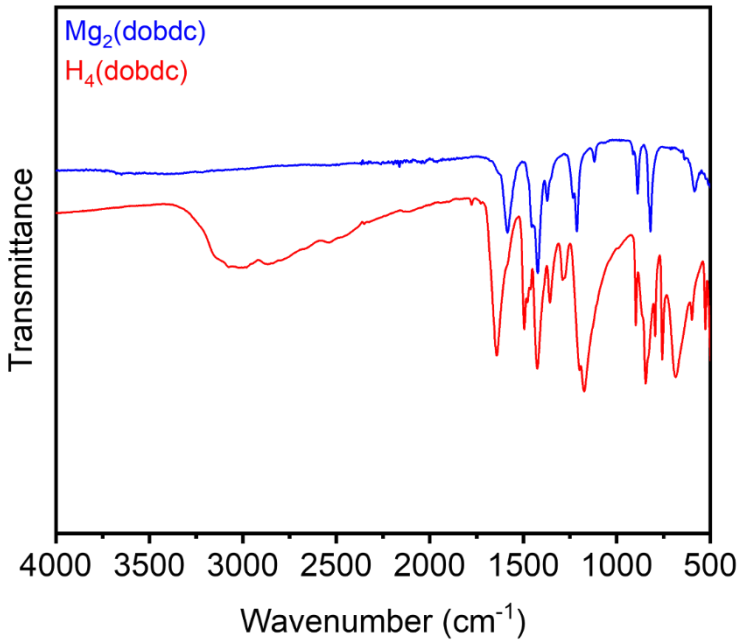

Figure S16. ATR-IR spectra of Mg_2(dobdc) synthesized at 0.5 M and the H_4dobdc linker.

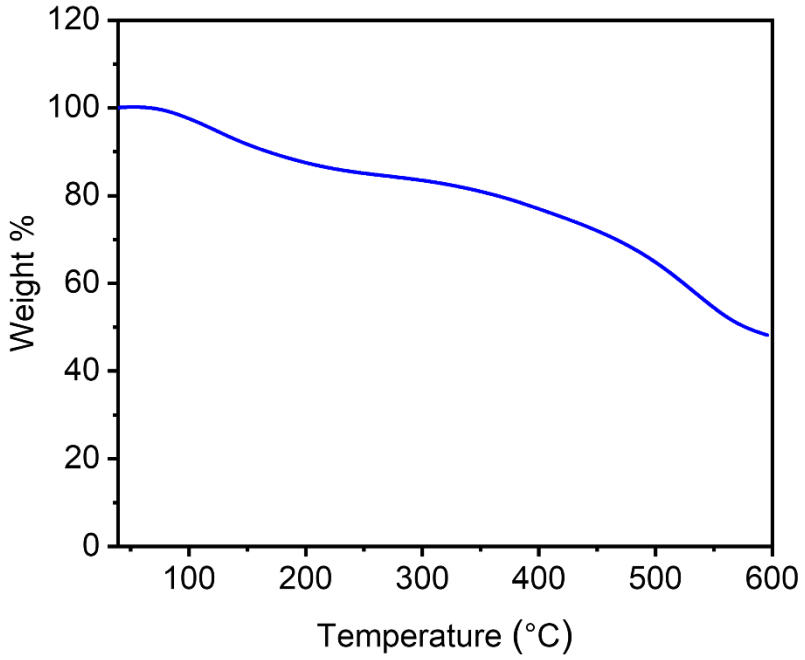

Figure S17. Thermogravimetric decomposition profile under N_2 of Mg_2(dobdc) synthesized at 0.5 M.

Table S2. Surface area data and yields for Mg_2(dobdc) at each synthesized concentration. Literature values for surface areas are included.

Concentration (M)	BET Surface Area (m^2/g)	Langmuir Surface Area (m^2/g)	Yield (%)
0.1	1532 ± 1	1792	42.7
0.5	1597 ± 1	1974	74.6
1.0	1569 ± 1	2092	71.5
Literature	1510[10]	2060[7]	-

3.2. Co_2(dobdc).

Prepared according to a modified literature procedure.[8] In a 20 mL scintillation vial, $Co(NO_3)_2$•$6H_2O$ (728 mg, 2.50 mmol, 2.50 equiv.) was dissolved in H_2O (5 mL, 1.0 mL, or 0.5 mL for 0.1 M, 0.5 M, and 1.0 M, respectively). In a separate 20 mL scintillation vial equipped with a stir bar, NaOH (160 mg, 4.00 mmol, 4.00 equiv.), H_4dobdc (198 mg, 1.00 mmol, 1.00 equiv.), and H_2O (5 mL, 1.0 mL, or 0.5 mL for 0.1 M, 0.5 M, and 1.0 M, respectively) were combined. The $Co(NO_3)_2$•H_2O solution was added all at once to the H_4dobdc solution via a plastic pipette. The mixture was stirred at room temperature for 1 h. The reaction mixture was vacuum-filtered, and the resulting solid was rinsed with MeOH (10–15 mL). The resulting dark red-orange solid was transferred to a new scintillation vial filled with MeOH (10–15 mL). The vial was transferred to an aluminum block on a hot plate that had been pre-heated to 60 °C and was allowed to stand at this temperature for at least 12 h. At this time, the heterogenous mixture was allowed to cool to room temperature, the solvent was decanted, and fresh MeOH (10–15 mL) was added. This process was repeated for a total of six MeOH soaks. After the final soak, the solvent was decanted, and the remaining solid was allowed to dry in air. The sample was then activated using supercritical CO_2 (See Section 1), yielding activated Co_2(dobdc) (28.4%, 51.6%, 52.4% yield for 0.1 M, 0.5 M, and 1.0 M, respectively) that was immediately transferred to a glass adsorption tube equipped with a Micromeritics *CheckSeal*. The sample was activated on the SmartVac under high vacuum (<10 μbar), ramping the temperature slowly to 180 °C (0.1 °C/min). The sample was allowed to stand at 180 °C under high vacuum (<10 μbar) for 12 h prior to gas adsorption analysis.

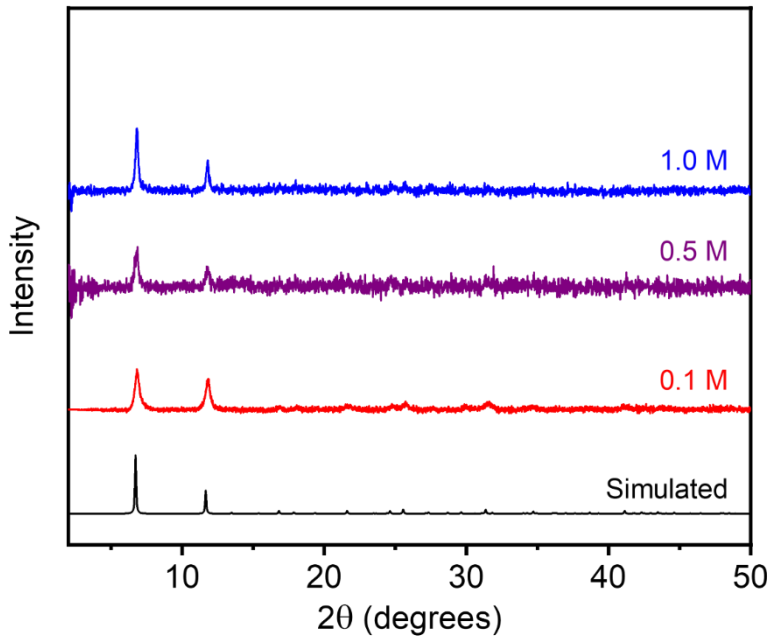

Figure S18. Baseline-corrected PXRD patterns (λ = 1.5406 Å) of MeOH-solvated Co_2(dobdc) at different concentrations after aqueous synthesis. The simulated pattern based on the previously reported SCXRD structure of the isostructural framework Zn_2(dobdc) is included for reference.[9]

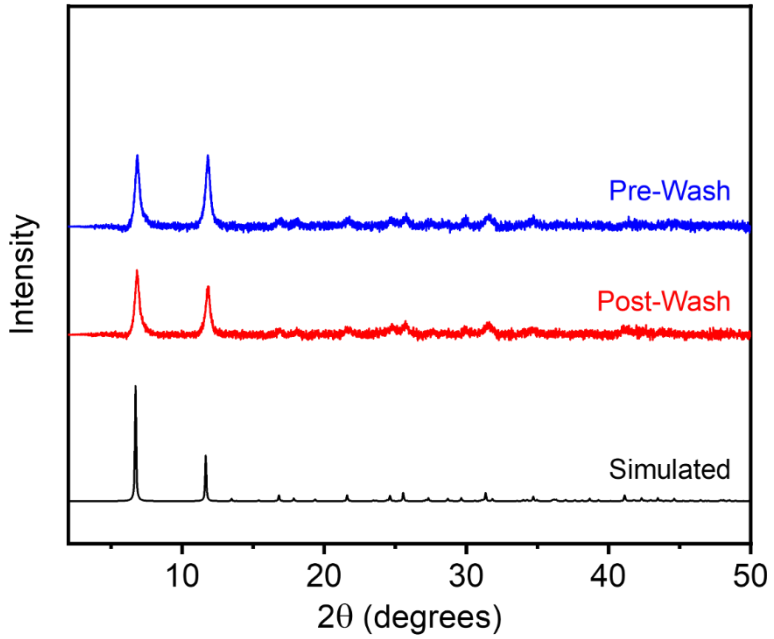

Figure S19. Baseline-corrected PXRD patterns (λ = 1.5406 Å) of Co_2(dobdc) synthesized at 0.1 M before (pre-wash) and after (post-wash) soaking in MeOH. The simulated pattern based on the previously reported SCXRD structure of the isostructural framework Zn_2(dobdc) is included for reference.[9] No significant change in the pattern was observed upon soaking the MOF in MeOH.

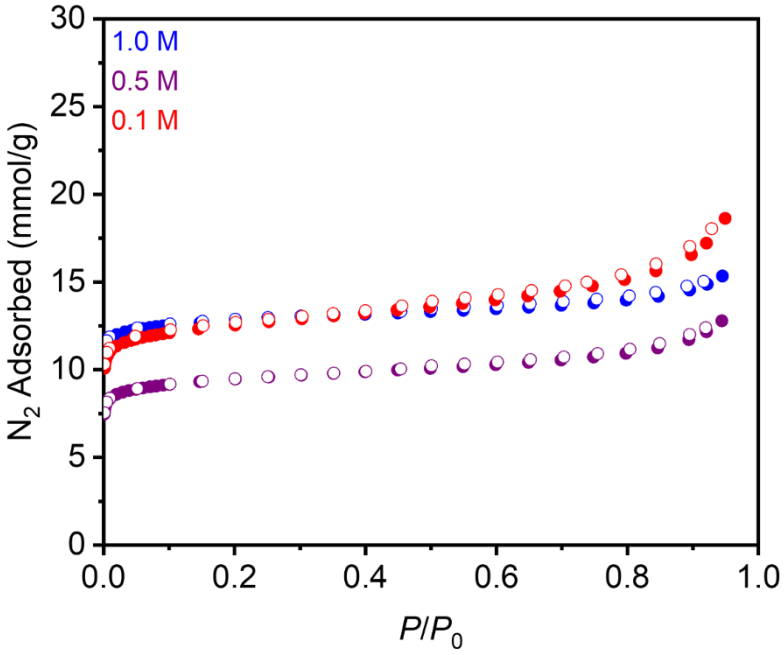

Figure S20. 77 K N_2 adsorption (filled circles) and desorption (open circles) isotherms of activated Co_2(dobdc) at different concentrations after aqueous synthesis. BET surface areas determined from these data are 1097 ± 1 m^2/g (0.1 M), 831 ± 1 m^2/g (0.5 M), and 1155 ± 1 m^2/g (1.0 M). The Langmuir surface areas determined from these data are 1559 m^2/g (0.1 M), 1115 m^2/g (0.5 M), and 1399 m^2/g (1.0 M).

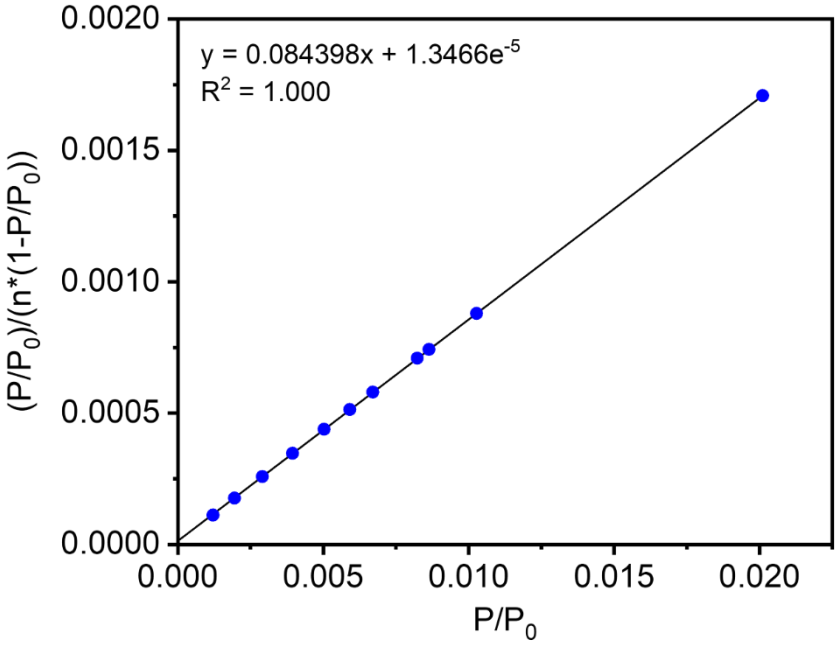

Figure S21. Linearized BET plot for the N_2 adsorption data of Co_2(dobdc) synthesized at 1.0 M.

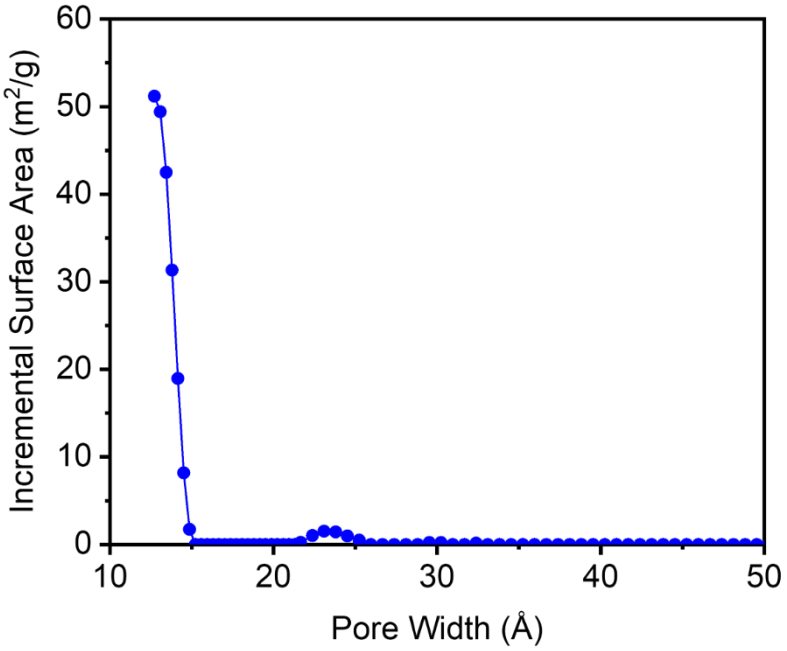

Figure S22. DFT-calculated pore size distribution for Co_2(dobdc) synthesized at 1.0 M, assuming a cylindrical pore geometry. The primary pore size is below the lower limit of the measurement.

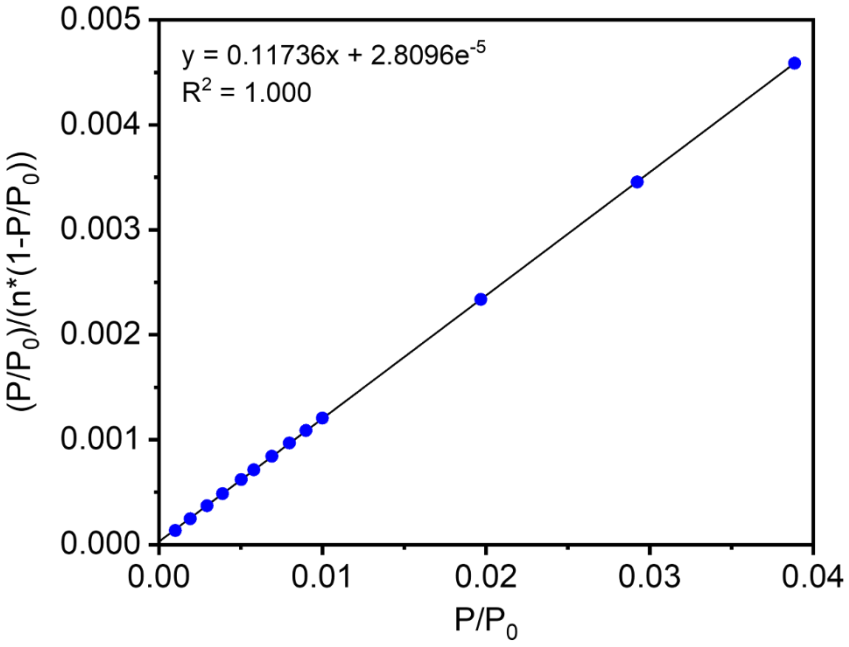

Figure S23. Linearized BET plot for the N_2 adsorption data of Co_2(dobdc) synthesized at 0.5 M.

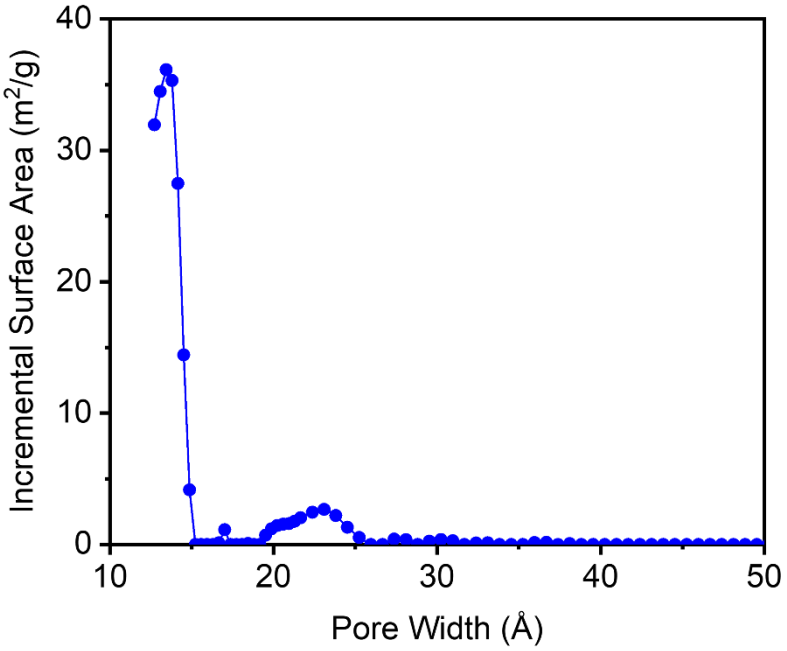

Figure S24. DFT-calculated pore size distribution for Co_2(dobdc) synthesized at 0.5 M, assuming a cylindrical pore geometry.

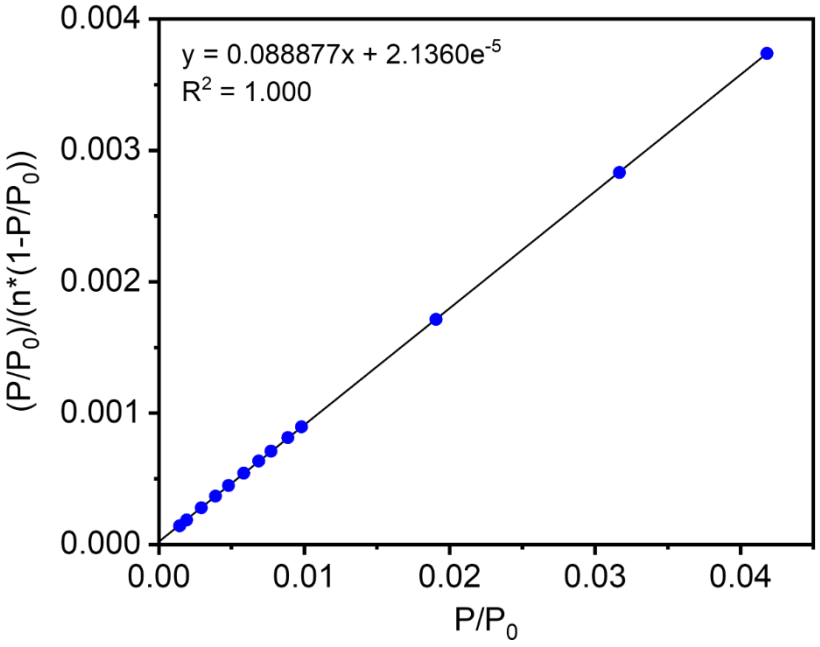

Figure S25. Linearized BET plot for the N_2 adsorption data of Co_2(dobdc) synthesized at 0.1 M.

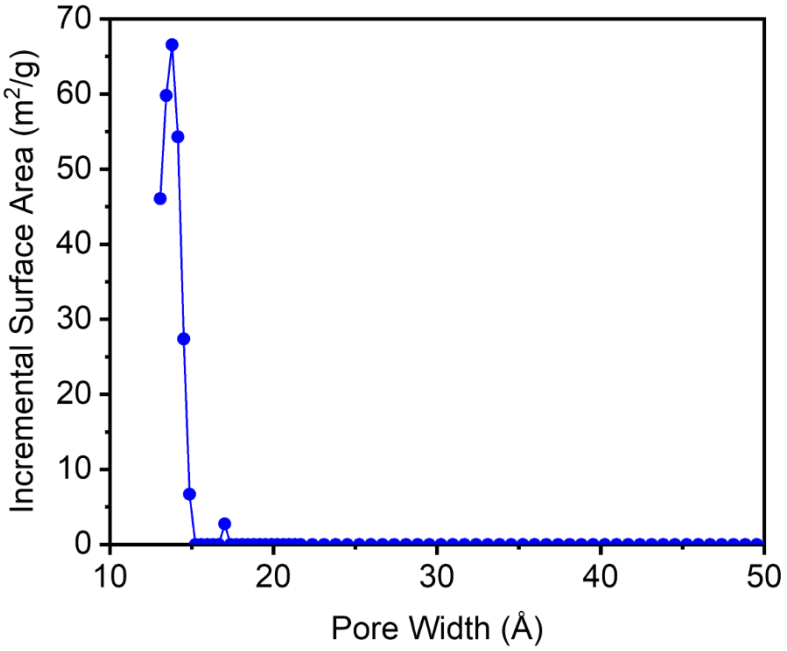

Figure S26. DFT-calculated pore size distribution for Co_2(dobdc) synthesized at 0.1 M, assuming a cylindrical pore geometry.

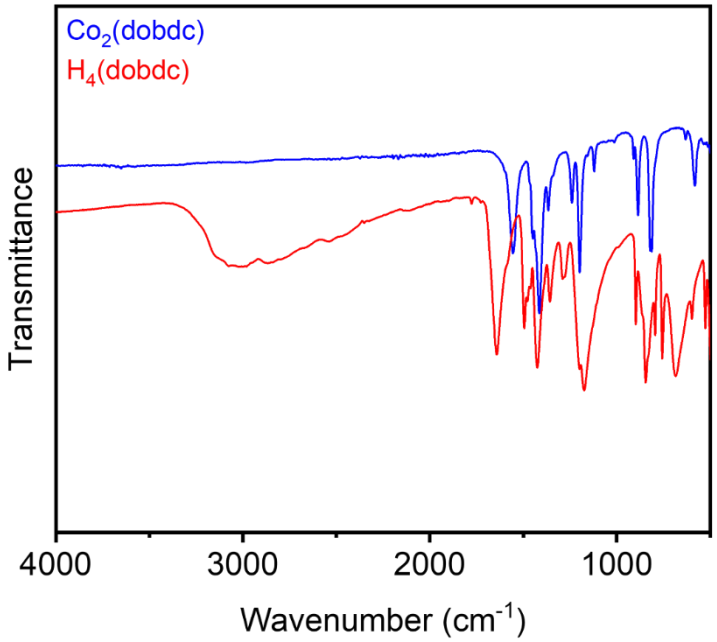

Figure S27. ATR-IR spectra of Co_2(dobdc) synthesized at 1.0 M and the H_4dobdc linker.

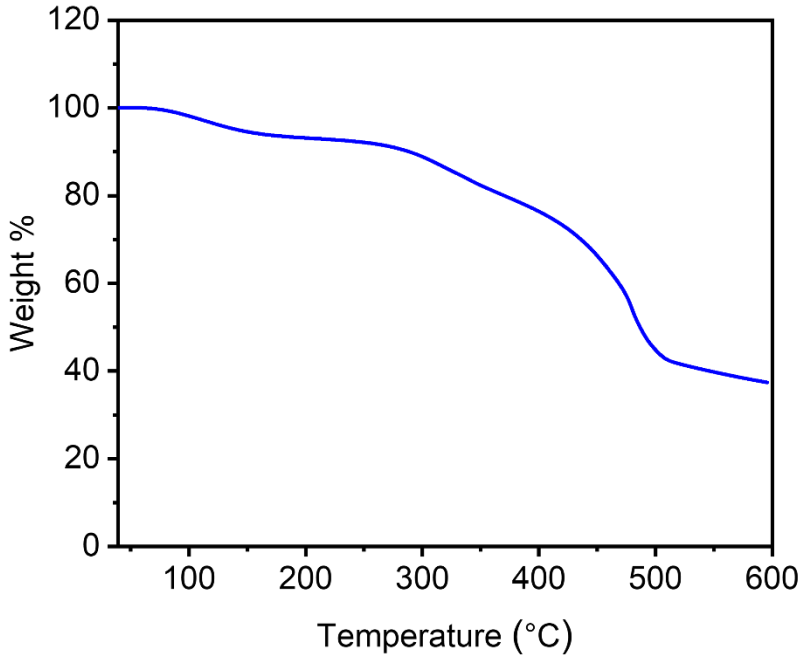

Figure S28. Thermogravimetric decomposition profile under N_2 of Co_2(dobdc) synthesized at 1.0 M.

Table S3. Surface area data and yields for Co_2(dobdc) at each synthesized concentration. Literature values for surface areas are included.

Concentration (M)	BET Surface Area (m^2/g)	Langmuir Surface Area (m^2/g)	Yield (%)
0.1	1097 ± 1	1559	28.4
0.5	831 ± 1	1115	51.6
1.0	1155 ± 1	1399	52.4
Literature	1341[7]	1432[7]	-

3.3. Ni_2(dobdc).

Prepared according to a modified literature procedure.[8] In a 20 mL scintillation vial, $Ni(NO_3)_2$•$6H_2O$ (727 mg, 2.50 mmol, 2.50 equiv.) was dissolved in H_2O (5 mL, 1.0 mL, or 0.5 mL for 0.1 M, 0.5 M, and 1.0 M, respectively). In a separate 20 mL scintillation vial equipped with a stir bar, NaOH (160 mg, 4.00 mmol, 4.00 equiv.), H_4dobdc (198 mg, 1.00 mmol, 1.00 equiv.), and H_2O (5 mL, 1.0 mL, or 0.5 mL for 0.1 M, 0.5 M, and 1.0 M, respectively) were combined. The $Ni(NO_3)_2$•H_2O solution was added all at once to the H_4dobdc solution via a plastic pipette. The mixture was stirred at room temperature for 1 h. The reaction mixture was vacuum-filtered, and the resulting solid was rinsed with MeOH (10–15 mL). The resulting dark brown solid was transferred to a new scintillation vial filled with MeOH (10–15 mL). The vial was transferred to an aluminum block on a hot plate that had been pre-heated to 60 °C and was allowed to stand at this temperature for at least 12 h. At this time, the heterogenous mixture was allowed to cool to room temperature, the solvent was decanted, and fresh MeOH (10–15 mL) was added. This process was repeated for a total of six MeOH soaks. After the final soak, the solvent was decanted, and the remaining solid was allowed to dry in air. The sample was then activated using supercritical CO_2 (See Section 1), yielding activated Ni_2(dobdc) (85.7%, 78.5%, and 57.1% yield for 0.1 M, 0.5 M, and 1.0 M, respectively) that was immediately transferred to a glass adsorption tube equipped with a Micromeritics *CheckSeal*. The sample was activated on the SmartVac under high vacuum (<10 μbar), ramping the temperature slowly to 180 °C (0.1°C/min). The sample was allowed to stand at 180 °C under high vacuum (<10 μbar) for 12 h prior to gas adsorption analysis.

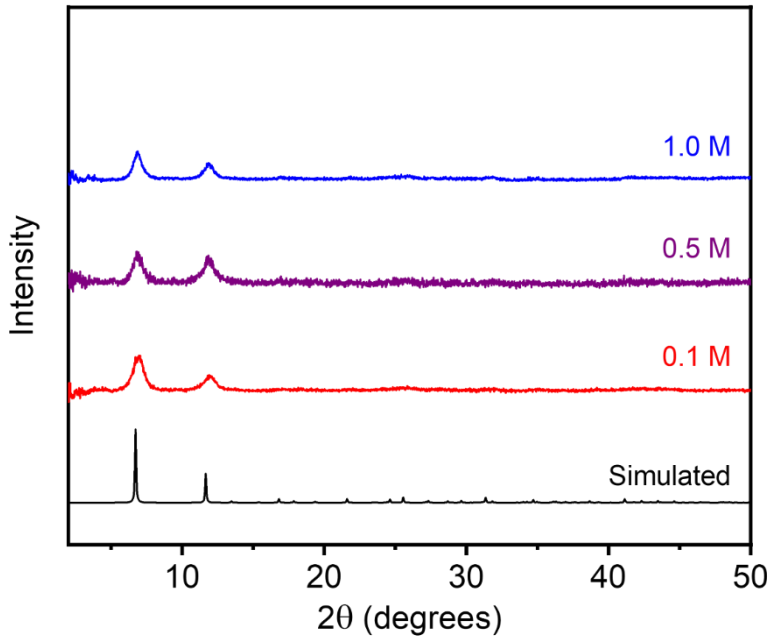

Figure S29. Baseline-corrected PXRD patterns (λ = 1.5406 Å) of MeOH-solvated Ni_2(dobdc) at different concentrations after aqueous synthesis. The simulated pattern based on the previously reported SCXRD structure of the isostructural framework Zn_2(dobdc) is included for reference.[9]

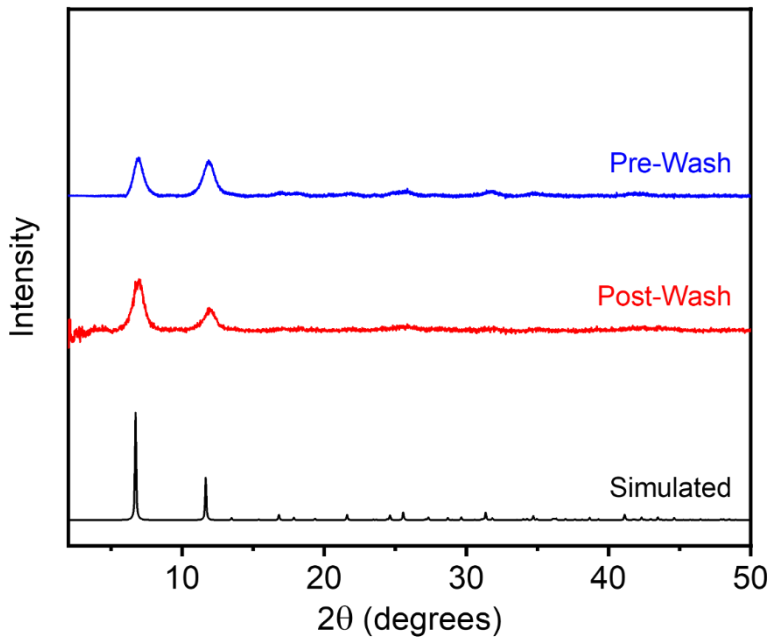

Figure S30. Baseline-corrected PXRD patterns (λ = 1.5406 Å) of Ni_2(dobdc) synthesized at 0.1 M before (pre-wash) and after (post-wash) soaking in MeOH. The simulated pattern based on the previously reported SCXRD structure of the isostructural framework Zn_2(dobdc) is included for reference.[9] No significant change in the pattern was observed upon soaking the MOF in MeOH.

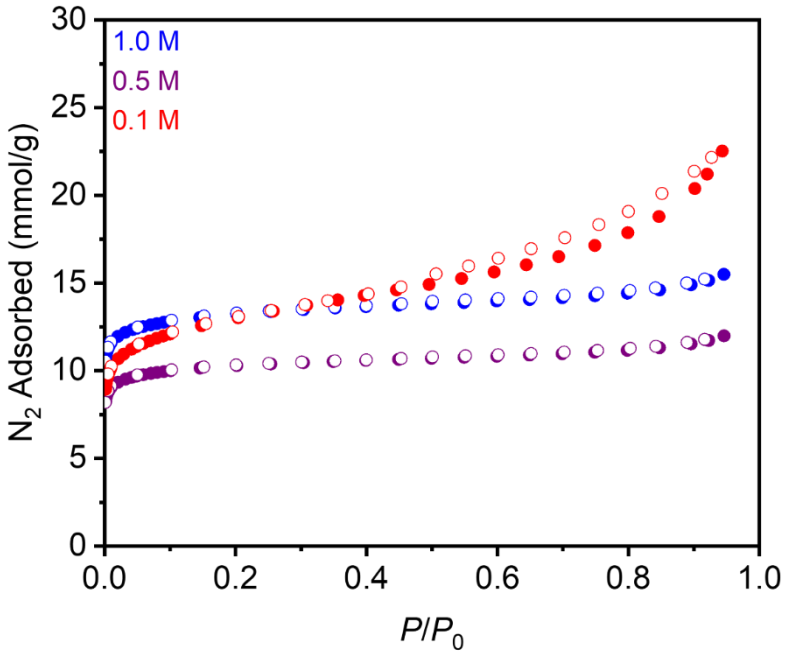

Figure S31. 77 K N_2 adsorption (filled circles) and desorption (open circles) isotherms of activated Ni_2(dobdc) at different concentrations after aqueous synthesis. BET surface areas determined from these data are 1071 ± 2 m^2/g (0.1 M), 906 ± 1 m^2/g (0.5 M), and 1160 ± 1 m^2/g (1.0 M). The Langmuir surface areas determined from these data are 1859 m^2/g (0.1 M), 1113 m^2/g (0.5 M), and 1438 m^2/g (1.0 M).

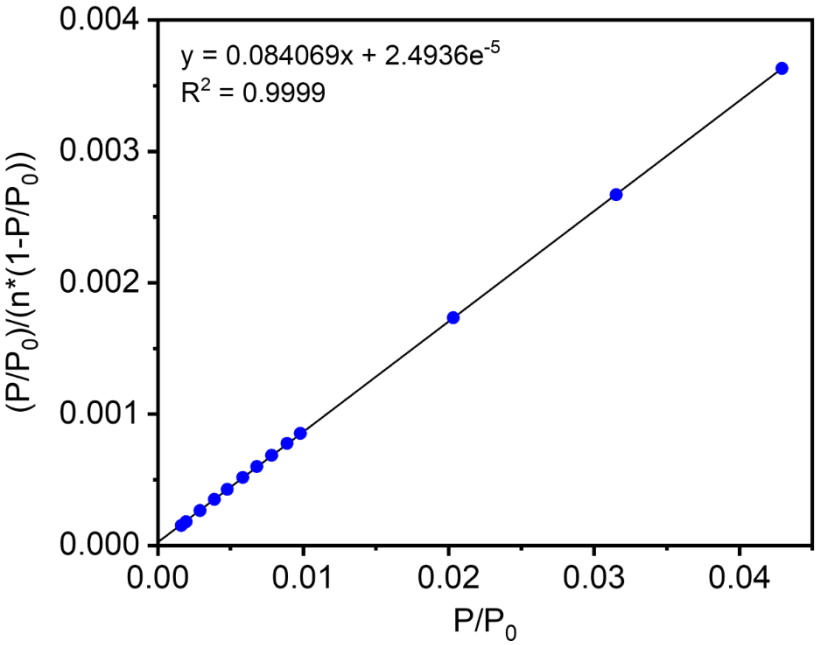

Figure S32. Linearized BET plot for the N_2 adsorption data of Ni_2(dobdc) synthesized at 1.0 M.

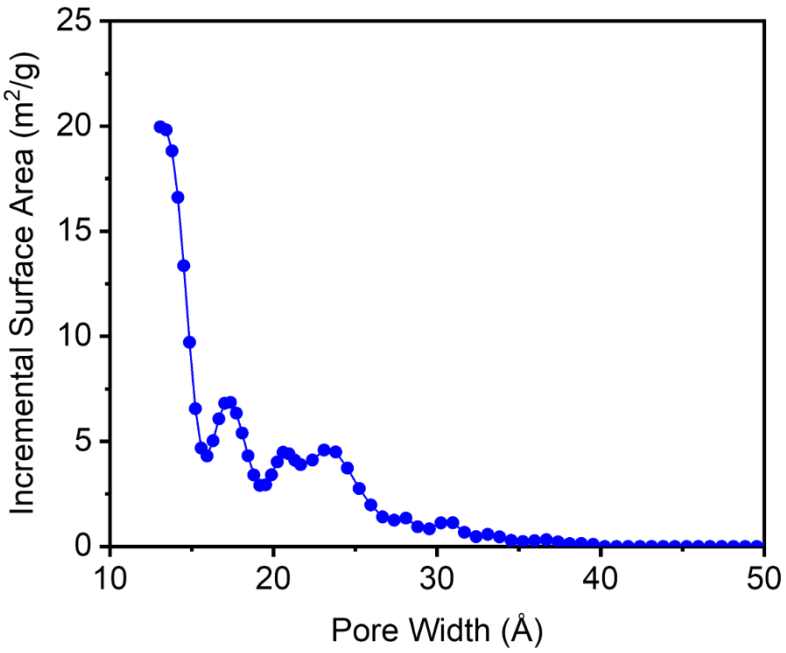

Figure S33. DFT-calculated pore size distribution for Ni_2(dobdc) synthesized at 1.0 M, assuming a cylindrical pore geometry. The primary pore size is below the lower limit of the measurement.

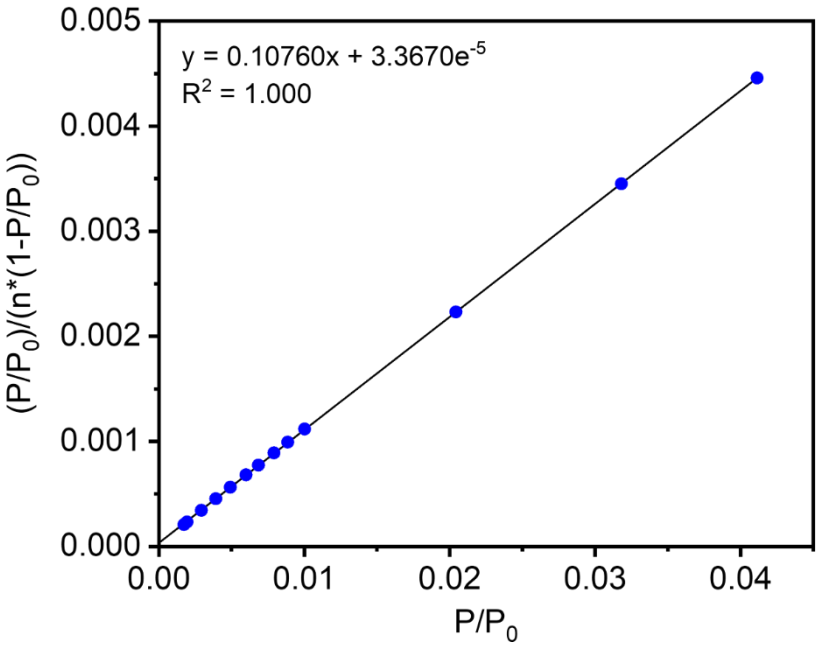

Figure S34. Linearized BET plot for the N_2 adsorption data of Ni_2(dobdc) synthesized at 0.5 M.

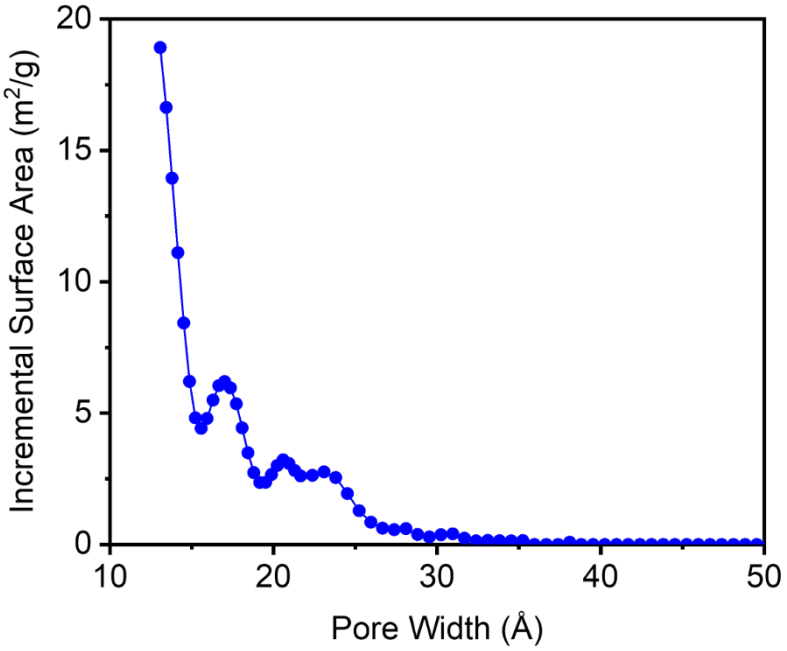

Figure S35. DFT-calculated pore size distribution for Ni_2(dobdc) synthesized at 0.5 M, assuming a cylindrical pore geometry. The primary pore size is below the lower limit of the measurement.

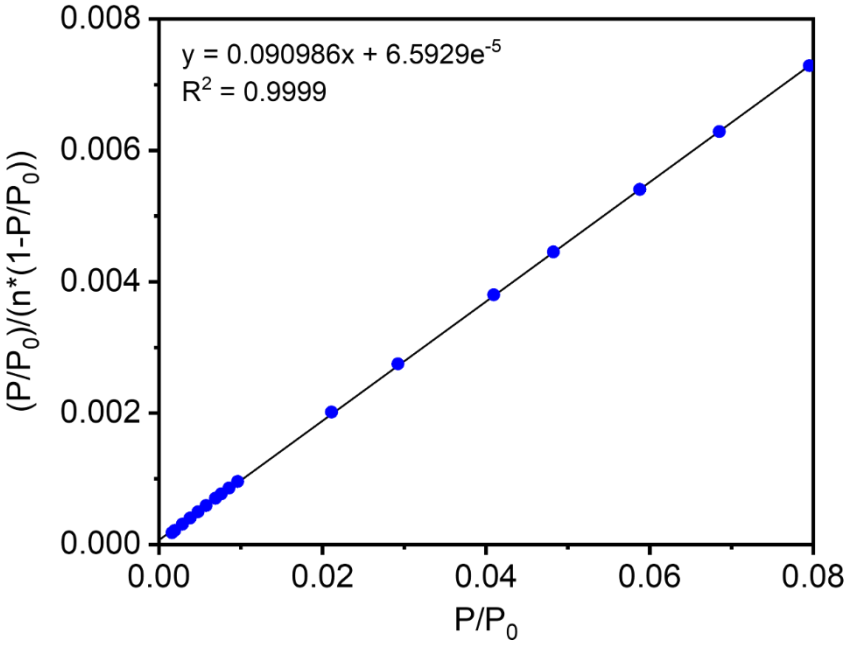

Figure S36. Linearized BET plot for the N_2 adsorption data of Ni_2(dobdc) synthesized at 0.1 M.

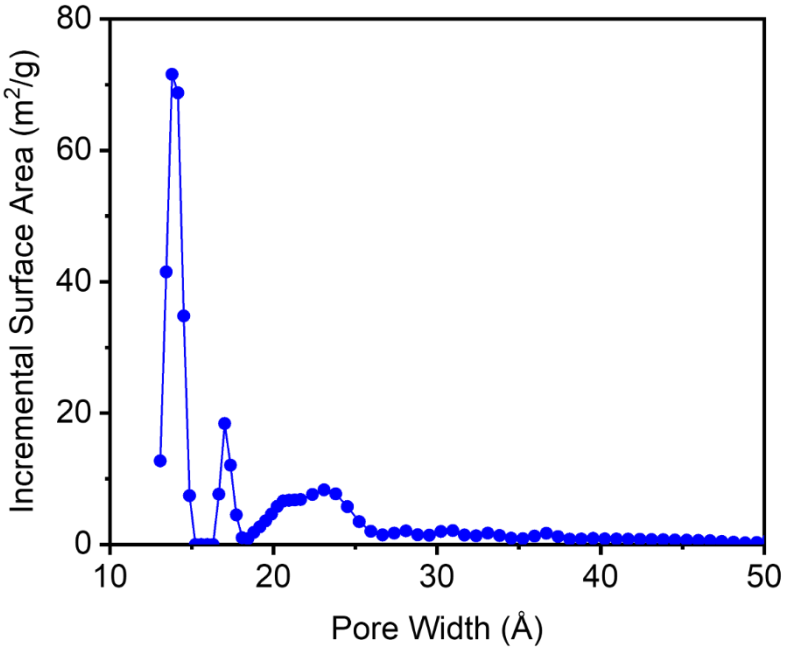

Figure S37. DFT-calculated pore size distribution for Ni_2(dobdc) synthesized at 0.1 M, assuming a cylindrical pore geometry.

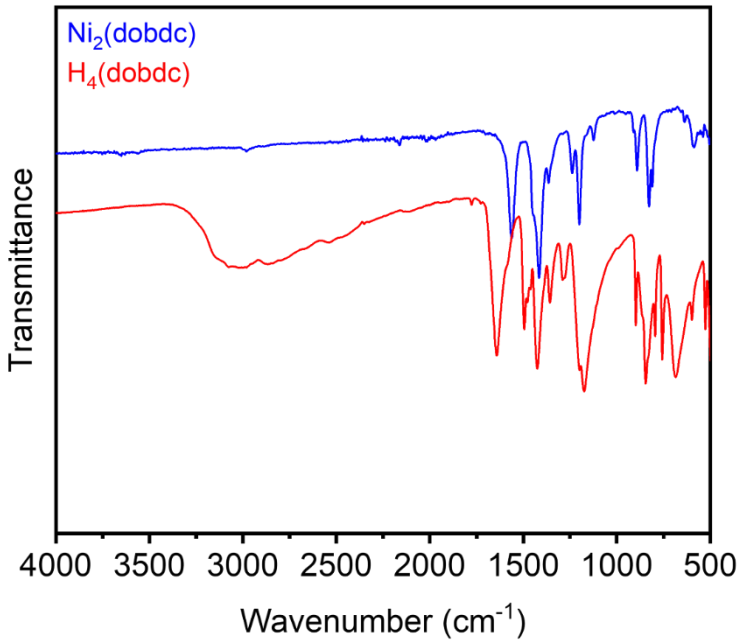

Figure S38. ATR-IR spectra of Ni_2(dobdc) synthesized at 1.0 M and the H_4dobdc linker.

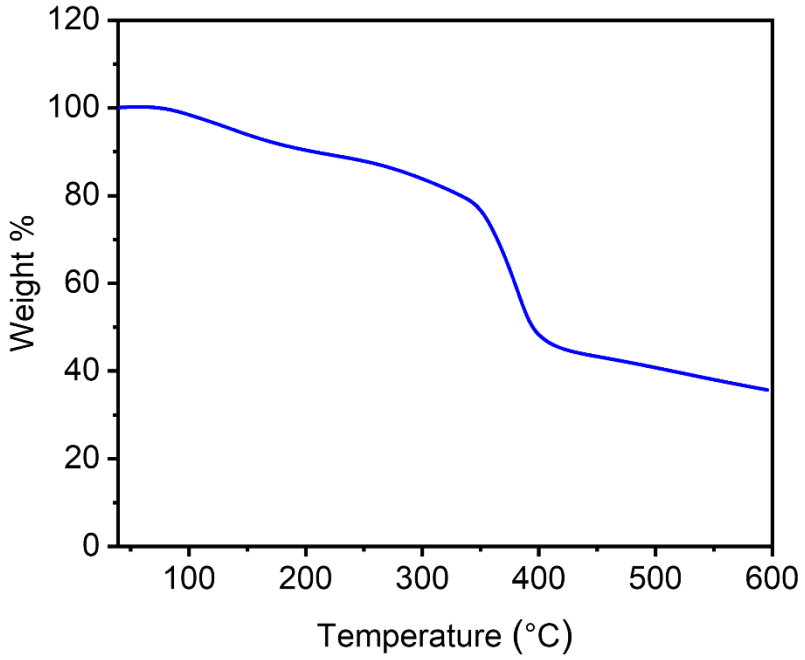

Figure S39. Thermogravimetric decomposition profile under N_2 of Ni_2(dobdc) synthesized at 1.0 M.

Table S4. Surface area data and yields for Ni_2(dobdc) at each synthesized concentration. Literature values for surface areas are included.

Concentration (M)	BET Surface Area (m^2/g)	Langmuir Surface Area (m^2/g)	Yield (%)
0.1	1071 ± 2	1859	85.7
0.5	906 ± 1	1113	78.5
1.0	1160 ± 1	1438	57.1
Literature	1218[7]	1312[7]	-

3.4. Zn_2(dobdc).

Prepared according to a modified literature procedure.[8] In a 20 mL scintillation vial, $Zn(NO_3)_2$•$6H_2O$ (744 mg, 2.50 mmol, 2.50 equiv.) was dissolved in H_2O (5 mL, 1.0 mL, or 0.5 mL for 0.1 M, 0.5 M, and 1.0 M, respectively). In a separate 20 mL scintillation vial equipped with a stir bar, NaOH (160 mg, 4.00 mmol, 4.00 equiv.), 2,5-dihydroxyterephthalic acid (198 mg, 1.00 mmol, 1.00 equiv.), and H_2O (5 mL, 1.0 mL, or 0.5 mL for 0.1 M, 0.5 M, and 1.0 M, respectively) were combined. The $Zn(NO_3)_2$•H_2O solution was added all at once to the H_4dobdc solution via a plastic pipette. The mixture was stirred at room temperature for 1 h. The reaction mixture was vacuum-filtered, and the resulting solid was rinsed with MeOH (10–15 mL). The resulting yellowish-brown solid was transferred to a new scintillation vial filled with MeOH (10–15 mL). The vial was transferred to an aluminum block on a hot plate that had been pre-heated to 60 °C and was allowed to stand at this temperature for at least 12 h. At this time, the heterogenous mixture was allowed to cool to room temperature, the solvent was decanted, and fresh MeOH (10–15 mL) was added. This process was repeated for a total of six MeOH soaks. After the final soak, the solvent was decanted, and the remaining solid was allowed to dry in air. The sample was then activated using supercritical CO_2 (See Section 1), yielding activated Zn_2(dobdc) (70.5%, 74.2%, 67.3% yield for 0.1 M, 0.5 M, and 1.0 M, respectively) that was immediately transferred to a glass adsorption tube equipped with a Micromeritics *CheckSeal*. The sample was activated on the SmartVac under high vacuum (<10 μbar), ramping the temperature slowly to 180 °C (0.1 °C/min). The sample was allowed to stand at 180 °C under high vacuum (<10 μbar) for 12 h prior to gas adsorption analysis.

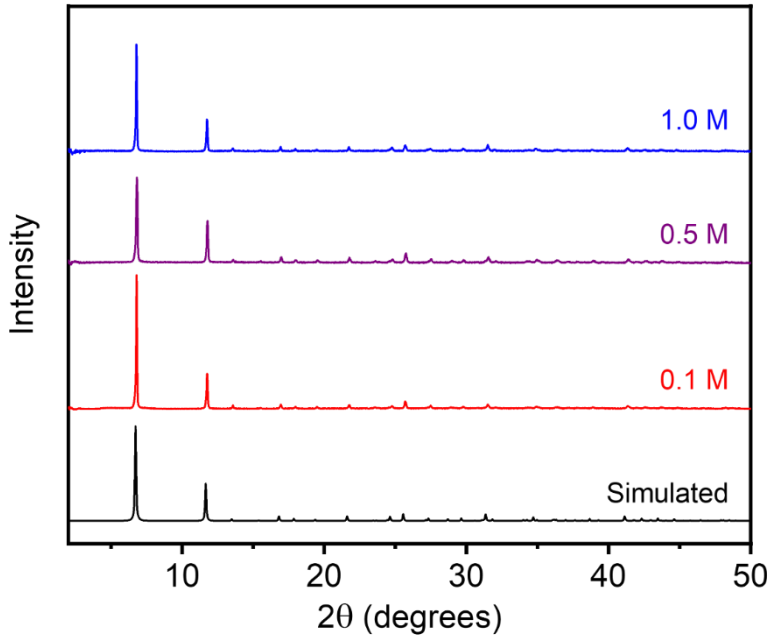

Figure S40. Baseline-corrected PXRD patterns (λ = 1.5406 Å) of MeOH-solvated Zn_2(dobdc) at different concentrations after aqueous synthesis. The simulated pattern based on the previously reported SCXRD structure of Zn_2(dobdc) is included for reference.[9]

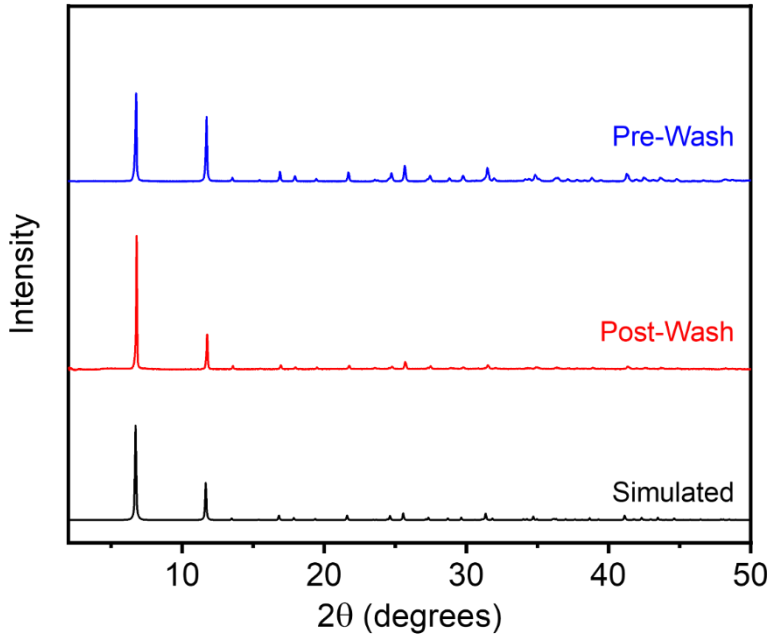

Figure S41. Baseline-corrected PXRD patterns (λ = 1.5406 Å) of Zn_2(dobdc) synthesized at 0.1 M before (pre-wash) and after (post-wash) soaking in MeOH. The simulated pattern based on the previously reported SCXRD structure of the isostructural framework Zn_2(dobdc) is included for reference.[9] Minimal changes in the PXRD pattern were observed upon soaking in MeOH.

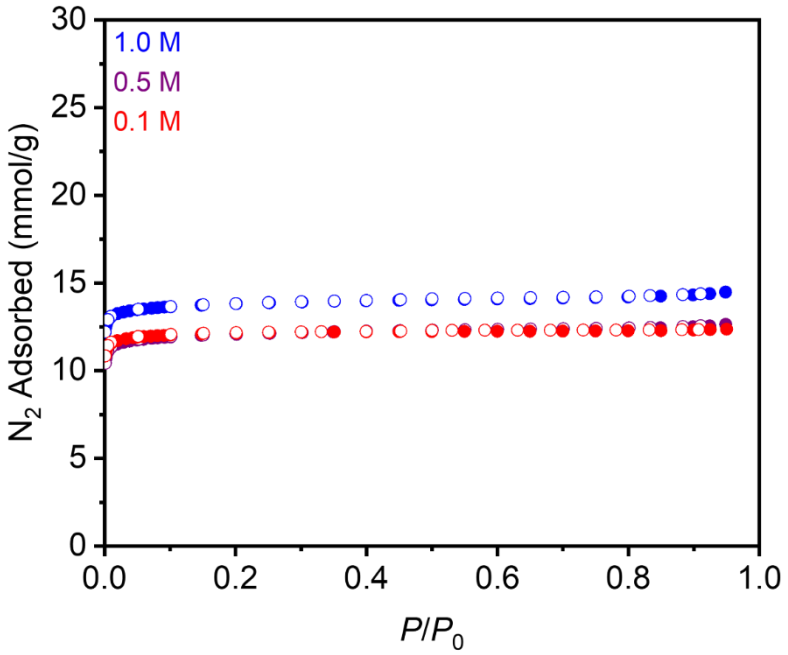

Figure S42. 77 K N_2 adsorption (filled circles) and desorption (open circles) isotherms of activated Zn_2(dobdc) at different concentrations after aqueous synthesis. BET surface areas determined from these data are 1127 ± 1 m^2/g (0.1 M), 1108 ± 1 m^2/g (0.5 M), and 1274 ± 1 m^2/g (1.0 M). The Langmuir surface areas determined from these data are 1202 m^2/g (0.1 M), 1219 m^2/g (0.5 M), and 1395 m^2/g (1.0 M).

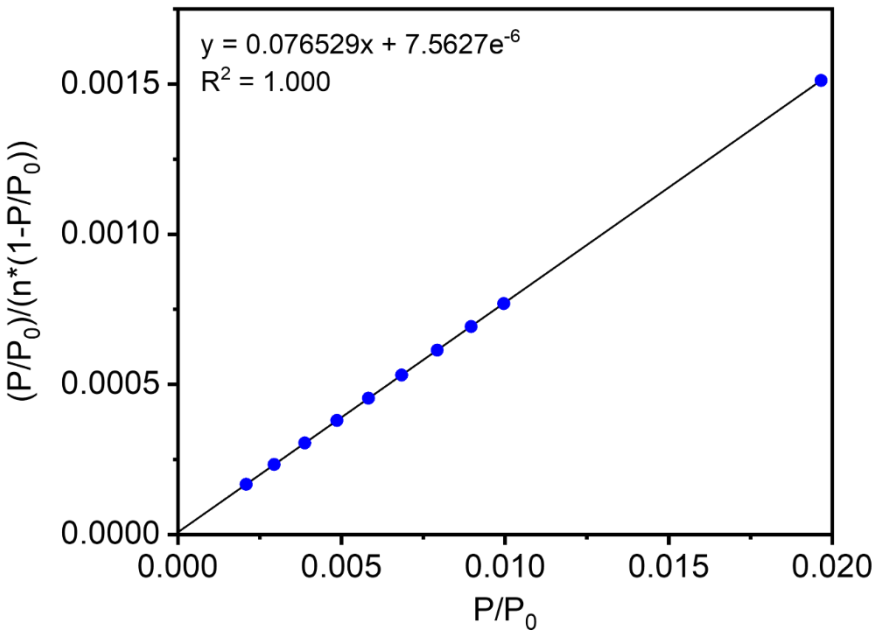

Figure S43. Linearized BET plot for the N_2 adsorption data of Zn_2(dobdc) synthesized at 1.0 M.

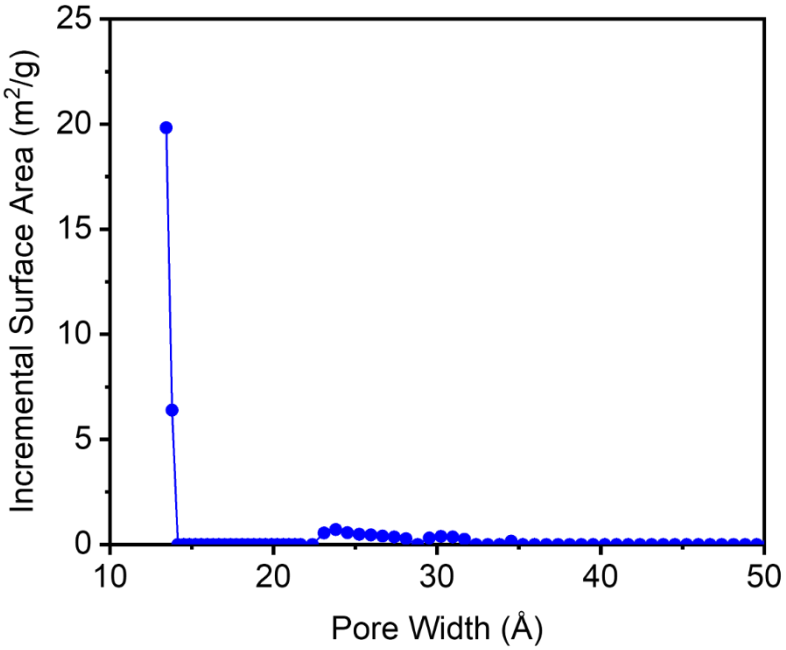

Figure S44. DFT-calculated pore size distribution for Zn_2(dobdc) synthesized at 1.0 M, assuming a cylindrical pore geometry. The primary pore size is below the lower limit of the measurement.

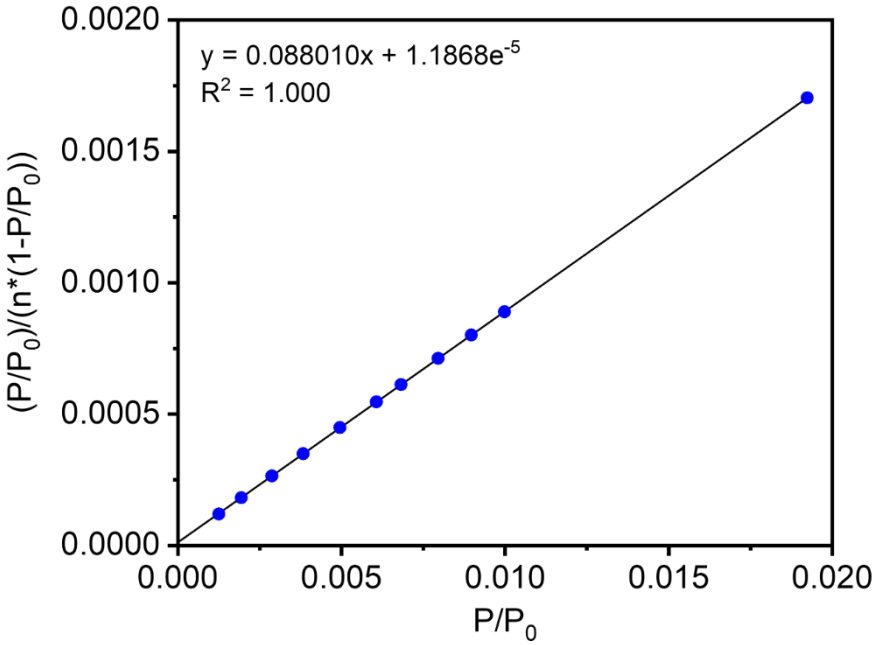

Figure S45. Linearized BET plot for the N_2 adsorption data of Zn_2(dobdc) synthesized at 0.5 M.

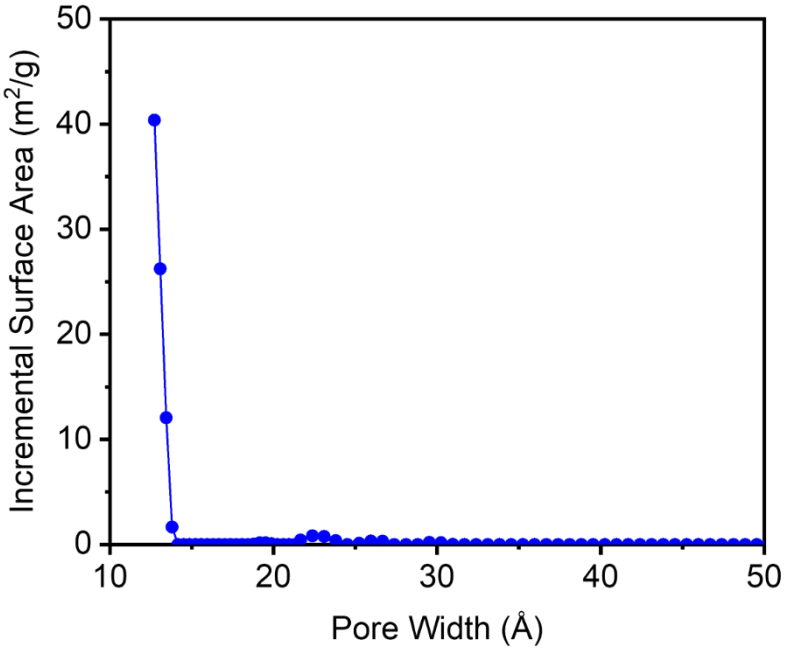

Figure S46. DFT-calculated pore size distribution for Zn_2(dobdc) synthesized at 0.5 M, assuming a cylindrical pore geometry. The primary pore size is below the lower limit of the measurement.

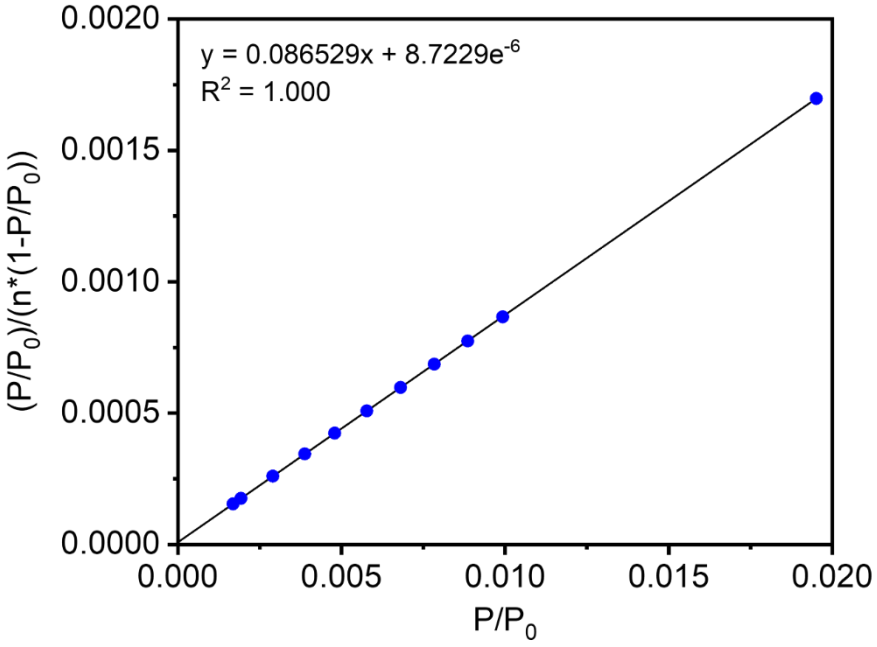

Figure S47. Linearized BET plot for the N_2 adsorption data of Zn_2(dobdc) synthesized at 0.1 M.

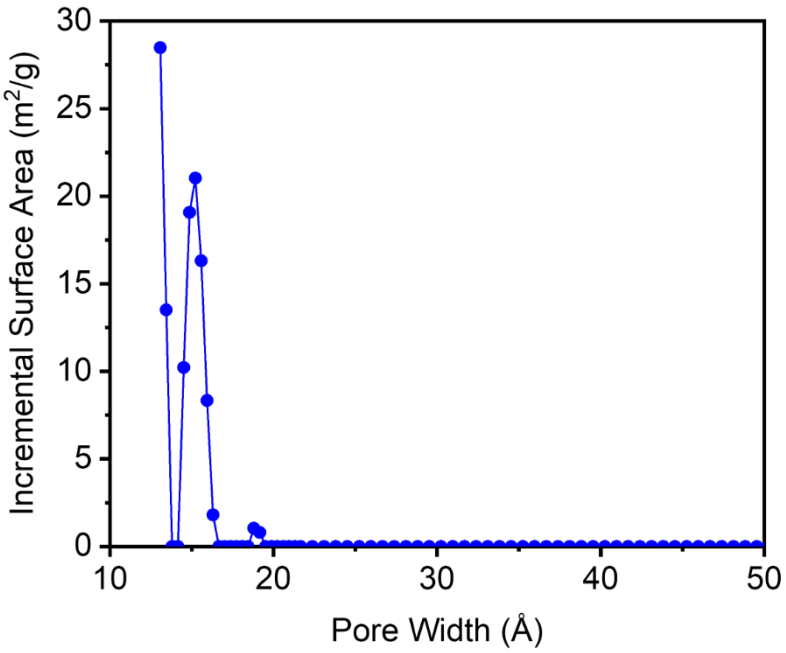

Figure S48. DFT-calculated pore size distribution for Zn_2(dobdc) synthesized at 0.1 M, assuming a cylindrical pore geometry. The primary pore size is below the lower limit of the measurement.

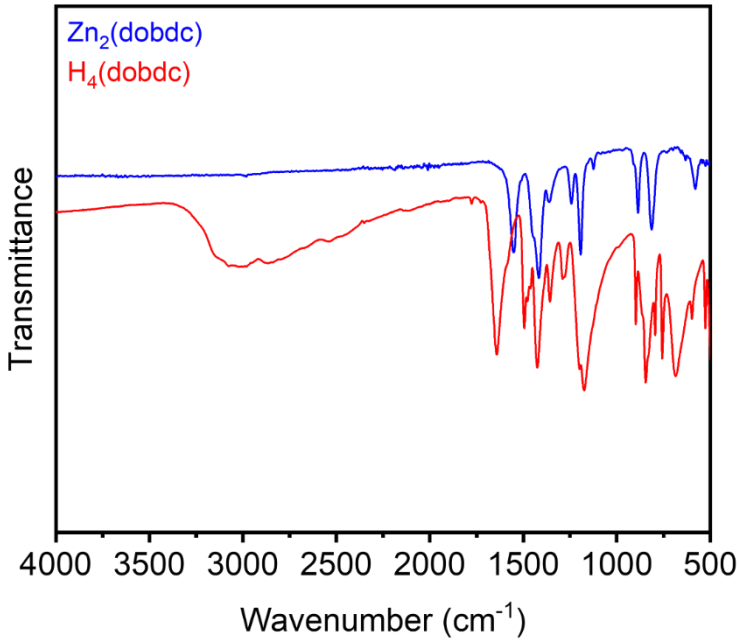

Figure S49. ATR-IR spectra of Zn_2(dobdc) synthesized at 1.0 M and the H_4dobdc linker.

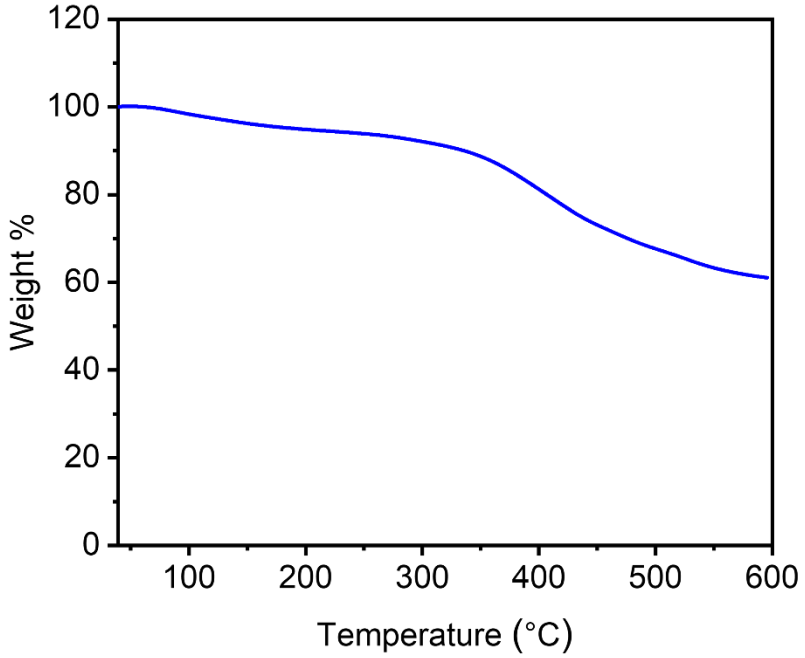

Figure S50. Thermogravimetric decomposition profile under N_2 of Zn_2(dobdc) synthesized at 1.0 M.

Table S5. Surface area data and yields for Zn_2(dobdc) at each synthesized concentration. Literature values for surface areas are included.

Concentration (M)	BET Surface Area (m^2/g)	Langmuir Surface Area (m^2/g)	Yield (%)
0.1	1127 ± 1	1202	70.5
0.5	1108 ± 1	1219	74.2
1.0	1274 ± 1	1395	67.3
Literature	1039[11]	1277[12]	-

4. High-concentration aqueous syntheses of M_2(dobpdc) MOFs.

4.1. Mg_2(dobpdc).

Prepared according to a modified literature procedure.[8] In a 20 mL scintillation vial, $Mg(NO_3)_2$•$6H_2O$ (321 mg, 1.25 mmol, 2.50 equiv.) was dissolved in H_2O (2.5 mL, 0.5 mL, or 0.25 mL for 0.1 M, 0.5 M, and 1.0 M, respectively). In a separate 20 mL scintillation vial equipped with a stir bar, NaOH (80.0 mg, 2.00 mmol, 4.00 equiv.), H_4dobpdc (137 mg, 0.50 mmol, 1.00 equiv.), and H_2O (2.5 mL, 0.5 mL, or 0.25 mL for 0.1 M, 0.5 M, and 1.0 M, respectively) were combined. The $Mg(NO_3)_2$•H_2O solution was added all at once to the H_4dobpdc solution via a plastic pipette. The mixture was stirred at room temperature for 1 h. The reaction mixture was vacuum-filtered, and the resulting solid was rinsed with MeOH (10–15 mL). The resulting yellow-white solid was transferred to a new scintillation vial filled with MeOH (10–15 mL). The vial was transferred to an aluminum block on a hot plate that had been pre-heated to 60 °C and was allowed to stand at this temperature for at least 12 h. At this time, the heterogenous mixture was allowed to cool to room temperature, the solvent was decanted, and fresh MeOH (10–15 mL) was added. This process was repeated for a total of six MeOH soaks. After the final soak, the solvent was decanted, and the remaining solid was allowed to dry in air. The sample was then activated using supercritical CO_2 (See Section 1), yielding activated Mg_2(dobpdc) (57.9%, 94.4%, and 50.9% yield for 0.1 M, 0.5 M, and 1.0 M, respectively) that was immediately transferred to a glass adsorption tube equipped with a Micromeritics *CheckSeal*. The sample was activated on the SmartVac under high vacuum (<10 μbar), ramping the temperature slowly to 180 °C (0.1°C/min). The sample was allowed to stand at 180 °C under high vacuum (<10 μbar) for 12 h prior to gas adsorption analysis.

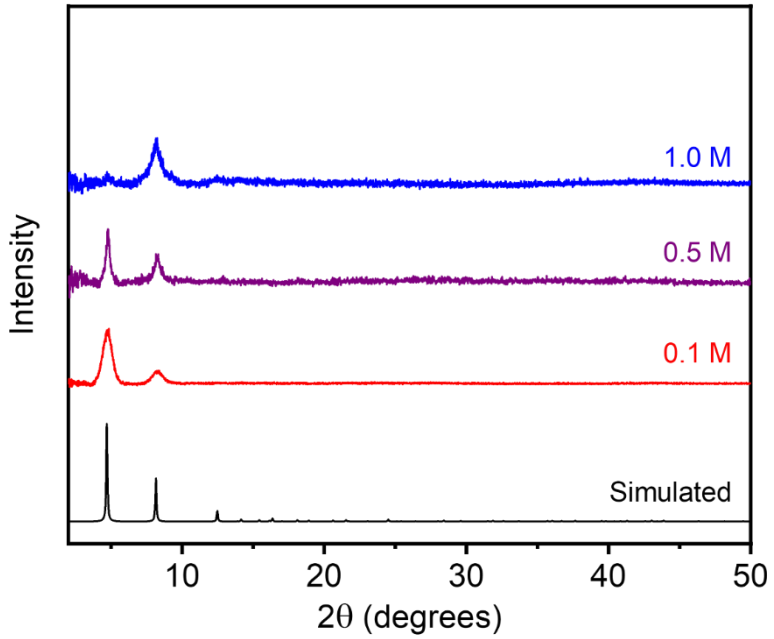

Figure S51. Baseline-corrected PXRD patterns (λ = 1.5406 Å) of MeOH-solvated Mg_2(dobpdc) at different concentrations after aqueous synthesis. The simulated pattern based on the previously reported SCXRD structure of the isostructural framework Zn_2(dobpdc) is included for reference.[13]

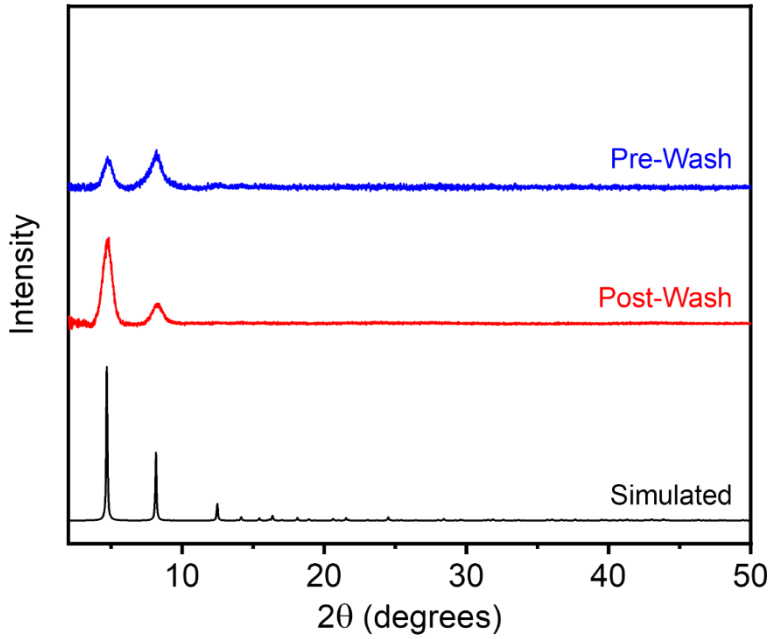

Figure S52. Baseline-corrected PXRD patterns (λ = 1.5406 Å) of MeOH-solvated Mg_2(dobpdc) synthesized at 0.1 M before (pre-wash) and after (post-wash) soaking in MeOH. The simulated pattern based on the previously reported SCXRD structure of the isostructural framework Zn_2(dobpdc) is included for reference.[13] The MOF shows improved crystallinity after soaking.

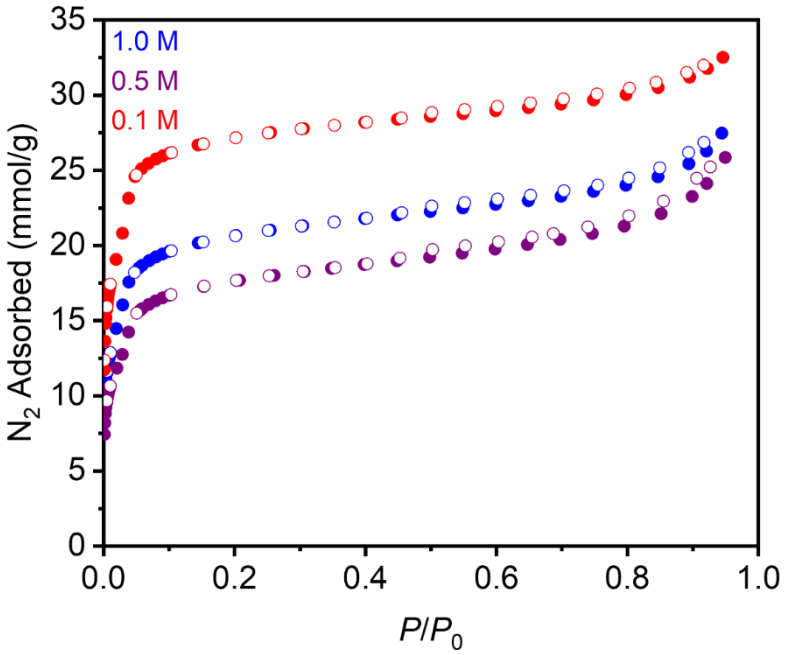

Figure S53. 77 K N_2 adsorption (filled circles) and desorption (open circles) isotherms of activated Mg_2(dobpdc) at different concentrations after aqueous synthesis. BET surface areas determined from these data are 2369 ± 40 m^2/g (0.1 M), 1514 ± 20 m^2/g (0.5 M), and 1785 ± 21 m^2/g (1.0 M). The Langmuir surface areas determined from these data are 3011 m^2/g (0.1 M), 2206 m^2/g (0.5 M), and 2445 m^2/g (1.0 M).

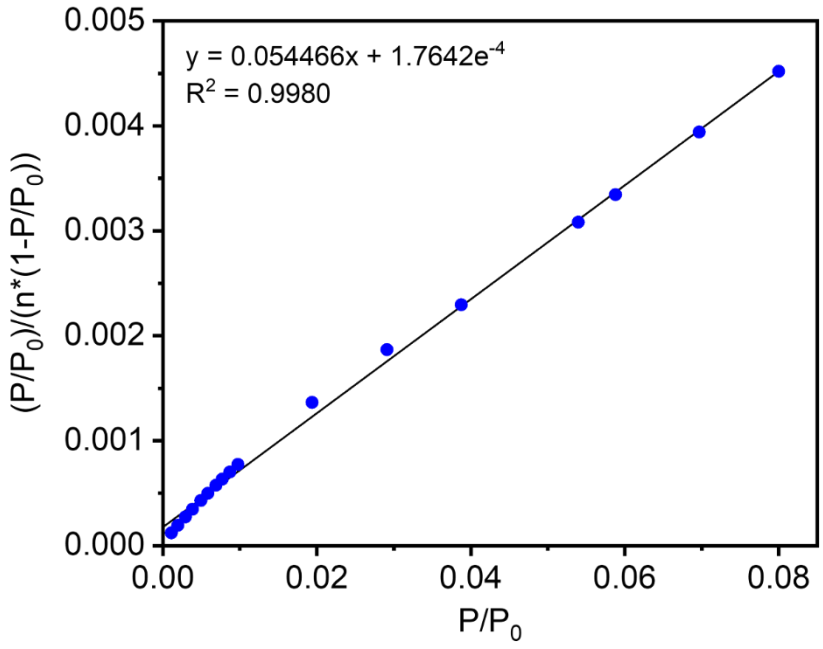

Figure S54. Linearized BET plot for the N_2 adsorption data of Mg_2(dobpdc) synthesized at 1.0 M.

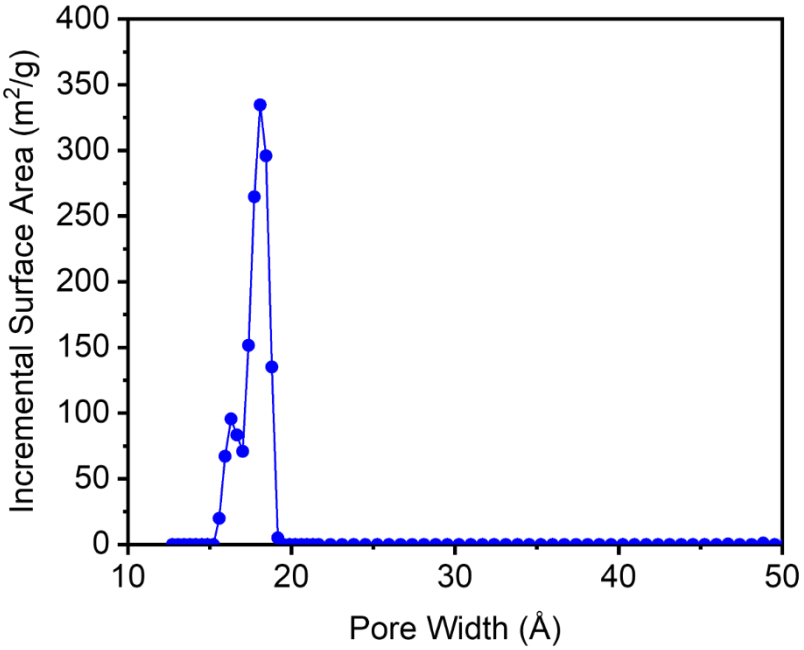

Figure S55. DFT-calculated pore size distribution for Mg_2(dobpdc) synthesized at 1.0 M, assuming a cylindrical pore geometry.

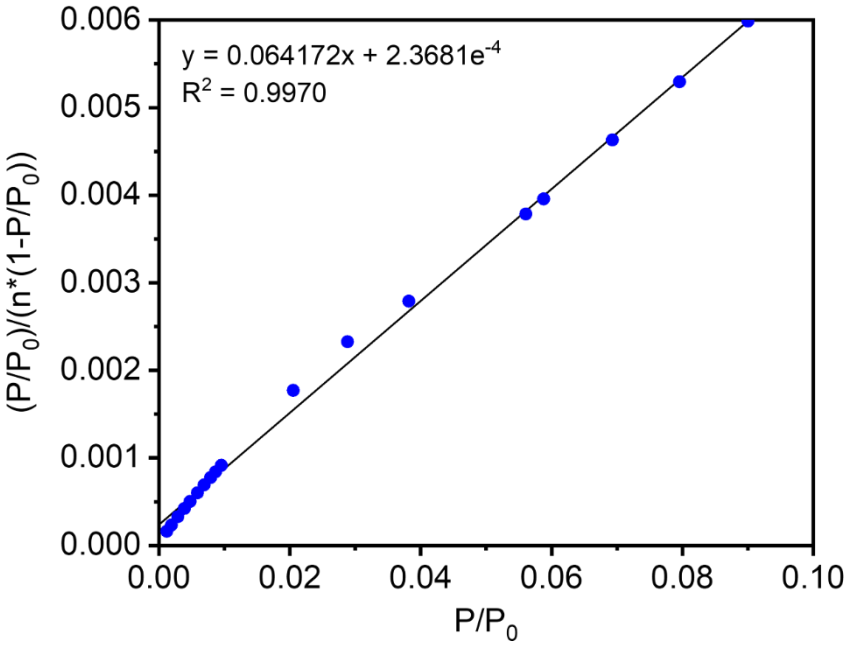

Figure S56. Linearized BET plot for the N_2 adsorption data of Mg_2(dobpdc) synthesized at 0.5 M.

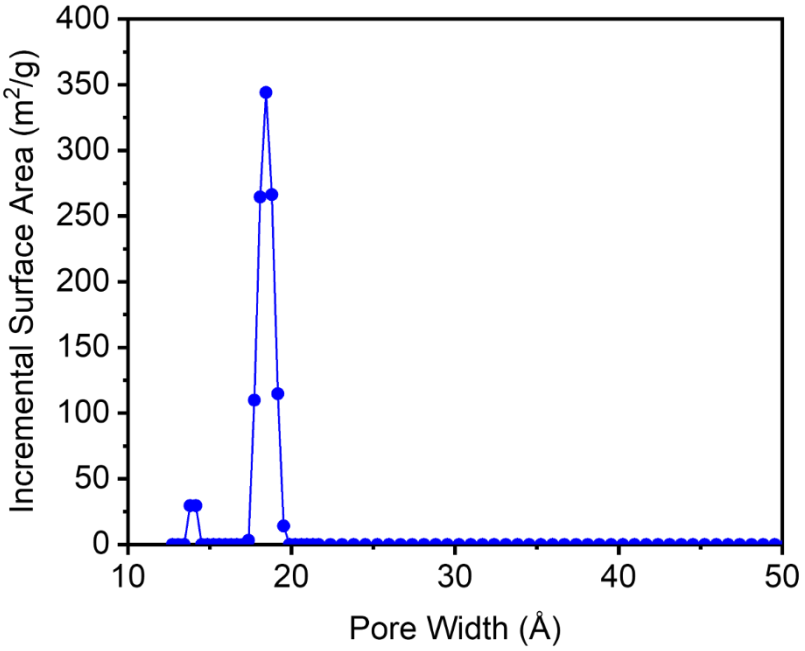

Figure S57. DFT-calculated pore size distribution for Mg_2(dobpdc) synthesized at 0.5 M, assuming a cylindrical pore geometry.

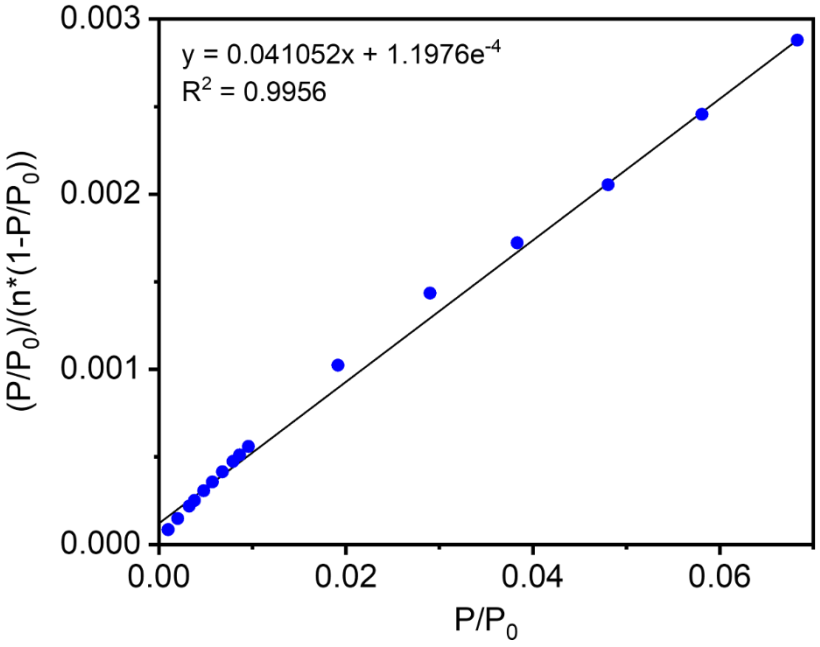

Figure S58. Linearized BET plot for the N_2 adsorption data of Mg_2(dobpdc) synthesized at 0.1 M.

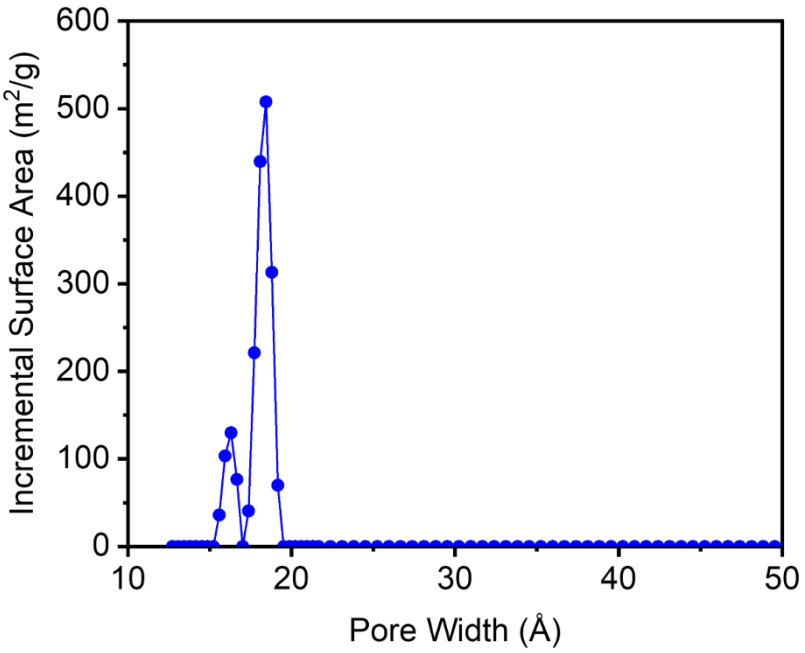

Figure S59. DFT-calculated pore size distribution for Mg_2(dobpdc) synthesized at 0.1 M, assuming a cylindrical pore geometry.

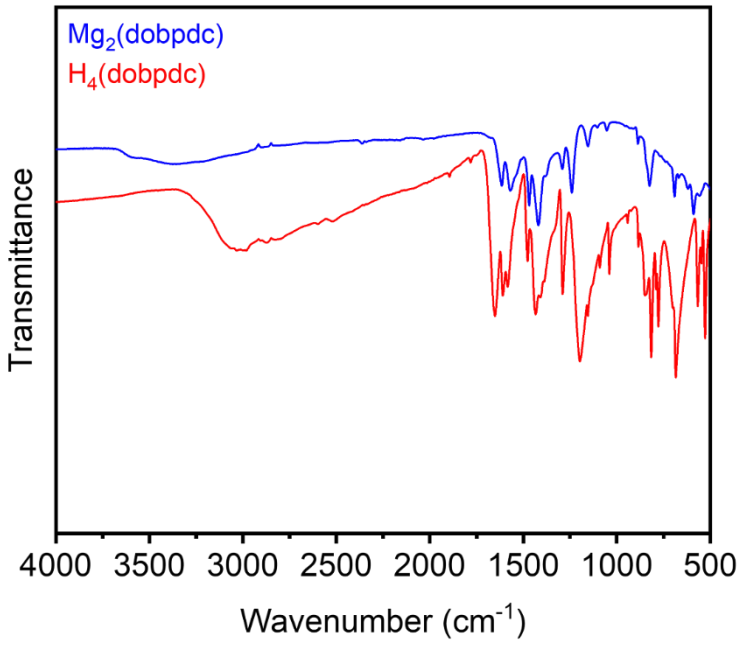

Figure S60. ATR-IR spectra of Mg_2(dobpdc) synthesized at 0.1 M and the H_4dobpdc linker.

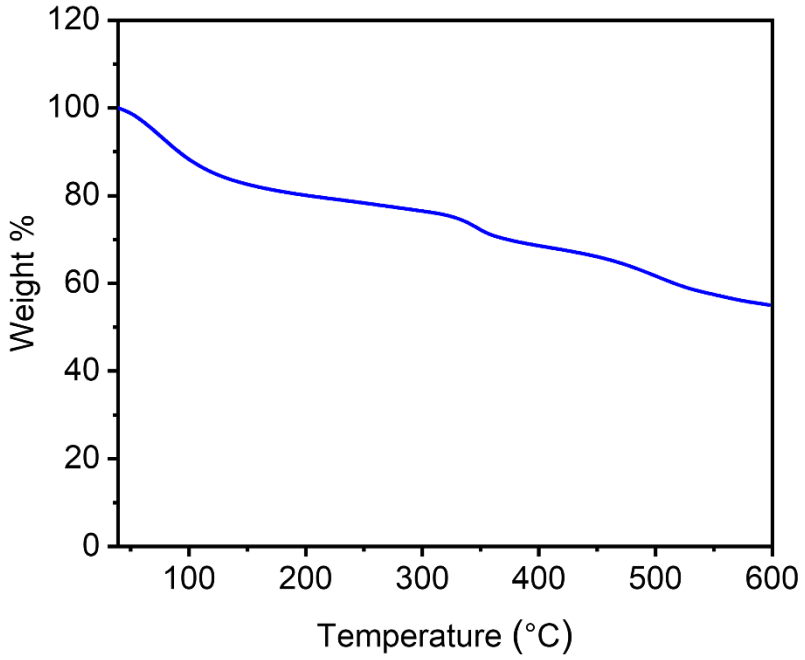

Figure S61. Thermogravimetric decomposition profile under N_2 of Mg_2(dobpdc) synthesized at 0.1 M.

Table S6. Surface area data and yields for Mg_2(dobpdc) at each synthesized concentration. Literature values for surface areas are included.

Concentration (M)	BET Surface Area (m^2/g)	Langmuir Surface Area (m^2/g)	Yield (%)
0.1	2369 ± 40	3011	57.9
0.5	1514 ± 20	2206	94.4
1.0	1785 ± 21	2445	50.9
Literature	3270[7]	3873[7]	-

4.2. Co_2(dobpdc).

Prepared according to a modified literature procedure.[8] In a 20 mL scintillation vial, $Co(NO_3)_2$•$6H_2O$ (364 mg, 1.25 mmol, 2.50 equiv.) was dissolved in H_2O (2.5 mL, 0.5 mL, or 0.25 mL for 0.1 M, 0.5 M, and 1.0 M, respectively). In a separate 20 mL scintillation vial equipped with a stir bar, NaOH (80.0 mg, 2.00 mmol, 4.00 equiv.), H_4dobpdc (137 mg, 0.50 mmol, 1.00 equiv.), and H_2O (2.5 mL, 0.5 mL, or 0.25 mL for 0.1 M, 0.5 M, and 1.0 M, respectively) were combined. The $Co(NO_3)_2$•H_2O solution was added all at once to the H_4dobpdc solution via a plastic pipette. The mixture was stirred at room temperature for 1 h. The reaction mixture was vacuum-filtered, and the resulting solid was rinsed with MeOH (10–15 mL). The resulting dark pink solid was transferred to a new scintillation vial filled with MeOH (10–15 mL). The vial was transferred to an aluminum block on a hot plate that had been pre-heated to 60 °C and was allowed to stand at this temperature for at least 12 h. At this time, the heterogenous mixture was allowed to cool to room temperature, the solvent was decanted, and fresh MeOH (10–15 mL) was added. This process was repeated for a total of six MeOH soaks. After the final soak, the solvent was decanted, and the remaining solid was allowed to dry in air. The sample was then activated using supercritical CO_2 (See Section 1), yielding activated Co_2(dobpdc) (84.9%, 90.2%, and 47.2% yield for 0.1 M, 0.5 M, and 1.0 M, respectively) that was immediately transferred to a glass adsorption tube equipped with a Micromeritics *CheckSeal*. The sample was activated on the SmartVac under high vacuum (<10 μbar), ramping the temperature slowly to 180 °C (0.1°C/min). The sample was allowed to stand at 180 °C under high vacuum (<10 μbar) for 12 h prior to gas adsorption analysis.

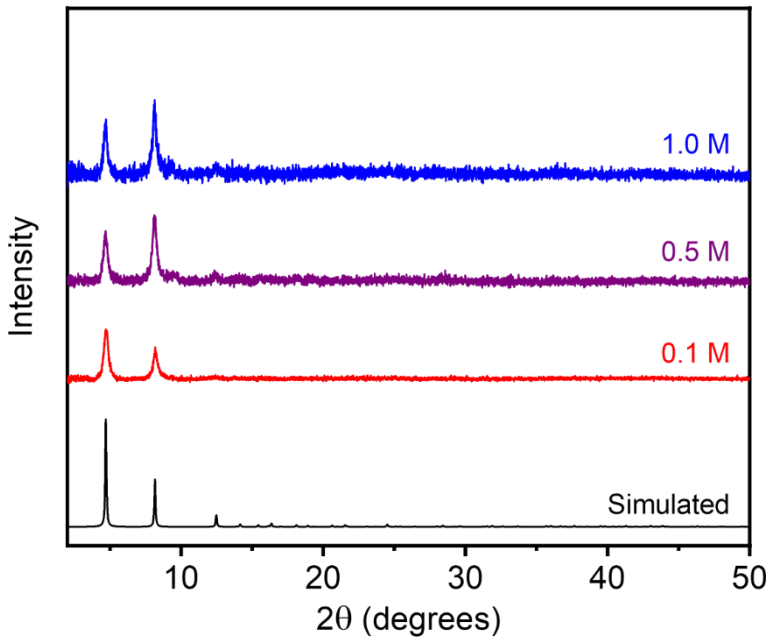

Figure S62. Baseline-corrected PXRD patterns (λ = 1.5406 Å) of MeOH-solvated Co_2(dobpdc) at different concentrations after aqueous synthesis. The simulated pattern based on the previously reported SCXRD structure of the isostructural framework Zn_2(dobpdc) is included for reference.[13]

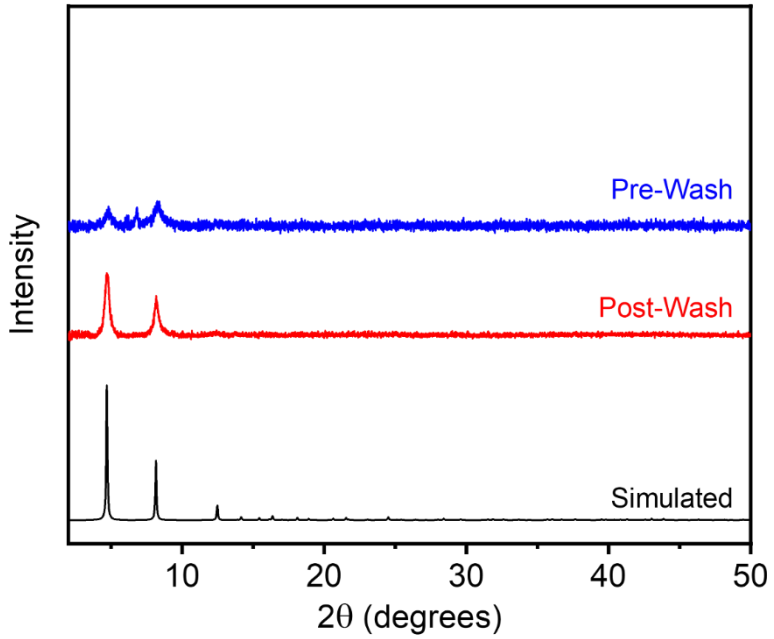

Figure S63. Baseline-corrected PXRD patterns (λ = 1.5406 Å) of MeOH-solvated Co_2(dobpdc) synthesized at 0.1 M before (pre-wash) and after (post-wash) soaking in MeOH. The simulated pattern based on the previously reported SCXRD structure of the isostructural framework Zn_2(dobpdc) is included for reference.[13] The MOF shows improved crystallinity after soaking.

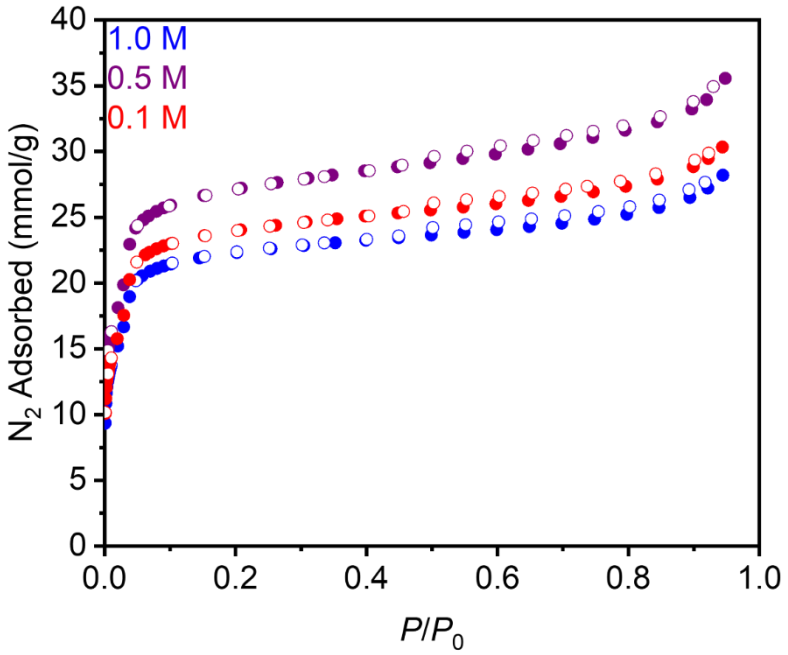

Figure S64. 77 K N_2 adsorption (filled circles) and desorption (open circles) isotherms of activated Co_2(dobpdc) at different concentrations after aqueous synthesis. BET surface areas determined from these data are 2102 ± 40 m^2/g (0.1 M), 2371 ± 42 m^2/g (0.5 M), 1946 ± 39 m^2/g (1.0 M). The Langmuir surface areas determined from these data are 2767 m^2/g (0.1 M), 3197 m^2/g (0.5 M), and 2549 m^2/g (1.0 M).

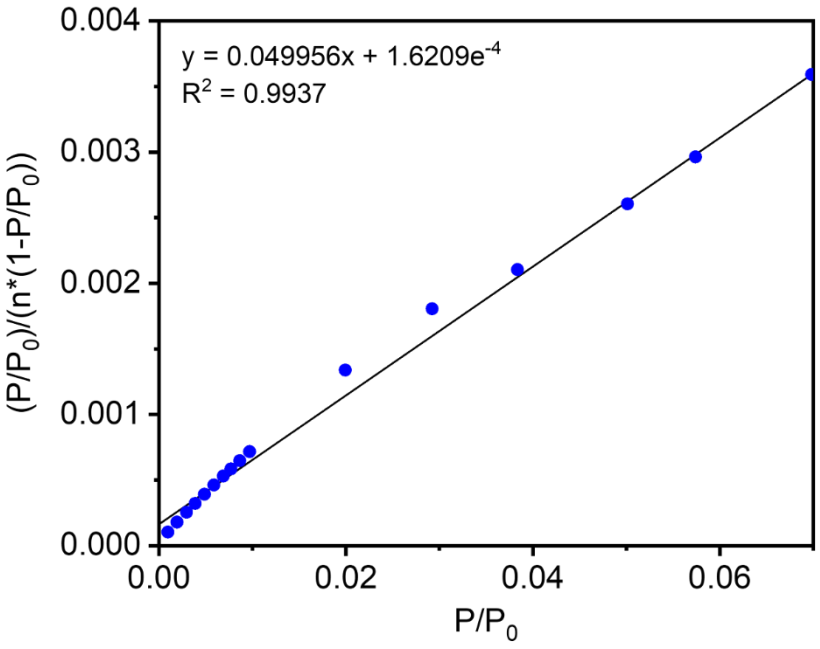

Figure S65. Linearized BET plot for the N_2 adsorption data of Co_2(dobpdc) synthesized at 1.0 M.

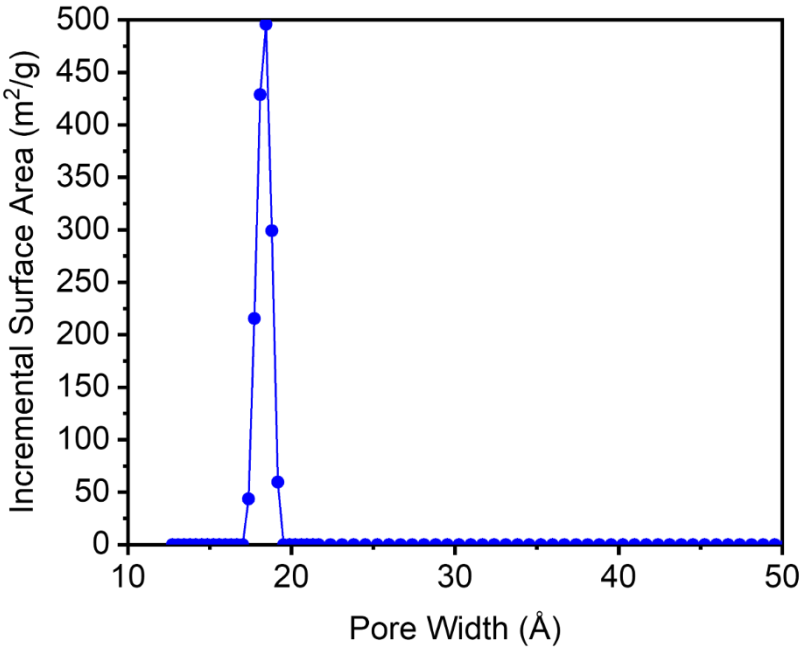

Figure S66. DFT-calculated pore size distribution for Co_2(dobpdc) synthesized at 1.0 M, assuming a cylindrical pore geometry.

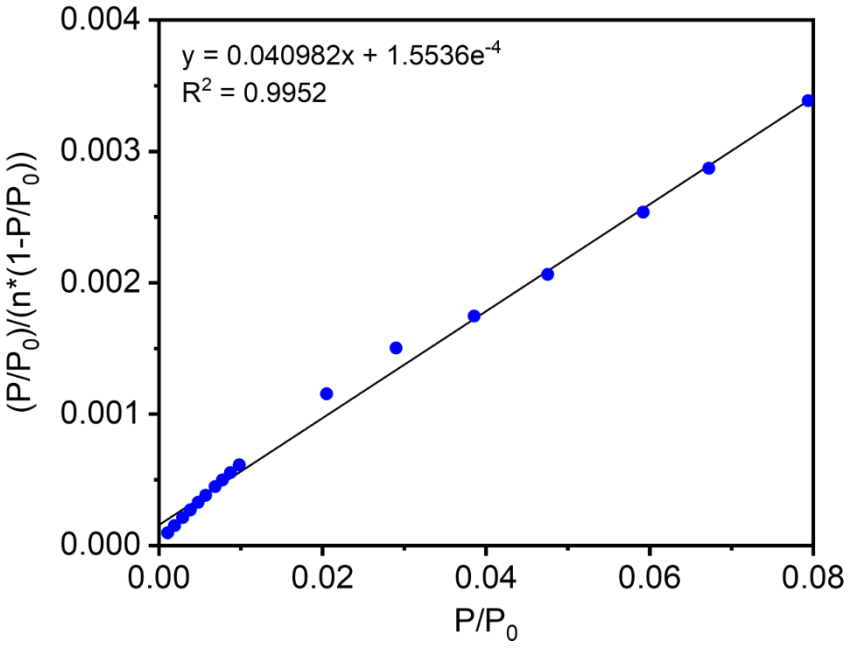

Figure S67. Linearized BET plot for the N_2 adsorption data of Co_2(dobpdc) synthesized at 0.5 M.

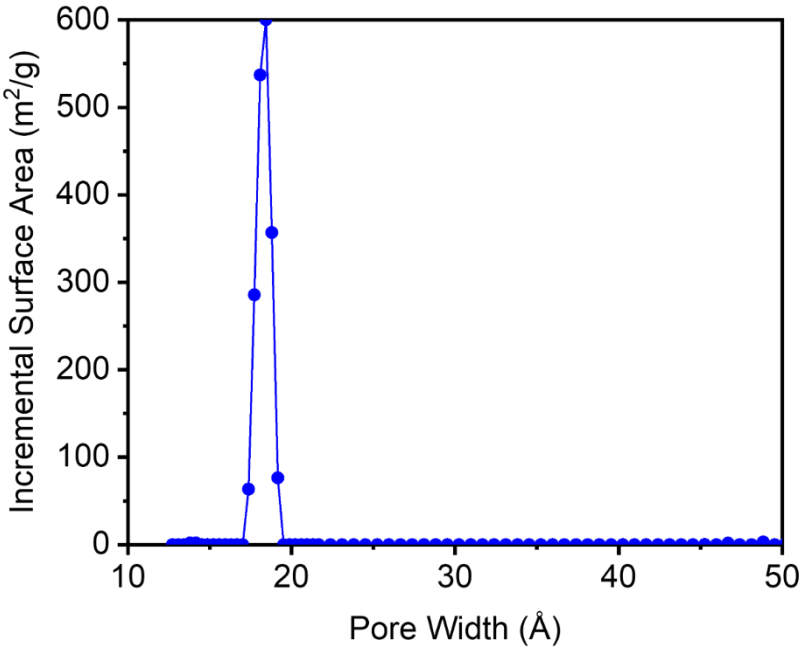

Figure S68. DFT-calculated pore size distribution for Co_2(dobpdc) synthesized at 0.5 M, assuming a cylindrical pore geometry. The primary pore size is below the lower limit of the measurement.

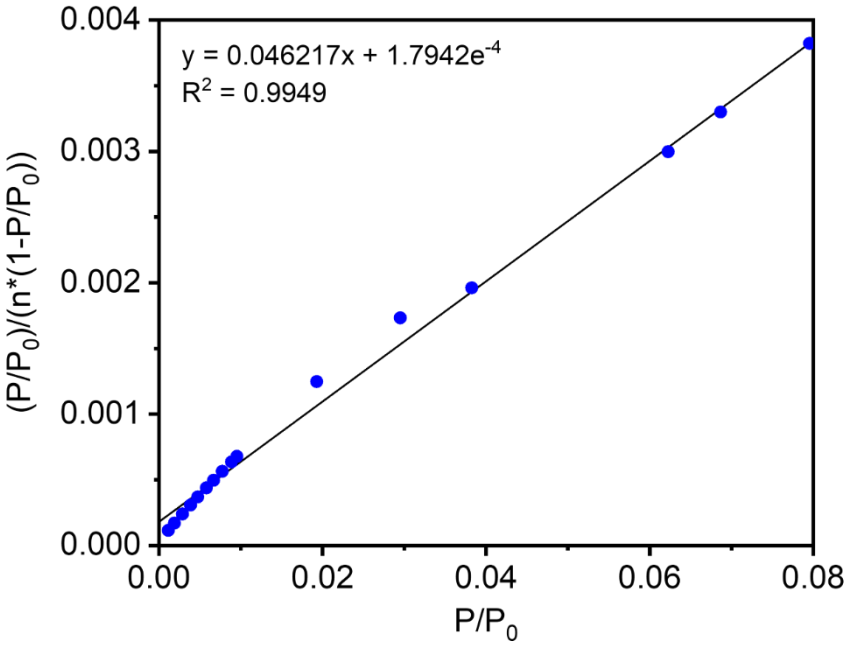

Figure S69. Linearized BET plot for the N_2 adsorption data of Co_2(dobpdc) synthesized at 0.1 M.

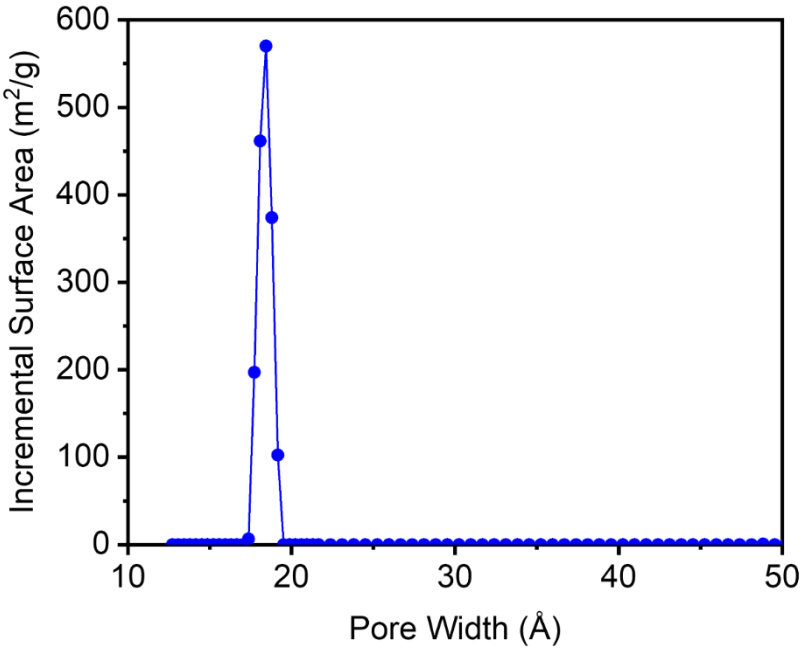

Figure S70. DFT-calculated pore size distribution for Co_2(dobpdc) synthesized at 0.1 M, assuming a cylindrical pore geometry. The primary pore size is below the lower limit of the measurement.

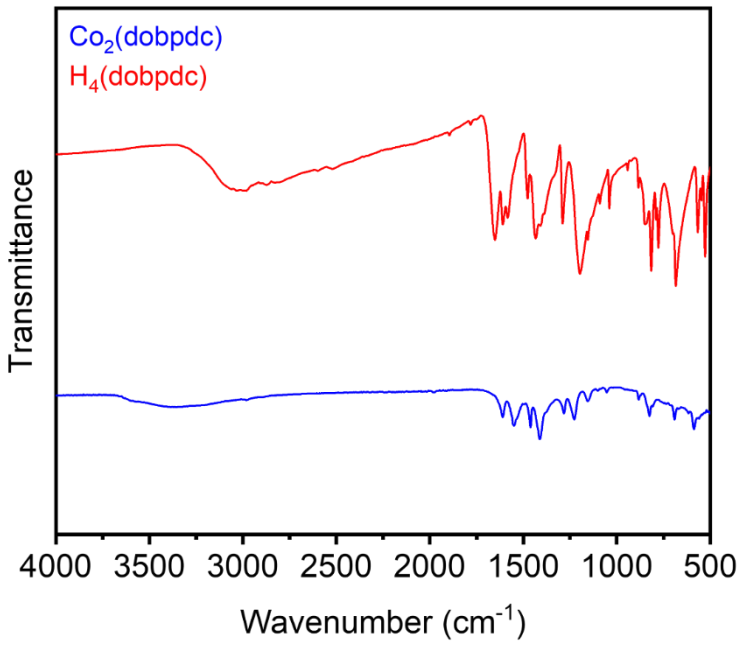

Figure S71. ATR-IR spectra of Co_2(dobpdc) synthesized at 0.5 M and the H_4dobpdc linker.

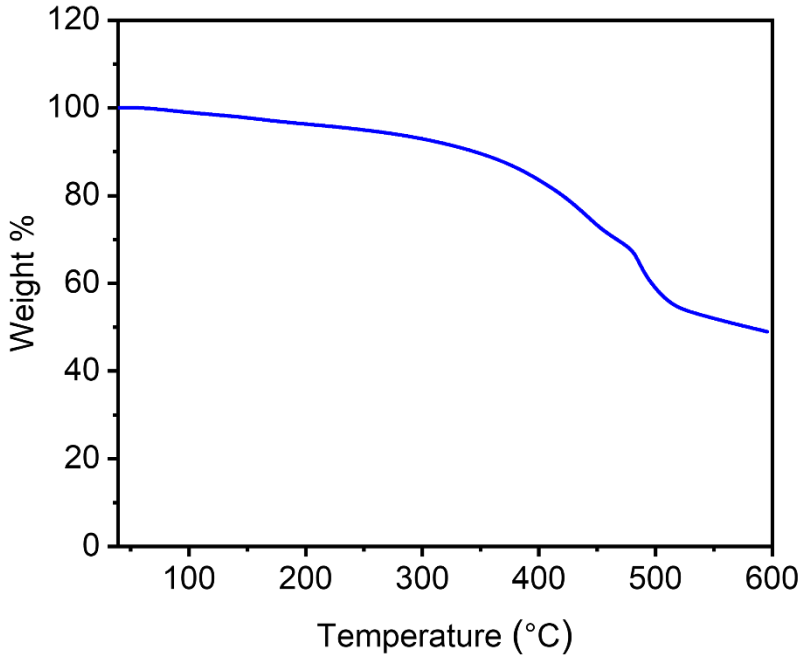

Figure S72. Thermogravimetric decomposition profile under N_2 of Co_2(dobpdc) synthesized at 0.5 M.

Table S7. Surface area data and yields for Co_2(dobpdc) at each synthesized concentration. Literature values for surface areas are included.

Concentration (M)	BET Surface Area (m^2/g)	Langmuir Surface Area (m^2/g)	Yield (%)
0.1	2102 ± 40	2767	84.9
0.5	2371 ± 42	3197	90.2
1.0	1946 ± 39	2549	47.2
Literature	2255[7]	3357[7]	-

4.3. Ni_2(dobpdc).

Prepared according to a modified literature procedure.[8] In a 20 mL scintillation vial, $Ni(NO_3)_2$•$6H_2O$ (364 mg, 1.25 mmol, 2.50 equiv.) was dissolved in H_2O (2.5 mL, 0.5 mL, or 0.25 mL for 0.1 M, 0.5 M, and 1.0 M, respectively). In a separate 20 mL scintillation vial equipped with a stir bar, NaOH (80.0 mg, 2.00 mmol, 4.00 equiv.), H_4dobpdc (137 mg, 0.50 mmol, 1.00 equiv.), and H_2O (2.5 mL, 0.5 mL, or 0.25 mL for 0.1 M, 0.5 M, and 1.0 M, respectively) were combined. The $Ni(NO_3)_2$•H_2O solution was added all at once to the H_4dobpdc solution via a plastic pipette. The mixture was stirred at room temperature for 1 h. The reaction mixture was vacuum-filtered, and the resulting solid was rinsed with MeOH (10–15 mL). The resulting green solid was transferred to a new scintillation vial filled with MeOH (10–15 mL). The vial was transferred to an aluminum block on a hot plate that had been pre-heated to 60 °C and was allowed to stand at this temperature for at least 12 h. At this time, the heterogenous mixture was allowed to cool to room temperature, the solvent was decanted, and fresh MeOH (10–15 mL) was added. This process was repeated for a total of six MeOH soaks. After the final soak, the solvent was decanted, and the remaining solid was allowed to dry in air. The sample was then activated using supercritical CO_2 (See Section 1), yielding activated Ni_2(dobpdc) (91.1%, 51.8%, and 30.5% yield for 0.1 M, 0.5 M, and 1.0 M, respectively) that was immediately transferred to a glass adsorption tube equipped with a Micromeritics *CheckSeal*. The sample was activated on the SmartVac under high vacuum (<10 μbar), ramping the temperature slowly to 180 °C (0.1°C/min). The sample was allowed to stand at 180 °C under high vacuum (<10 μbar) for 12 h prior to gas adsorption analysis.

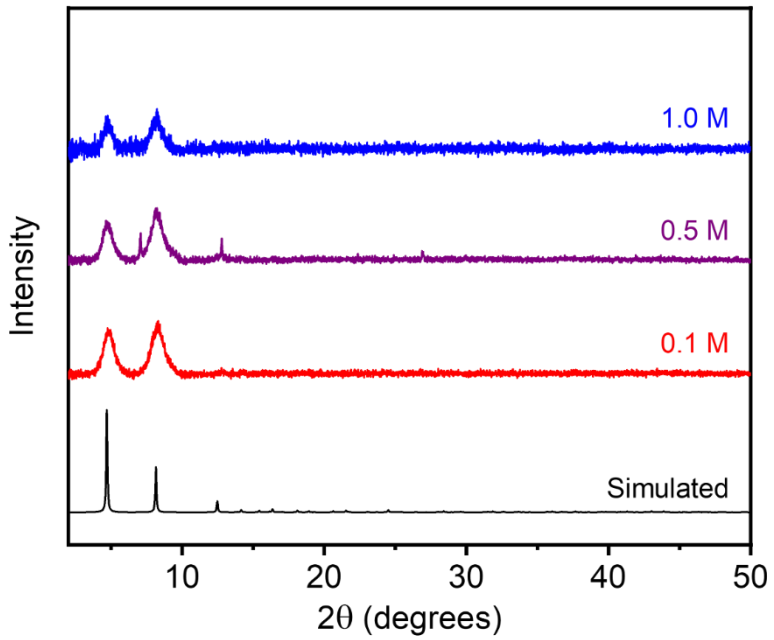

Figure S73. Baseline-corrected PXRD patterns (λ = 1.5406 Å) of MeOH-solvated Ni_2(dobpdc) at different concentrations after aqueous synthesis. The simulated pattern based on the previously reported SCXRD structure of the isostructural framework Zn_2(dobpdc) is included for reference.[13]

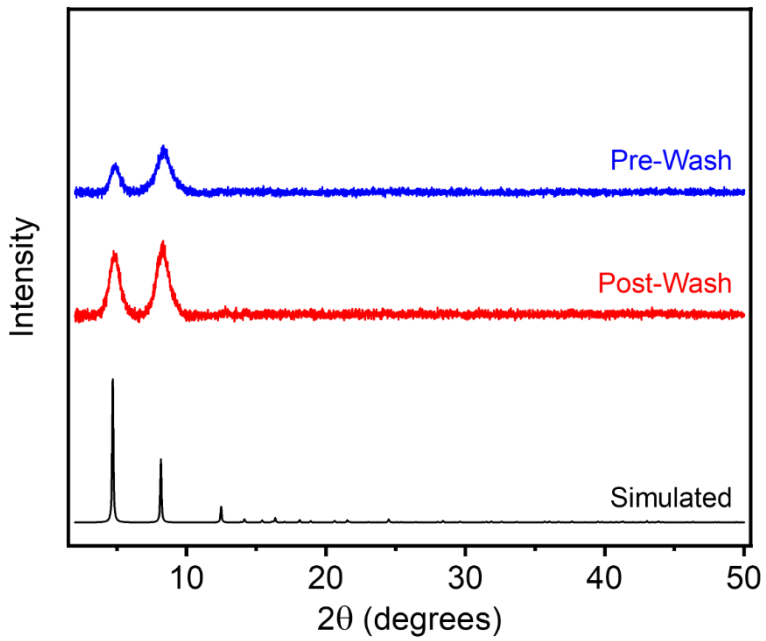

Figure S74. Baseline-corrected PXRD patterns (λ = 1.5406 Å) of MeOH-solvated Ni_2(dobpdc) synthesized at 0.1 M before (pre-wash) and after (post-wash) soaking in MeOH. The simulated pattern based on the previously reported SCXRD structure of the isostructural framework Zn_2(dobpdc) is included for reference.[13] No significant change in the pattern was observed upon soaking the MOF in MeOH.

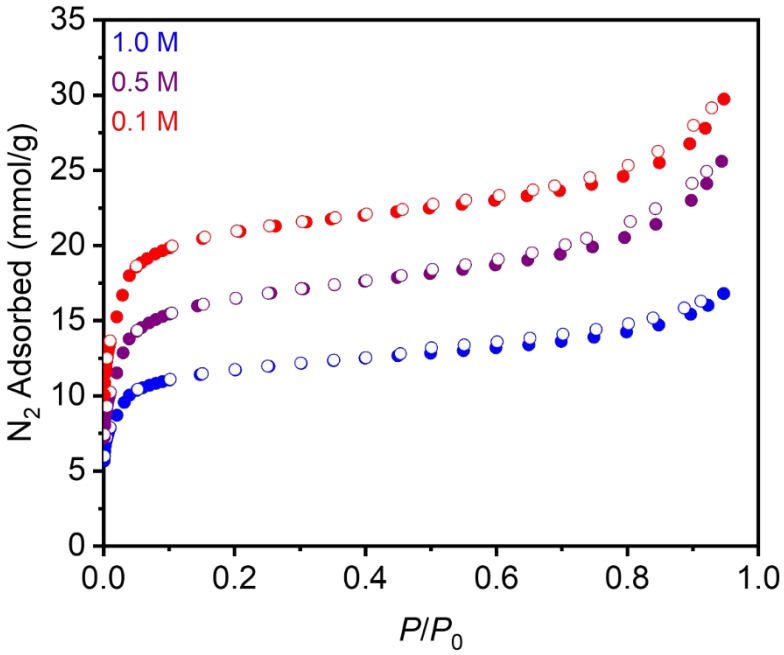

Figure S75. 77 K N_2 adsorption (filled circles) and desorption (open circles) isotherms of activated Ni_2(dobpdc) at different concentrations after aqueous synthesis. BET surface areas determined from these data are 1794 ± 17 m^2/g (0.1 M), 1393 ± 12 m^2/g (0.5 M), and 992 ± 8 m^2/g (1.0 M). The Langmuir surface areas determined from these data are 2542 m^2/g (0.1 M), 2143 m^2/g (0.5 M), and 1459 m^2/g (1.0 M).

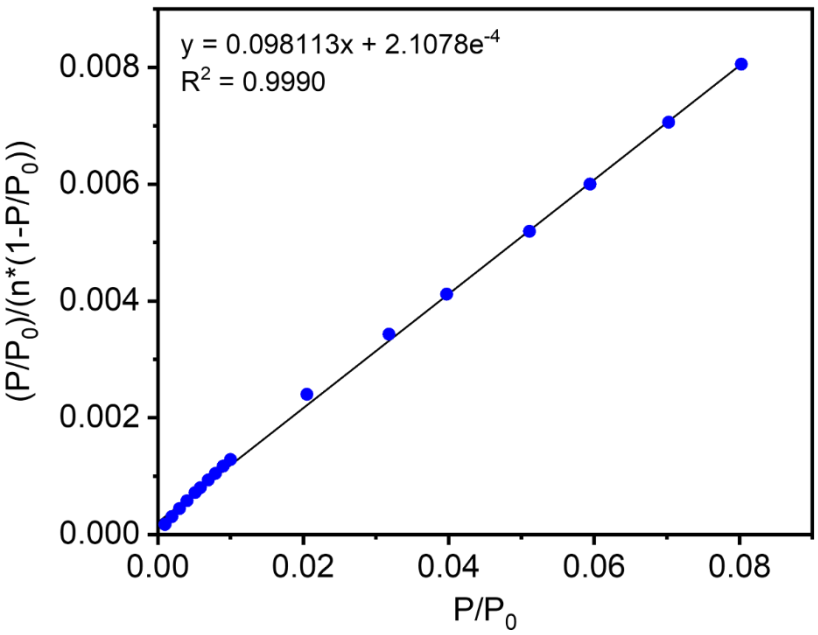

Figure S76. Linearized BET plot for the N_2 adsorption data of Ni_2(dobpdc) synthesized at 1.0 M.

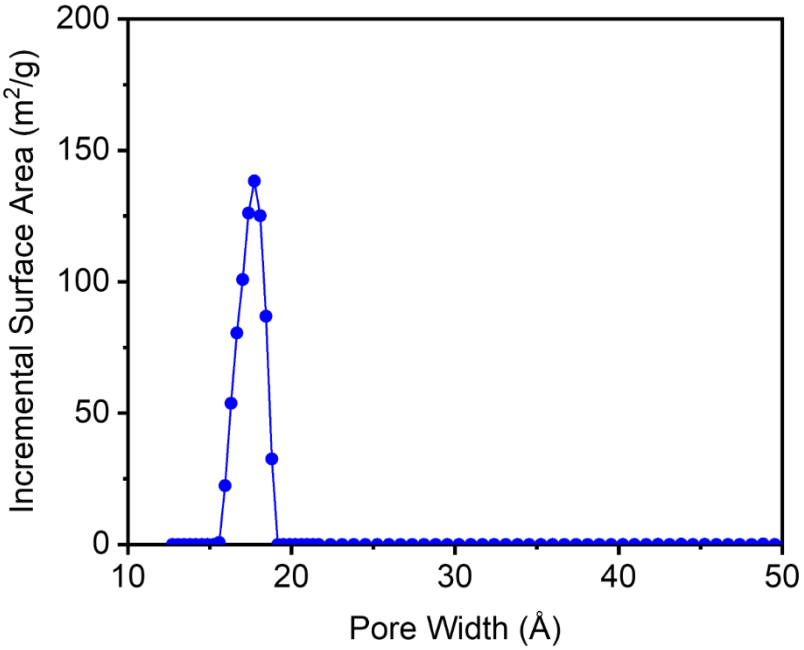

Figure S77. DFT-calculated pore size distribution for Ni_2(dobpdc) synthesized at 1.0 M, assuming a cylindrical pore geometry.

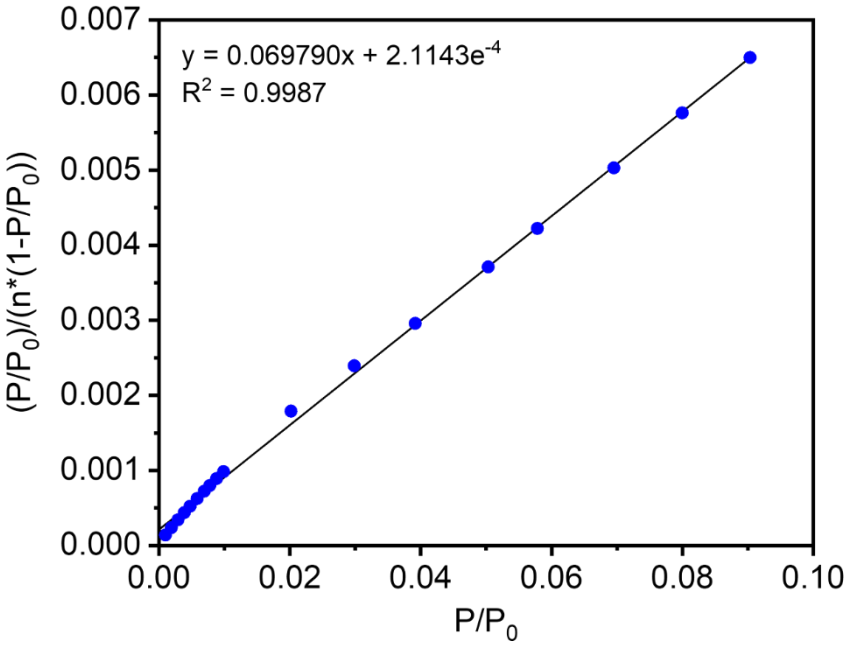

Figure S78. Linearized BET plot for the N_2 adsorption data of Ni_2(dobpdc) synthesized at 0.5 M.

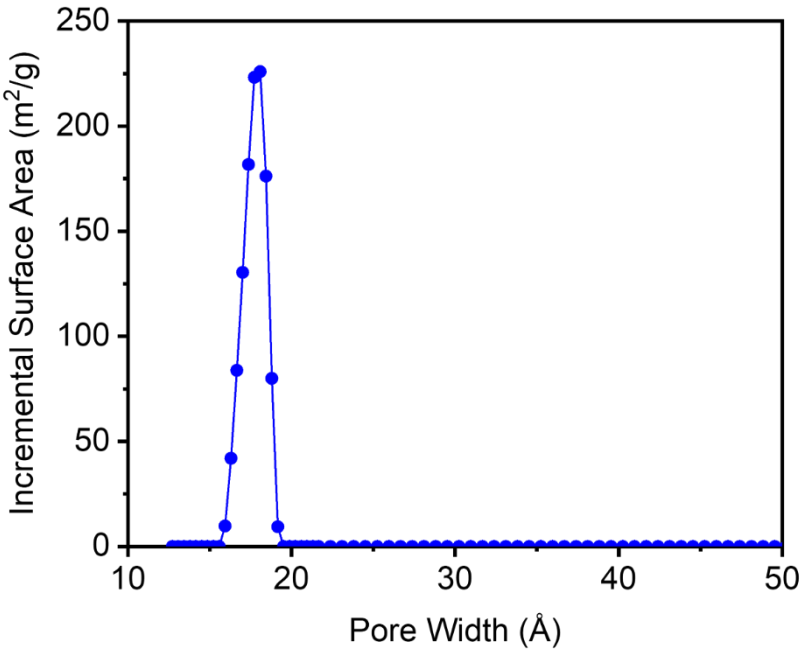

Figure S79. DFT-calculated pore size distribution for Ni_2(dobpdc) synthesized at 0.5 M, assuming a cylindrical pore geometry.

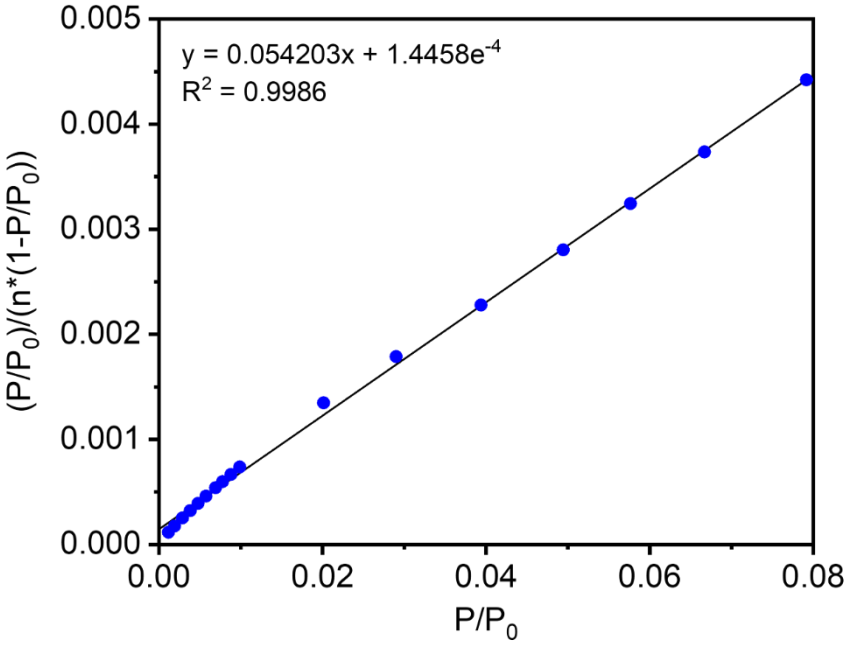

Figure S80. Linearized BET plot for the N_2 adsorption data of Ni_2(dobpdc) synthesized at 0.1 M.

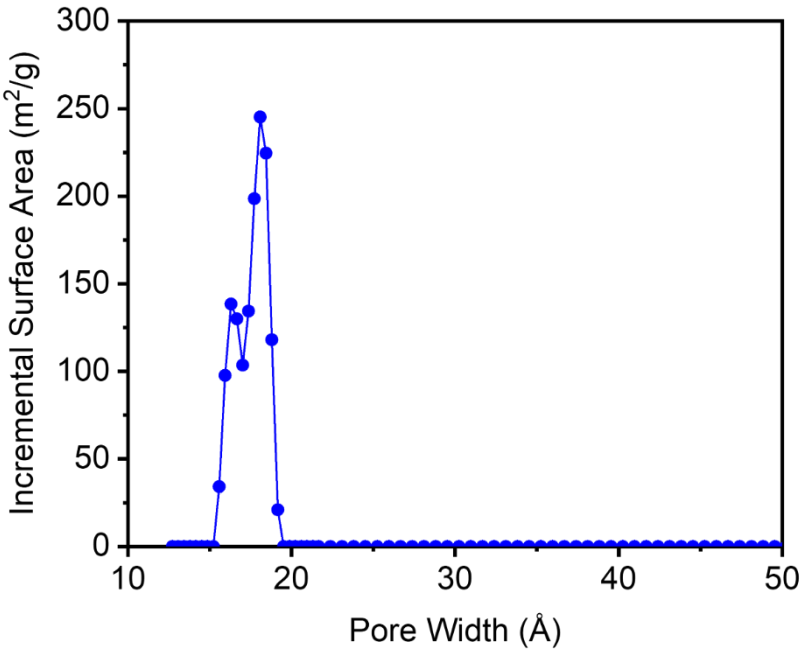

Figure S81. DFT-calculated pore size distribution for Ni_2(dobpdc) synthesized at 0.1 M, assuming a cylindrical pore geometry.

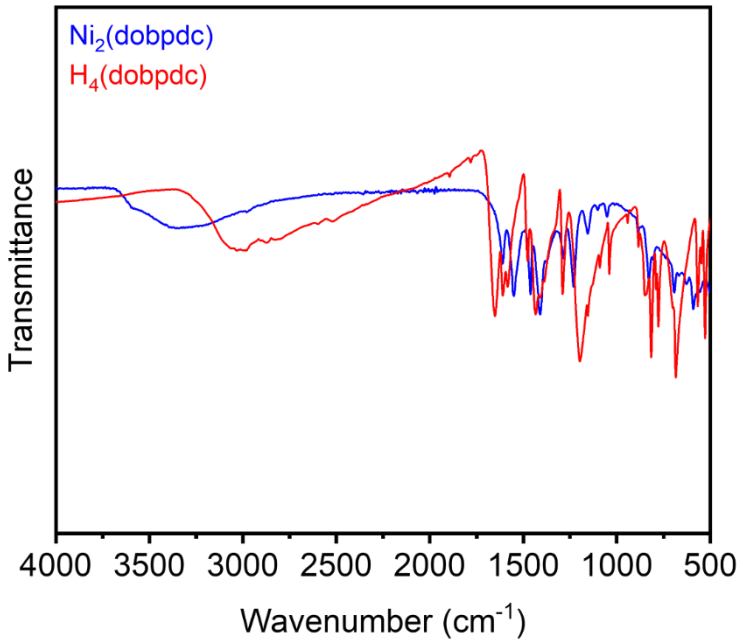

Figure S82. ATR-IR spectra of Ni_2(dobpdc) synthesized at 0.1 M and the H_4dobpdc linker.

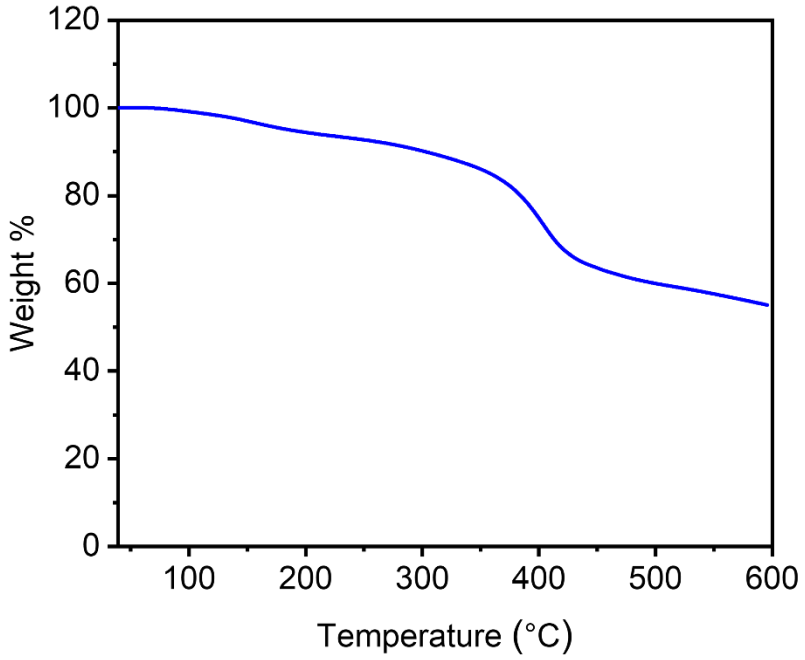

Figure S83. Thermogravimetric decomposition profile under N_2 of Ni_2(dobpdc) synthesized at 0.1 M.

Table S8. Surface area data and yields for Ni_2(dobpdc) at each synthesized concentration. Literature values for surface areas are included.

Concentration (M)	BET Surface Area (m^2/g)	Langmuir Surface Area (m^2/g)	Yield (%)
0.1	1794 ± 17	2542	91.1
0.5	1393 ± 12	2143	51.8
1.0	992 ± 8	1459	30.5
Literature	2059[7]	3108[7]	-

4.4. Zn_2(dobpdc).

Prepared according to a modified literature procedure.[8] In a 20 mL scintillation vial, $Zn(NO_3)_2$•$6H_2O$ (372 mg, 1.25 mmol, 2.50 equiv.) was dissolved in H_2O (2.5 mL, 0.5 mL, or 0.25 mL for 0.1 M, 0.5 M, and 1.0 M, respectively). In a separate 20 mL scintillation vial equipped with a stir bar, NaOH (80.0 mg, 2.00 mmol, 4.00 equiv.), H_4dobpdc (137 mg, 0.50 mmol, 1.00 equiv.), and H_2O (2.5 mL, 0.5 mL, or 0.25 mL for 0.1 M, 0.5 M, and 1.0 M, respectively) were combined. The $Zn(NO_3)_2$•H_2O solution was added all at once to the H_4dobpdc solution via a plastic pipette. The mixture was stirred at room temperature for 1 h. The reaction mixture was vacuum-filtered, and the resulting solid was rinsed with MeOH (10–15 mL). The resulting off-white solid was transferred to a new scintillation vial filled with MeOH (10–15 mL). The vial was transferred to an aluminum block on a hot plate that had been pre-heated to 60 °C and was allowed to stand at this temperature for at least 12 h. At this time, the heterogenous mixture was allowed to cool to room temperature, the solvent was decanted, and fresh MeOH (10–15 mL) was added. This process was repeated for a total of six MeOH soaks. After the final soak, the solvent was decanted, and the remaining solid was allowed to dry in air. The sample was then activated using supercritical CO_2 (See Section 1), yielding activated Zn_2(dobpdc) (87.8%, 59.6%, and 69.0% yield for 0.1 M, 0.5 M, and 1.0 M, respectively) that was immediately transferred to a glass adsorption tube equipped with a Micromeritics *CheckSeal*. The sample was activated on the SmartVac under high vacuum (<10 μbar), ramping the temperature slowly to 180 °C (0.1°C/min). The sample was allowed to stand at 180 °C under high vacuum (<10 μbar) for 12 h prior to gas adsorption analysis.

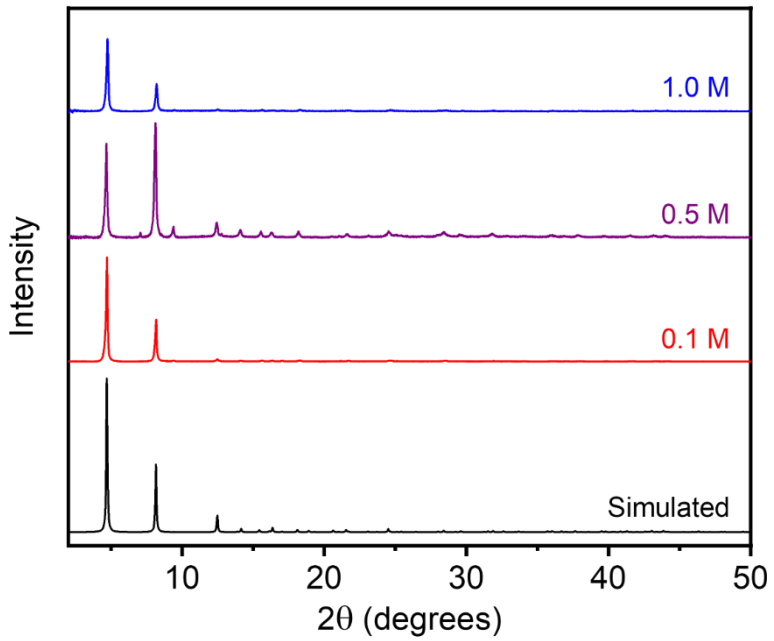

Figure S84. Baseline-corrected PXRD patterns (λ = 1.5406 Å) of MeOH-solvated Zn_2(dobpdc) at different concentrations after aqueous synthesis. The simulated pattern based on the previously reported SCXRD structure of the isostructural framework Zn_2(dobpdc) is included for reference.[13]

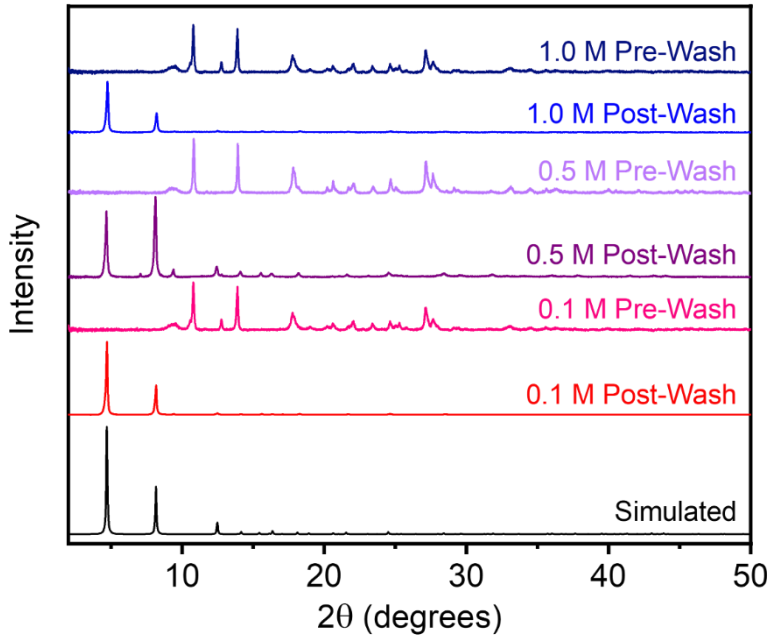

Figure S85. Baseline-corrected PXRD patterns (λ = 1.5406 Å) of MeOH-solvated Zn_2(dobpdc) synthesized at different concentrations before (pre-wash) and after (post-wash) soaking in MeOH. The simulated pattern based on the previously reported SCXRD structure of the isostructural framework Zn_2(dobpdc) is included for reference.[13] A different phase or mixture of phases is obtained initially at all concentrations that transformations into Zn_2(dobpdc) upon soaking in MeOH. Indexing the powder data of these samples did not produce definitive unit cell parameters.

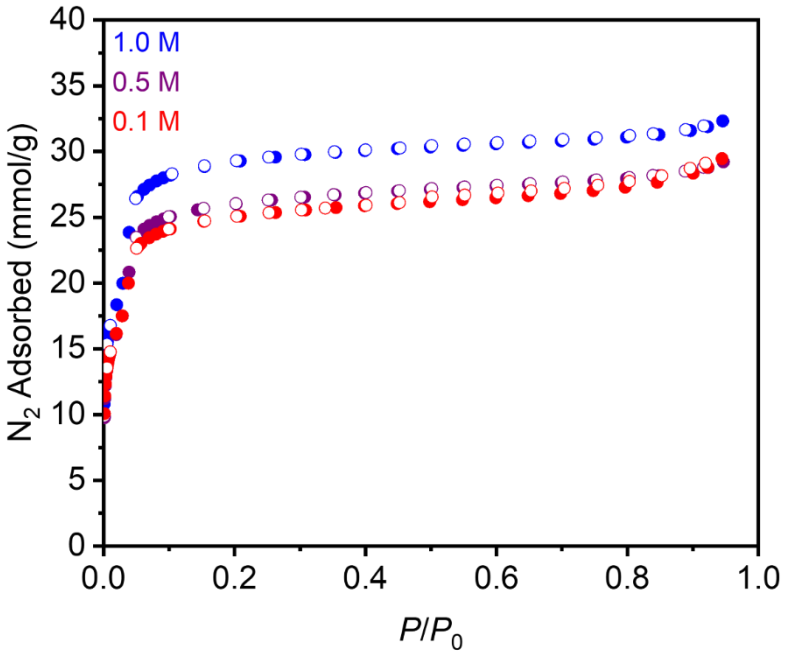

Figure S86. 77 K N_2 adsorption (filled circles) and desorption (open circles) isotherms of activated Zn_2(dobpdc) at different concentrations after aqueous synthesis. BET surface areas determined from these data are 2190 ± 60 m^2/g (0.1 M), 2285 ± 70 m^2/g (0.5 M), 2574 ± 77 m^2/g (1.0 M). The Langmuir surface areas determined from these data are 2743 m^2/g (0.1 M), 2783 m^2/g (0.5 M), and 3090 m^2/g (1.0 M).

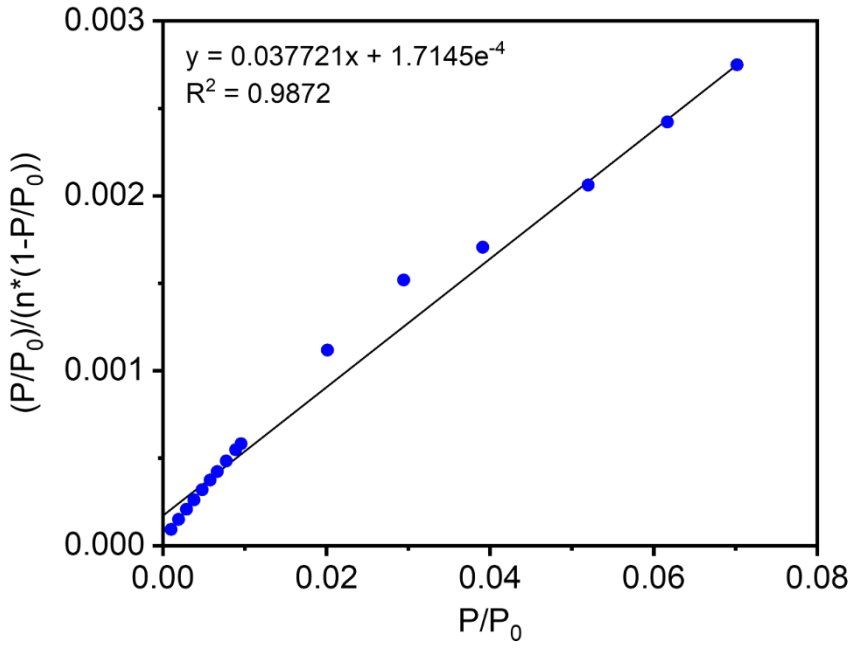

Figure S87. Linearized BET plot for the N_2 adsorption data of Zn_2(dobpdc) synthesized at 1.0 M.

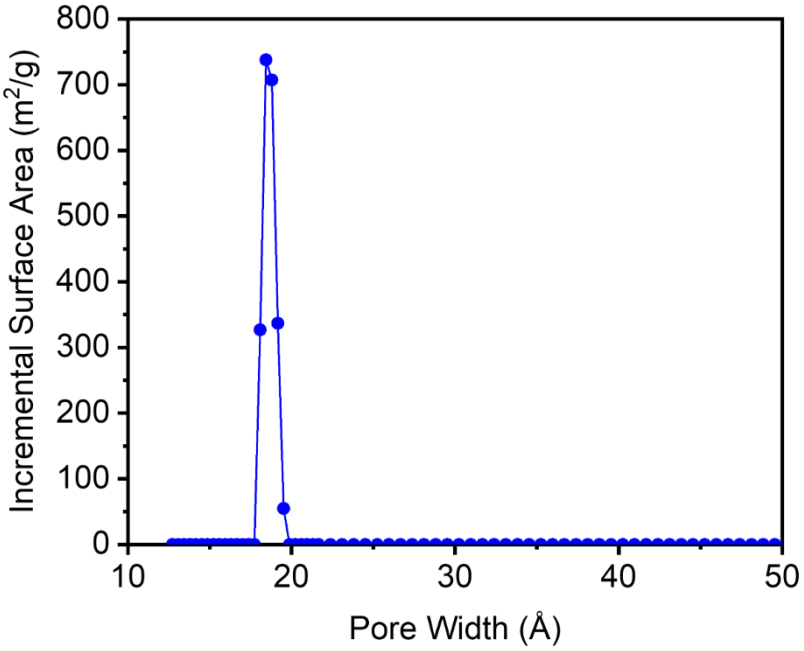

Figure S88. DFT-calculated pore size distribution for Zn_2(dobpdc) synthesized at 1.0 M, assuming a cylindrical pore geometry.

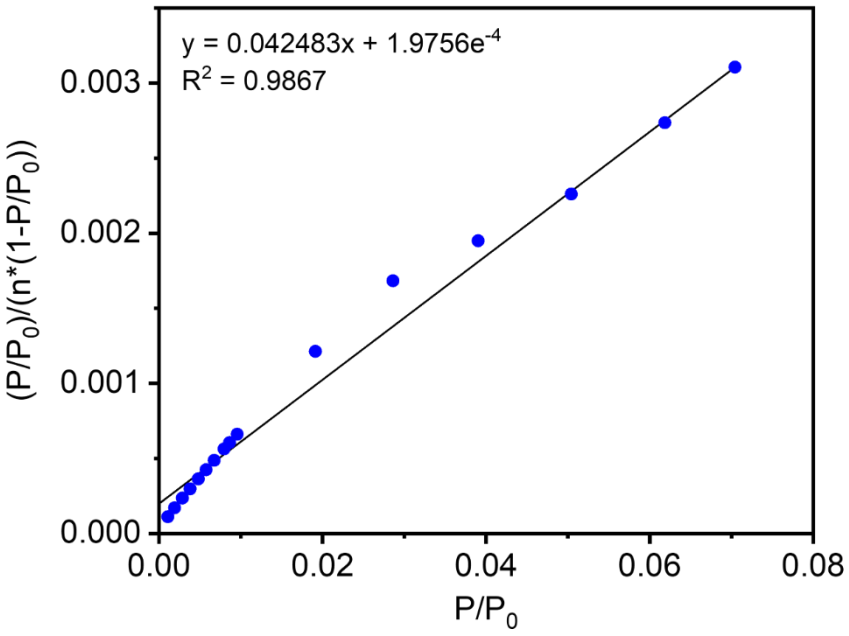

Figure S89. Linearized BET plot for the N_2 adsorption data of Zn_2(dobpdc) synthesized at 0.5 M.

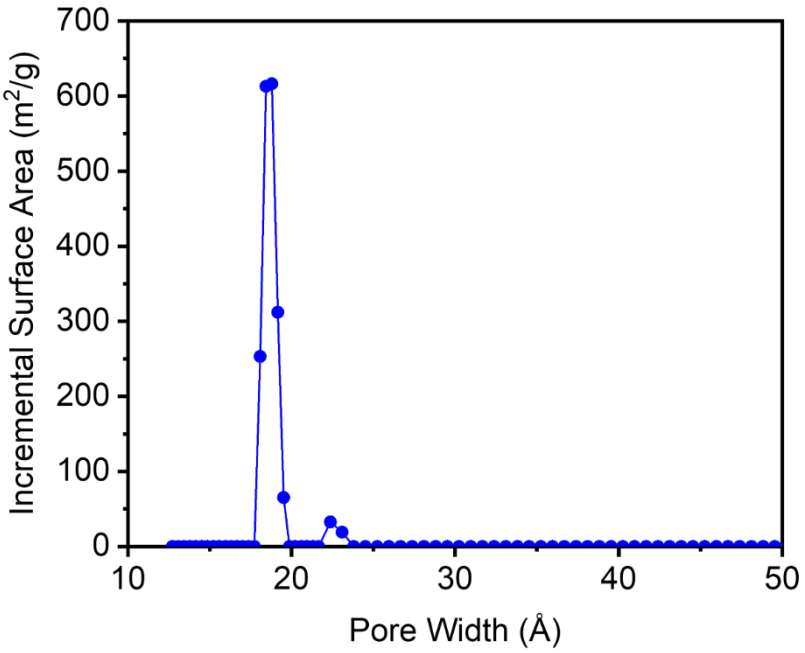

Figure S90. DFT-calculated pore size distribution for Zn_2(dobpdc) synthesized at 0.5 M, assuming a cylindrical pore geometry.

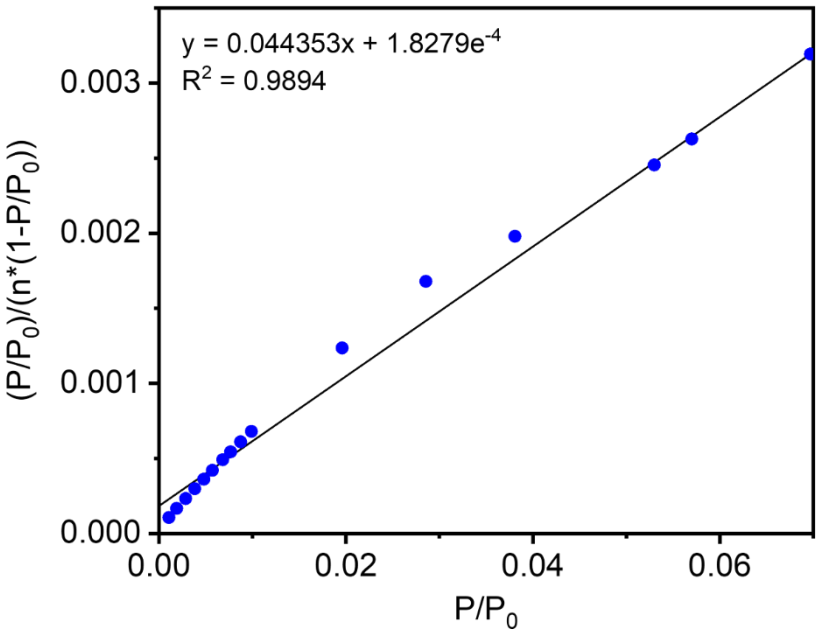

Figure S91. Linearized BET plot for the N_2 adsorption data of Zn_2(dobpdc) synthesized at 0.1 M.

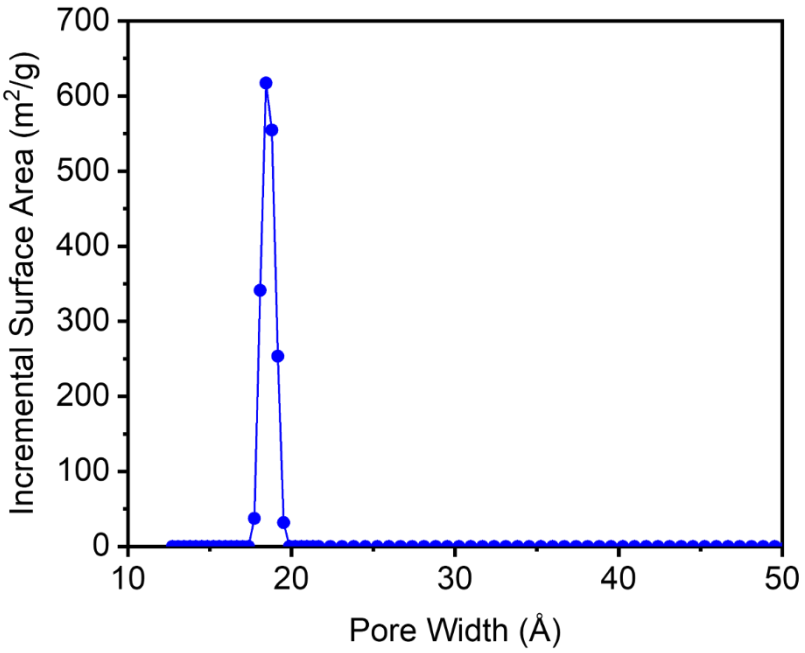

Figure S92. DFT-calculated pore size distribution for Zn_2(dobpdc) synthesized at 0.1 M, assuming a cylindrical pore geometry.

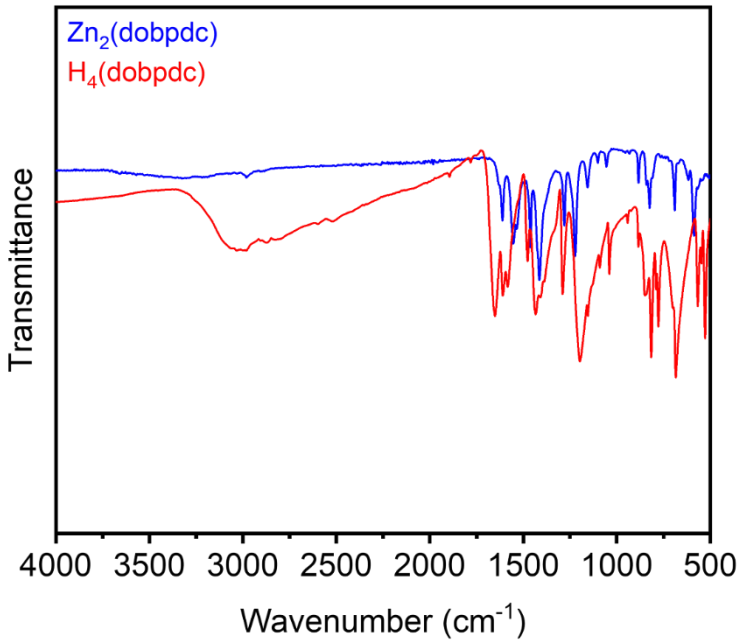

Figure S93. ATR-IR spectra of Zn_2(dobpdc) synthesized at 1.0 M and the H_4dobpdc linker.

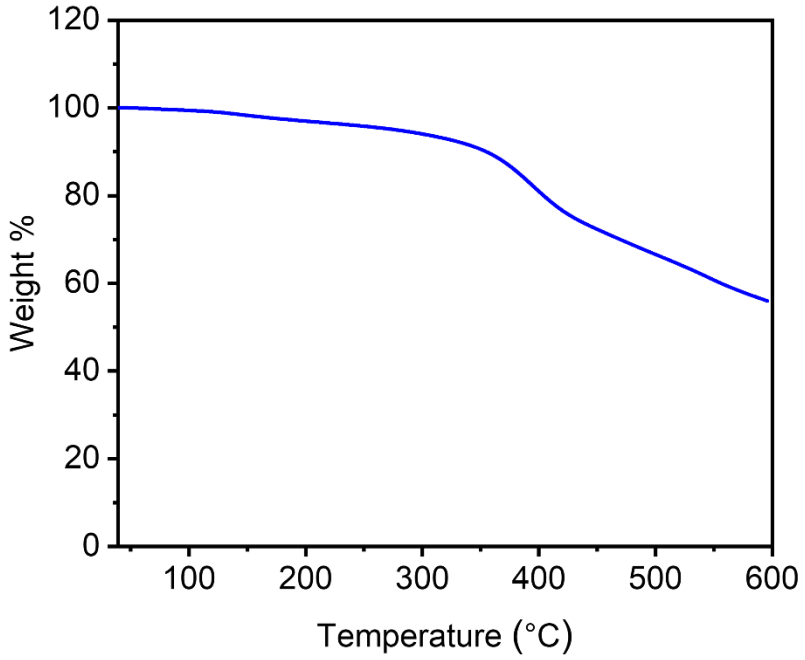

Figure S94. Thermogravimetric decomposition profile under N_2 of Zn_2(dobpdc) synthesized at 1.0 M.

Table S9. Surface area data and yields for Zn_2(dobpdc) at each synthesized concentration. Literature values for surface areas are included.

Concentration (M)	BET Surface Area (m^2/g)	Langmuir Surface Area (m^2/g)	Yield (%)
0.1	2190 ± 60	2743	87.8
0.5	2285 ± 70	2783	59.6
1.0	2574 ± 77	3090	69.0
Literature	1873[7]	2974[7]	-

5. High-concentration aqueous syntheses of M_2(*m*-dobdc) MOFs.

5.1. Mg_2(*m*-dobdc).

Prepared according to a modified literature procedure.[8] In a 20 mL scintillation vial, $Mg(NO_3)_2$•$6H_2O$ (321 mg, 1.25 mmol, 2.50 equiv.) was dissolved in H_2O (2.5 mL, 0.5 mL, or 0.25 mL for 0.1 M, 0.5 M, and 1.0 M, respectively). In a separate 20 mL scintillation vial equipped with a stir bar, NaOH (80.0 mg, 2.00 mmol, 4.00 equiv.), H_4*m*-dobdc (99.0 mg, 0.50 mmol, 1.00 equiv.), and H_2O (2.5 mL, 0.5 mL, or 0.25 mL for 0.1 M, 0.5 M, and 1.0 M, respectively) were combined. The $Mg(NO_3)_2$•H_2O solution was added all at once to the H_4*m*-dobdc solution via a plastic pipette. The mixture was stirred at room temperature for 1 h. The reaction mixture was vacuum-filtered, and the resulting solid was rinsed with MeOH (10–15 mL). The resulting off-white/salmon-colored solid was transferred to a new scintillation vial filled with MeOH (10–15 mL). The vial was transferred to an aluminum block on a hot plate that had been pre-heated to 60 °C and was allowed to stand at this temperature for at least 12 h. At this time, the heterogenous mixture was allowed to cool to room temperature, the solvent was decanted, and fresh MeOH (10–15 mL) was added. This process was repeated for a total of six MeOH soaks. After the final soak, the solvent was decanted, and the remaining solid was allowed to dry in air. The sample was then activated using supercritical CO_2 (See Section 1), yielding activated Mg_2(*m*-dobdc) (26.8%, 43.7%, and 69.2% yield for 0.1 M, 0.5 M, and 1.0 M, respectively) that was immediately transferred to a glass adsorption tube equipped with a Micromeritics *CheckSeal*. The sample was activated on the SmartVac under high vacuum (<10 μbar), ramping the temperature slowly to 180 °C (0.1°C/min). The sample was allowed to stand at 180 °C under high vacuum (<10 μbar) for 12 h prior to gas adsorption analysis.

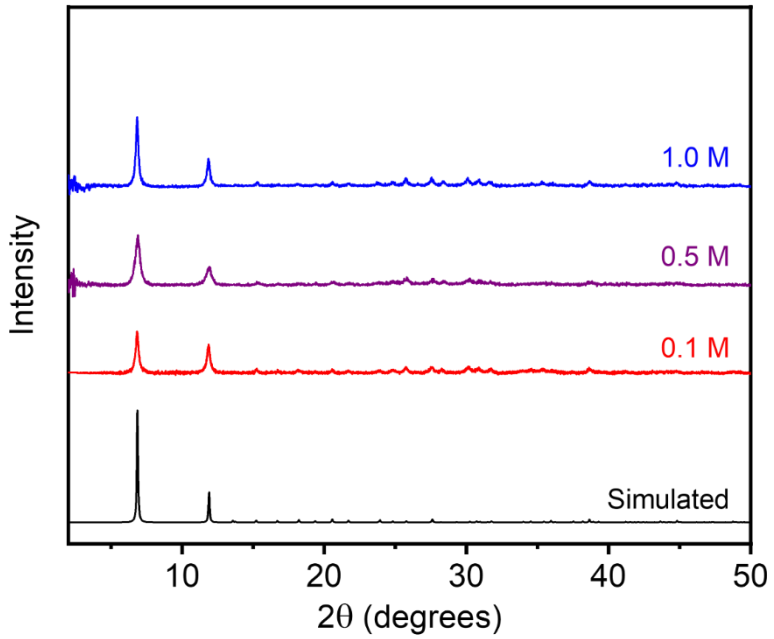

Figure S95. Baseline-corrected PXRD patterns (λ = 1.5406 Å) of MeOH-solvated Mg_2(*m*-dobdc) at different concentrations after aqueous synthesis. The simulated pattern based on the previously reported SCXRD structure of the isostructural framework Co_2(*m*-dobdc) is included for reference.[14]

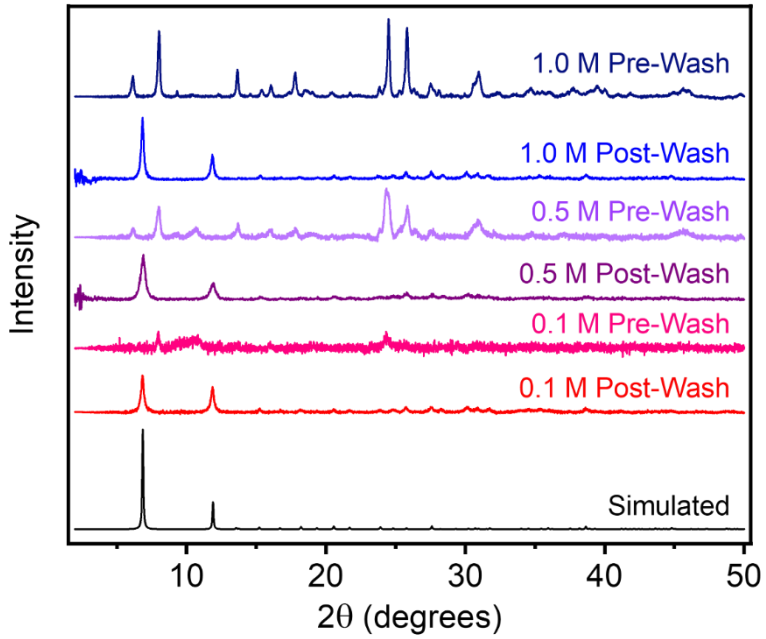

Figure S96. Baseline-corrected PXRD patterns (λ = 1.5406 Å) of Mg_2(*m*-dobdc) synthesized at different concentrations before (pre-wash) and after (post-wash) soaking in MeOH. The simulated pattern based on the previously reported SCXRD structure of the isostructural framework Co_2(*m*-dobdc) is included for reference.[14] A different phase or mixture of phases is obtained initially at all concentrations that transformations into Mg_2(*m*-dobdc) upon soaking in MeOH. Indexing the powder data did not produce definitive unit cell parameters.

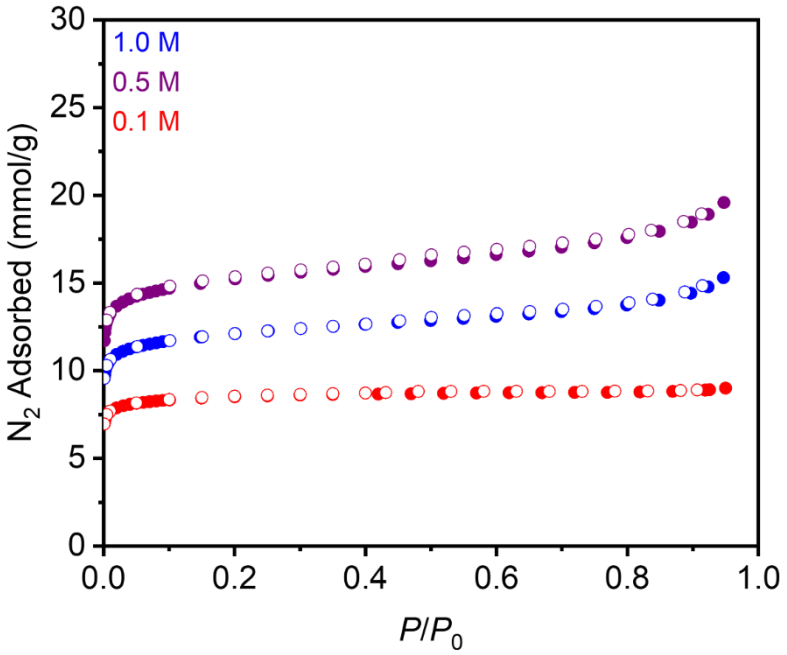

Figure S97. 77 K N_2 adsorption (filled circles) and desorption (open circles) isotherms of activated Mg_2(*m*-dobdc) at different concentrations after aqueous synthesis. BET surface areas determined from these data are 762 ± 1 m^2/g (0.1 M), 1330 ± 2 m^2/g (0.5 M), and 1060 ± 1 m^2/g (1.0 M). The Langmuir surface areas determined from these data are 865 m^2/g (0.1 M), 1767 m^2/g (0.5 M), and 1383 m^2/g (1.0 M).

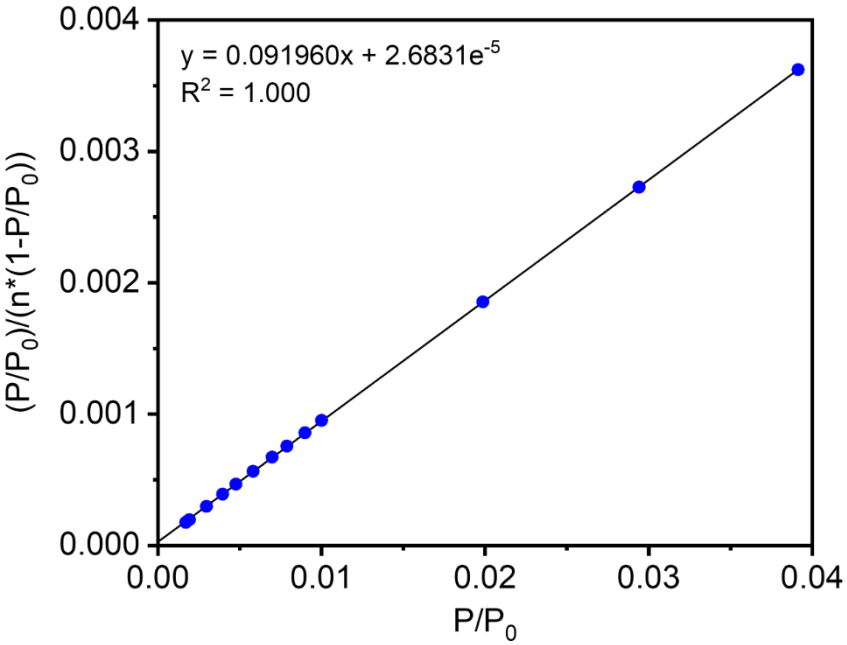

Figure S98. Linearized BET plot for the N_2 adsorption data of Mg_2(*m*-dobdc) synthesized at 1.0 M.

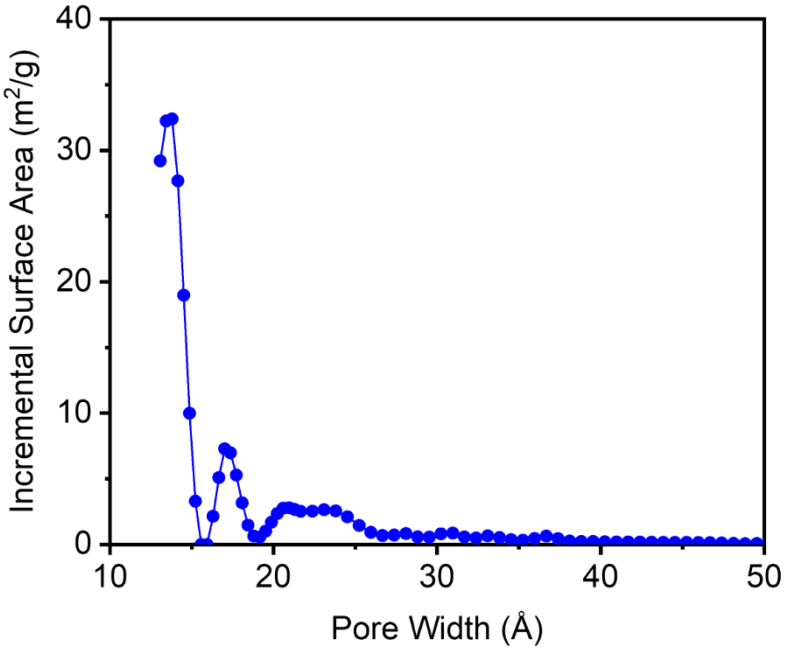

Figure S99. DFT-calculated pore size distribution for Mg_2(*m*-dobdc) synthesized at 1.0 M, assuming a cylindrical pore geometry.

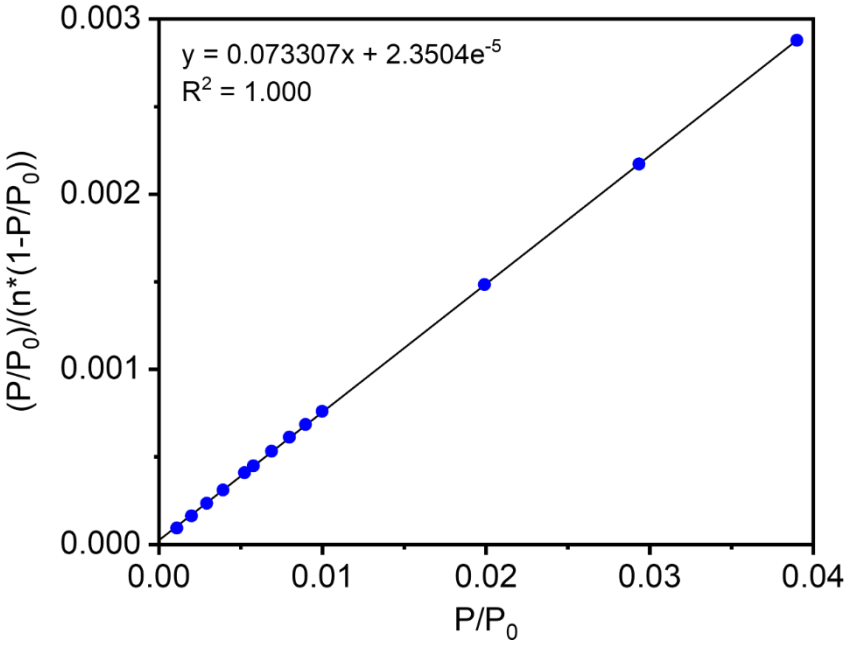

Figure S100. Linearized BET plot for the N_2 adsorption data of Mg_2(*m*-dobdc) synthesized at 0.5 M.

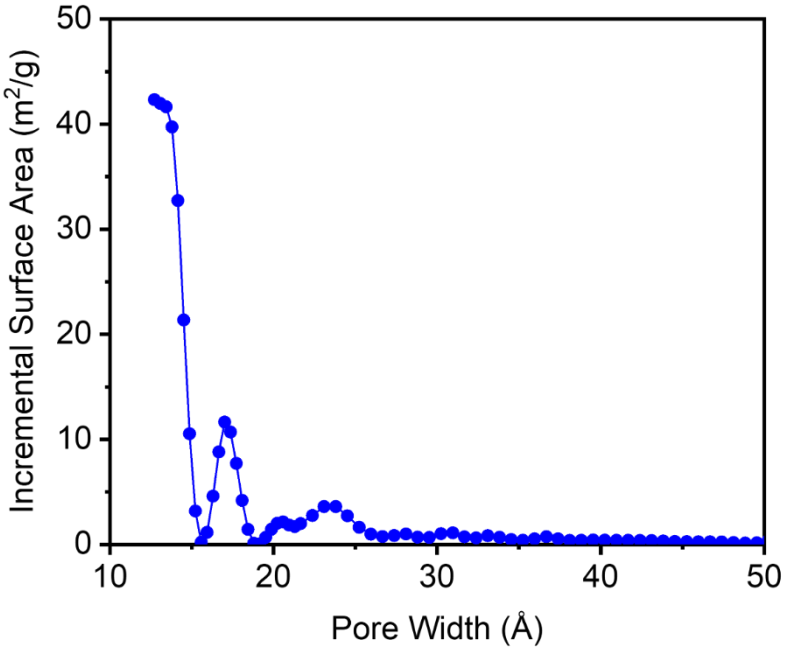

Figure S101. DFT-calculated pore size distribution for Mg_2(*m*-dobdc) synthesized at 0.5 M, assuming a cylindrical pore geometry. The primary pore size is below the lower limit of the measurement.

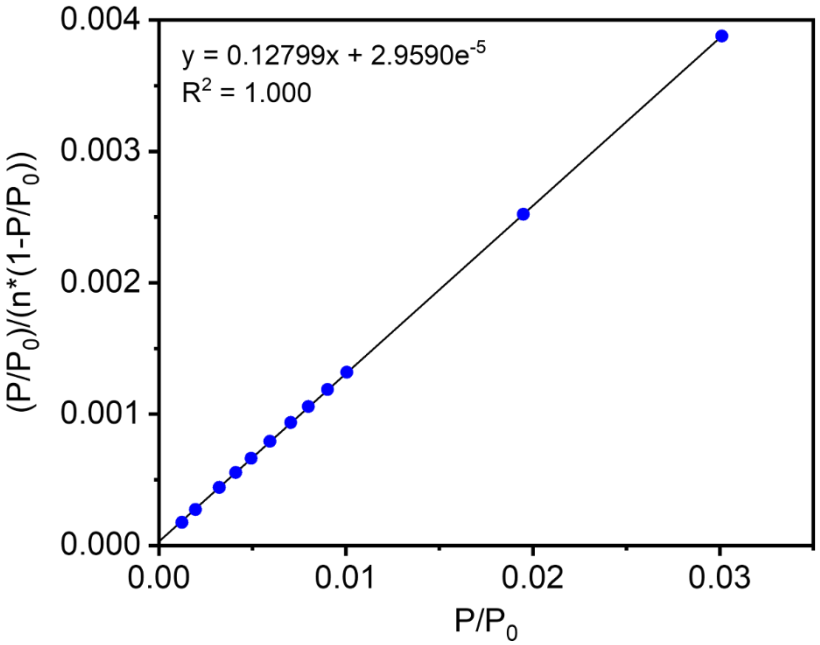

Figure S102. Linearized BET plot for the N_2 adsorption data of Mg_2(*m*-dobdc) synthesized at 0.1 M.

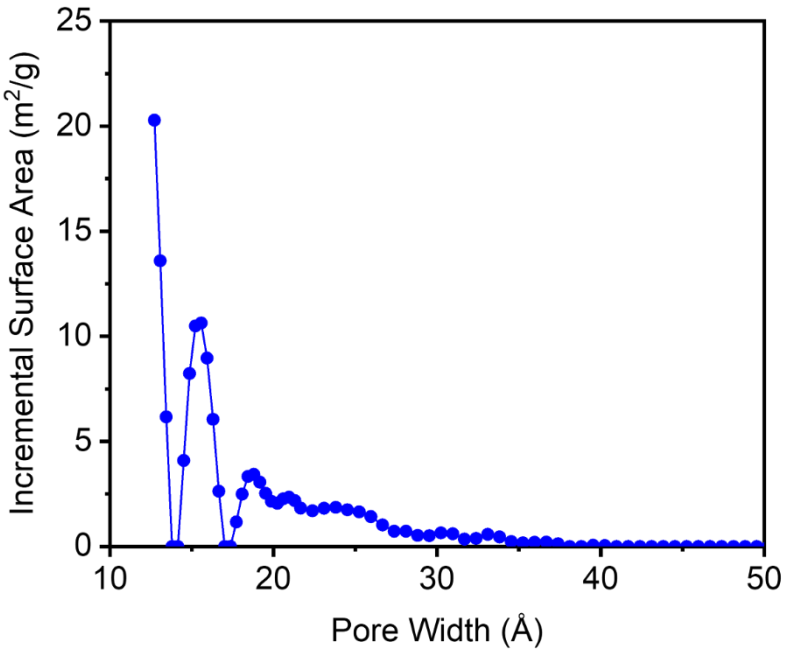

Figure S103. DFT-calculated pore size distribution for Mg_2(*m*-dobdc) synthesized at 0.1 M, assuming a cylindrical pore geometry. The primary pore size is below the lower limit of the measurement.

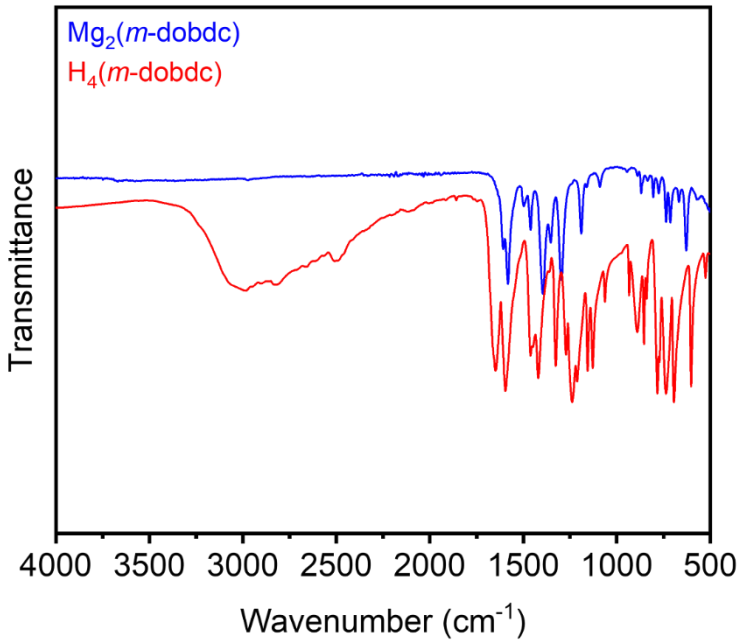

Figure S104. ATR-IR spectra of Mg_2(*m*-dobdc) synthesized at 0.5 M and the H_4(*m*-dobdc) linker.

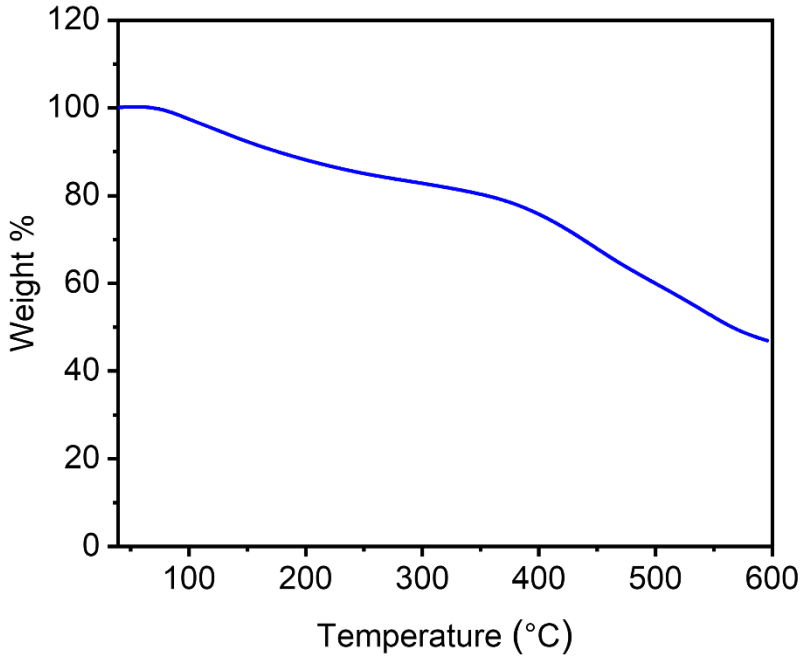

Figure S105. Thermogravimetric decomposition profile under N_2 of Mg_2(*m*-dobdc) synthesized at 0.5 M.

Table S10. Surface area data and yields for Mg_2(*m*-dobdc) at each synthesized concentration. Literature values for surface areas are included.

Concentration (M)	BET Surface Area (m^2/g)	Langmuir Surface Area (m^2/g)	Yield (%)
0.1	762 ± 1	865	26.8
0.5	1330 ± 2	1767	43.7
1.0	1060 ± 1	1383	69.2
Literature	1556[15]	1971[15]	-

5.2. Co_2(*m*-dobdc).

Prepared according to a modified literature procedure.[8] In a 20 mL scintillation vial, $Co(NO_3)_2$•$6H_2O$ (364 mg, 1.25 mmol, 2.50 equiv.) was dissolved in H_2O (2.5 mL, 0.5 mL, or 0.25 mL for 0.1 M, 0.5 M, and 1.0 M, respectively). In a separate 20 mL scintillation vial equipped with a stir bar, NaOH (80.0 mg, 2.00 mmol, 4.00 equiv.), H_4*m*-dobdc (99.0 mg, 0.50 mmol, 1.00 equiv.), and H_2O (2.5 mL, 0.5 mL, or 0.25 mL for 0.1 M, 0.5 M, and 1.0 M, respectively) were combined. The $Co(NO_3)_2$•H_2O solution was added all at once to the H_4*m*-dobdc solution via a plastic pipette. The mixture was stirred at room temperature for 1 h. The reaction mixture was vacuum-filtered, and the resulting solid was rinsed with MeOH (10–15 mL). The resulting pink solid was transferred to a new scintillation vial filled with MeOH (10–15 mL). The vial was transferred to an aluminum block on a hot plate that had been pre-heated to 60 °C and was allowed to stand at this temperature for at least 12 h. At this time, the heterogenous mixture was allowed to cool to room temperature, the solvent was decanted, and fresh MeOH (10–15 mL) was added. This process was repeated for a total of six MeOH soaks. After the final soak, the solvent was decanted, and the remaining solid was allowed to dry in air. The sample was then activated using supercritical CO_2 (See Section 1), yielding activated Co_2(*m*-dobdc) (56.8%, 57.3%, and 38.5% yield for 0.1 M, 0.5 M, and 1.0 M, respectively) that was immediately transferred to a glass adsorption tube equipped with a Micromeritics *CheckSeal*. The sample was activated on the SmartVac under high vacuum (<10 μbar), ramping the temperature slowly to 180 °C (0.1°C/min). The sample was allowed to stand at 180 °C under high vacuum (<10 μbar) for 12 h prior to gas adsorption analysis.

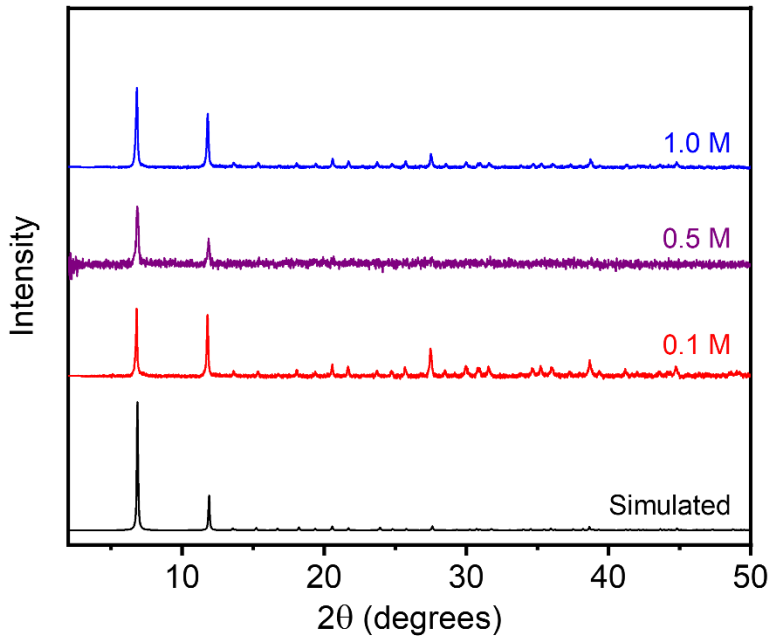

Figure S106. Baseline-corrected PXRD patterns (λ = 1.5406 Å) of MeOH-solvated Co_2(*m*-dobdc) at different concentrations after aqueous synthesis. The simulated pattern based on the previously reported SCXRD structure of Co_2(*m*-dobdc) is included for reference.[14]

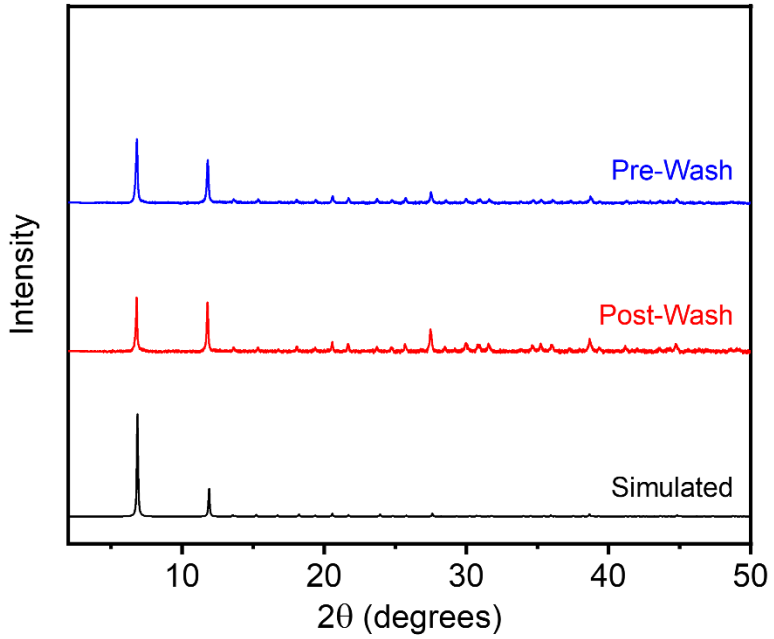

Figure S107. Baseline-corrected PXRD patterns (λ = 1.5406 Å) of Co_2(*m*-dobdc) synthesized at 0.1 M before (pre-wash) and after (post-wash) soaking in MeOH. The simulated pattern based on the previously reported SCXRD structure of Co_2(*m*-dobdc) is included for reference.[14] No significant change in the pattern was observed upon soaking the MOF in MeOH.

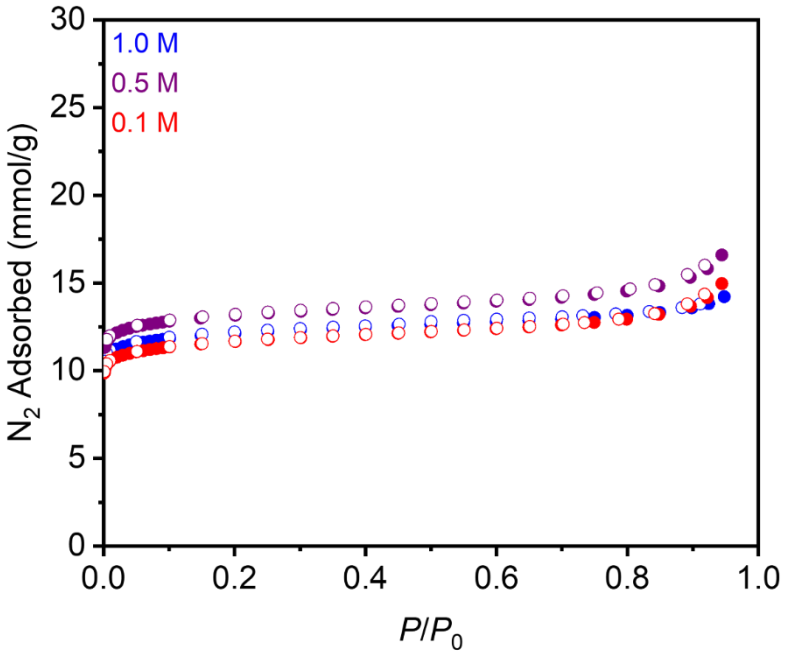

Figure S108. 77 K N_2 adsorption (filled circles) and desorption (open circles) isotherms of activated Co_2(*m*-dobdc) at different concentrations after aqueous synthesis. BET surface areas determined from these data are 1034 ± 1 m^2/g (0.1 M), 1169 ± 1 m^2/g (0.5 M), and 1081 ± 1 m^2/g (1.0 M). The Langmuir surface areas determined from these data are 1314 m^2/g (0.1 M), 1472 m^2/g (0.5 M), and 1313 m^2/g (1.0 M).

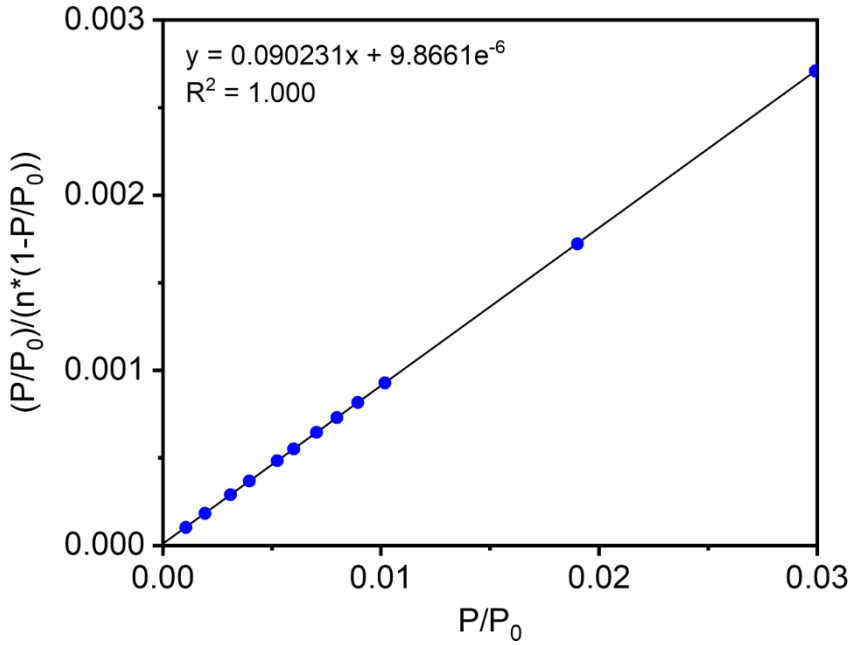

Figure S109. Linearized BET plot for the N_2 adsorption data of Co_2(*m*-dobdc) synthesized at 1.0 M.

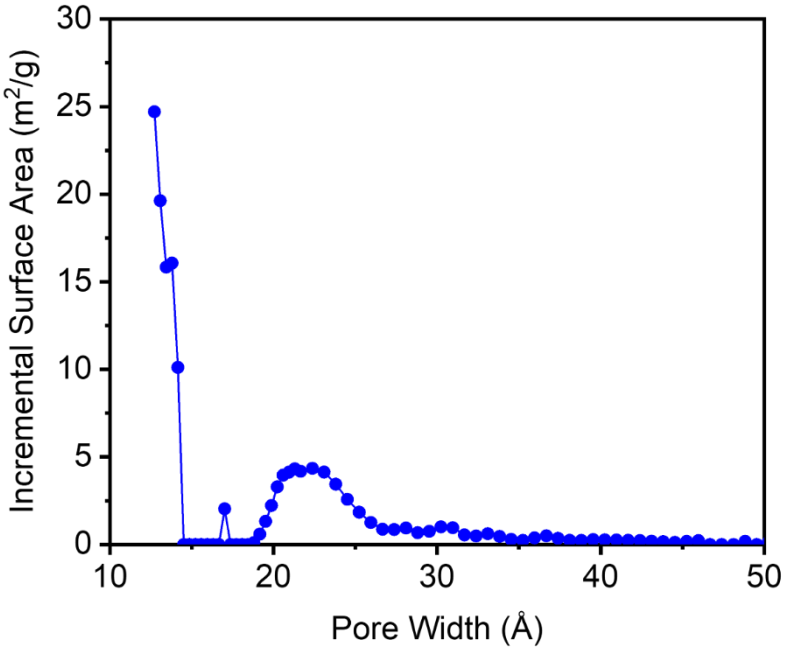

Figure S110. DFT-calculated pore size distribution for Co_2(*m*-dobdc) synthesized at 1.0 M, assuming a cylindrical pore geometry. The primary pore size is below the lower limit of the measurement.

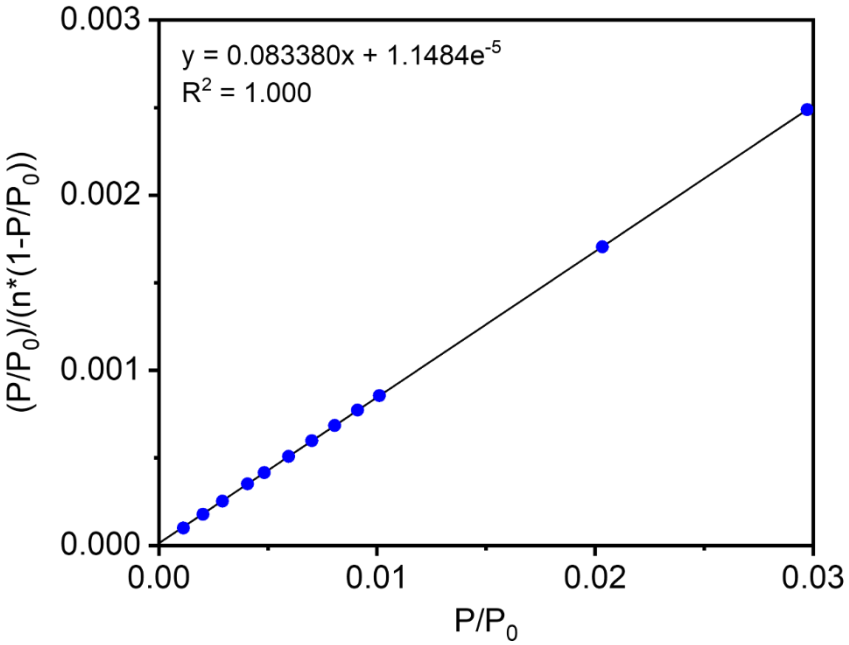

Figure S111. Linearized BET plot for the N_2 adsorption data of Co_2(*m*-dobdc) synthesized at 0.5 M.

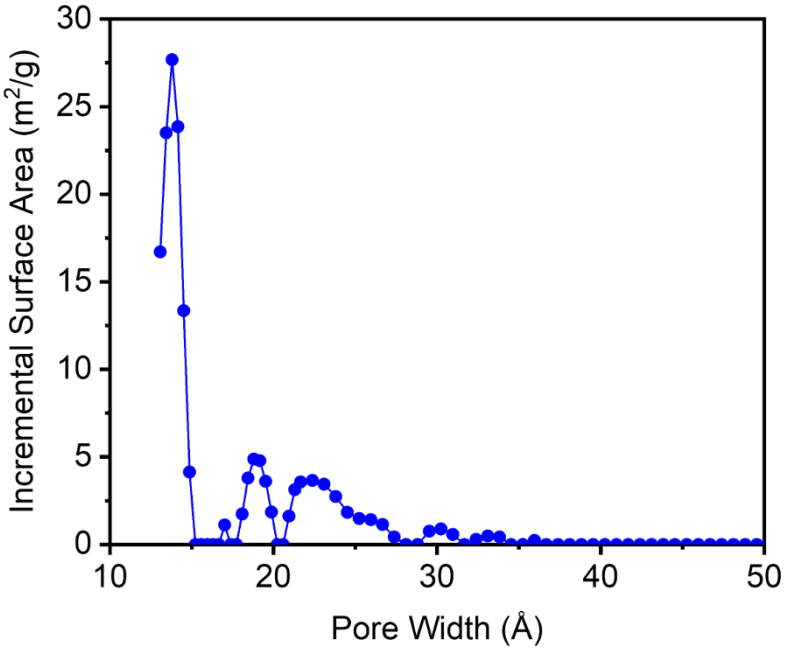

Figure S112. DFT-calculated pore size distribution for Co_2(*m*-dobdc) synthesized at 0.5 M, assuming a cylindrical pore geometry.

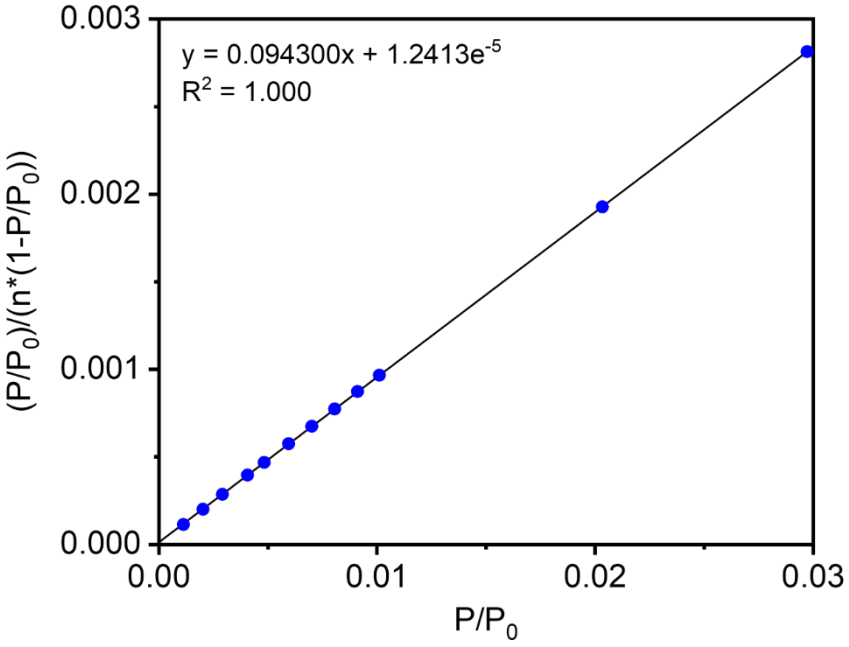

Figure S113. Linearized BET plot for the N_2 adsorption data of Co_2(*m*-dobdc) synthesized at 0.1 M.

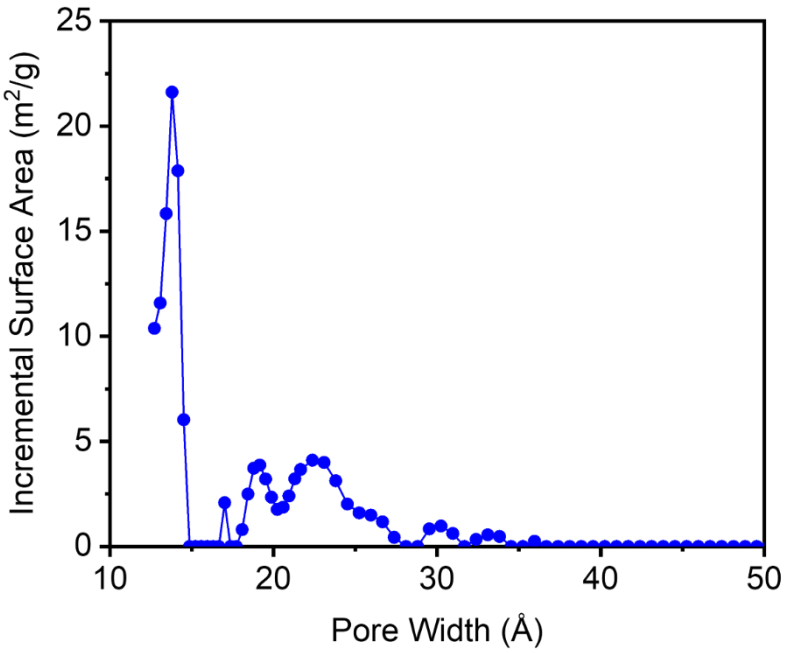

Figure S114. DFT-calculated pore size distribution for Mg_2(*m*-dobdc) synthesized at 0.1 M, assuming a cylindrical pore geometry.

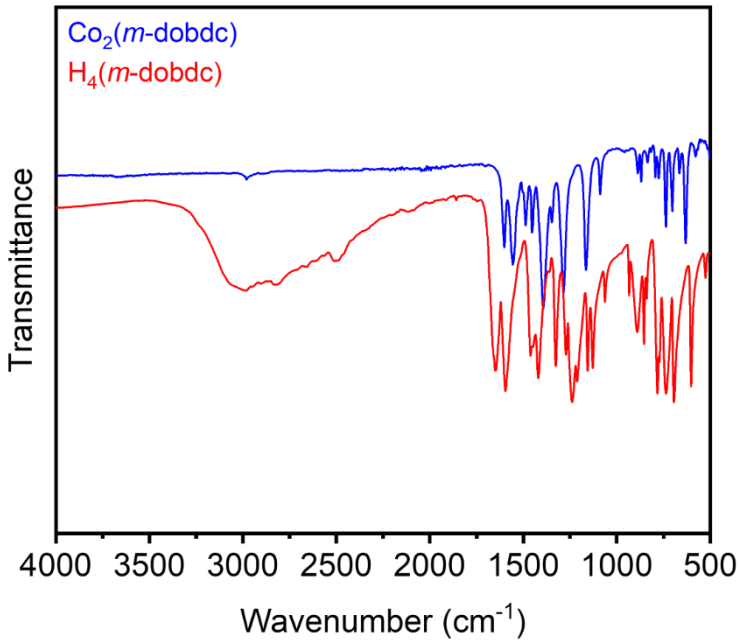

Figure S115. ATR-IR spectra of Co_2(*m*-dobdc) synthesized at 0.5 M and the H_4(*m*-dobdc) linker.

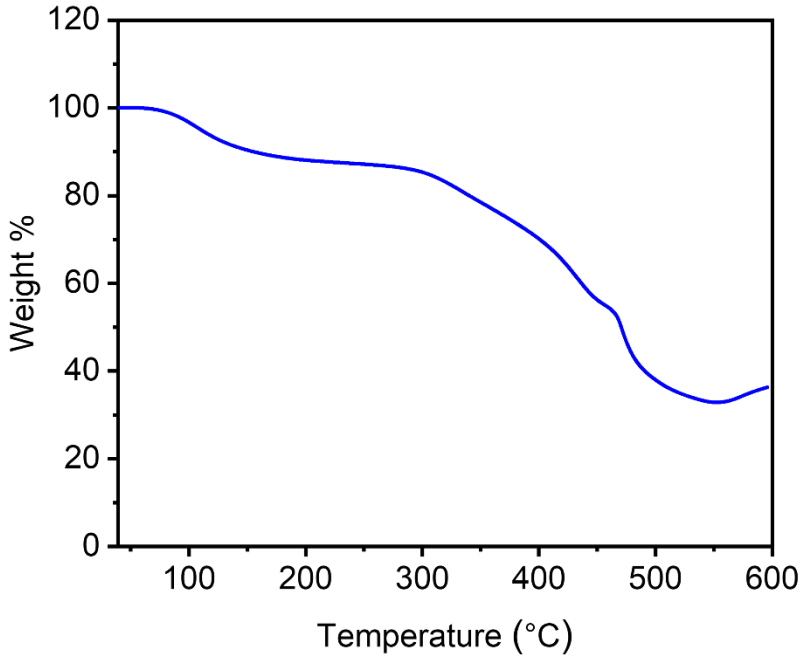

Figure S116. Thermogravimetric decomposition profile under N_2 of Co_2(*m*-dobdc) synthesized at 0.5 M.

Table S11. Surface area data and yields for Co_2(*m*-dobdc) at each synthesized concentration. Literature values for surface areas are included.

Concentration (M)	BET Surface Area (m^2/g)	Langmuir Surface Area (m^2/g)	Yield (%)
0.1	1034 ± 1	1314	56.8
0.5	1169 ± 1	1472	57.3
1.0	1081 ± 1	1313	38.5
Literature	1264[16]	1504[16]	-

5.3. Ni_2(*m*-dobdc).

Prepared according to a modified literature procedure.[8] In a 20 mL scintillation vial, $Ni(NO_3)_2$•$6H_2O$ (364 mg, 1.25 mmol, 2.50 equiv.) was dissolved in H_2O (2.5 mL, 0.5 mL, or 0.25 mL for 0.1 M, 0.5 M, and 1.0 M, respectively). In a separate 20 mL scintillation vial equipped with a stir bar, NaOH (80.0 mg, 2.00 mmol, 4.00 equiv.), H_4*m*-dobdc (99.0 mg, 0.50 mmol, 1.00 equiv.), and H_2O (2.5 mL, 0.5 mL, or 0.25 mL for 0.1 M, 0.5 M, and 1.0 M, respectively) were combined. The $Ni(NO_3)_2$•H_2O solution was added all at once to the H_4*m*-dobdc solution via a plastic pipette. The mixture was stirred at room temperature for 1 h. The reaction mixture was vacuum-filtered, and the resulting solid was rinsed with MeOH (10–15 mL). The resulting green solid was transferred to a new scintillation vial filled with MeOH (10–15 mL). The vial was transferred to an aluminum block on a hot plate that had been pre-heated to 60 °C and was allowed to stand at this temperature for at least 12 h. At this time, the heterogenous mixture was allowed to cool to room temperature, the solvent was decanted, and fresh MeOH (10–15 mL) was added. This process was repeated for a total of six MeOH soaks. After the final soak, the solvent was decanted, and the remaining solid was allowed to dry in air. The sample was then activated using supercritical CO_2 (See Section 1), yielding activated Ni_2(*m*-dobdc) (83.3%, 47.7%, and 55.2% yield for 0.1 M, 0.5 M, and 1.0 M, respectively) that was immediately transferred to a glass adsorption tube equipped with a Micromeritics *CheckSeal*. The sample was activated on the SmartVac under high vacuum (<10 μbar), ramping the temperature slowly to 180 °C (0.1°C/min). The sample was allowed to stand at 180 °C under high vacuum (<10 μbar) for 12 h prior to gas adsorption analysis.

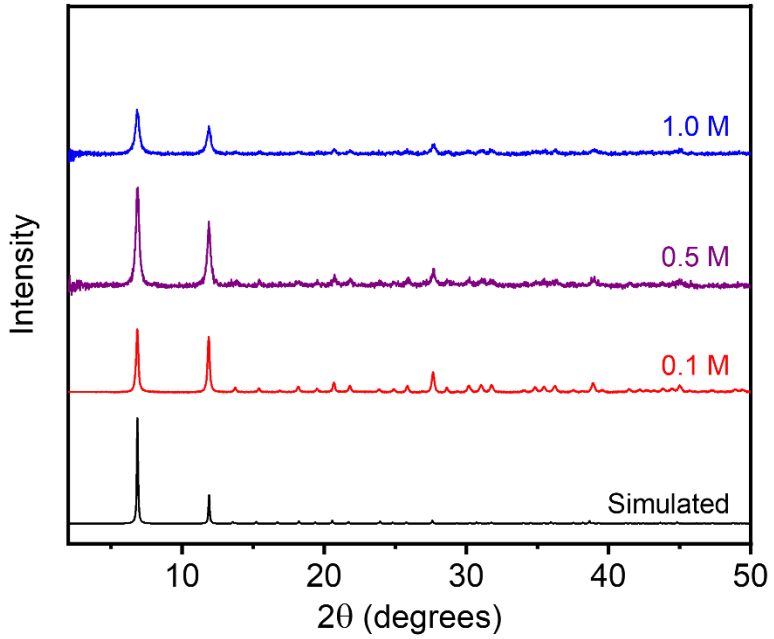

Figure S117. Baseline-corrected PXRD patterns (λ = 1.5406 Å) of MeOH-solvated Ni_2(*m*-dobdc) at different concentrations after aqueous synthesis. The simulated pattern based on the previously reported SCXRD structure of the isostructural framework Co_2(*m*-dobdc) is included for reference.[14]

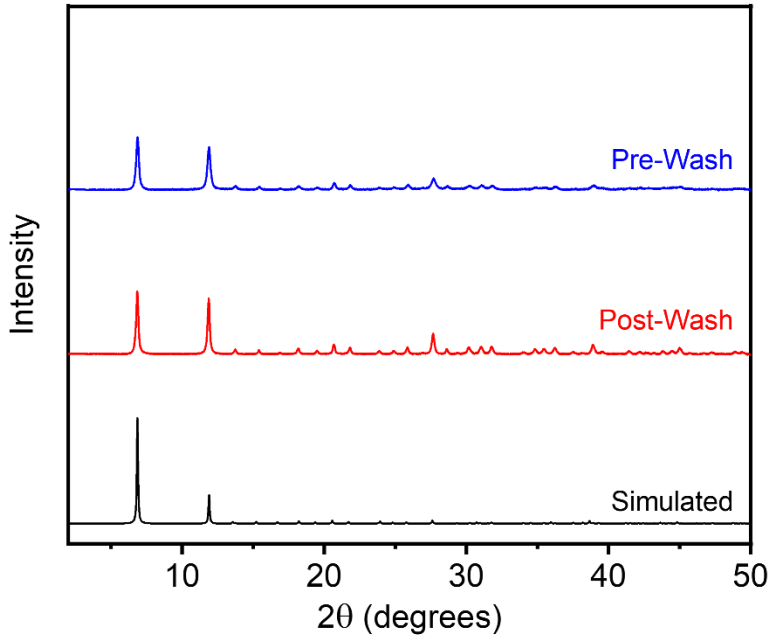

Figure S118. Baseline-corrected PXRD patterns (λ = 1.5406 Å) of MeOH-solvated Ni_2(*m*-dobdc) synthesized at 0.1 M before (pre-wash) and after (post-wash) soaking in MeOH. The simulated pattern based on the previously reported SCXRD structure of the isostructural framework Co_2(*m*-dobdc) is included for reference.[14] No significant change in the pattern was observed upon soaking the MOF in MeOH.

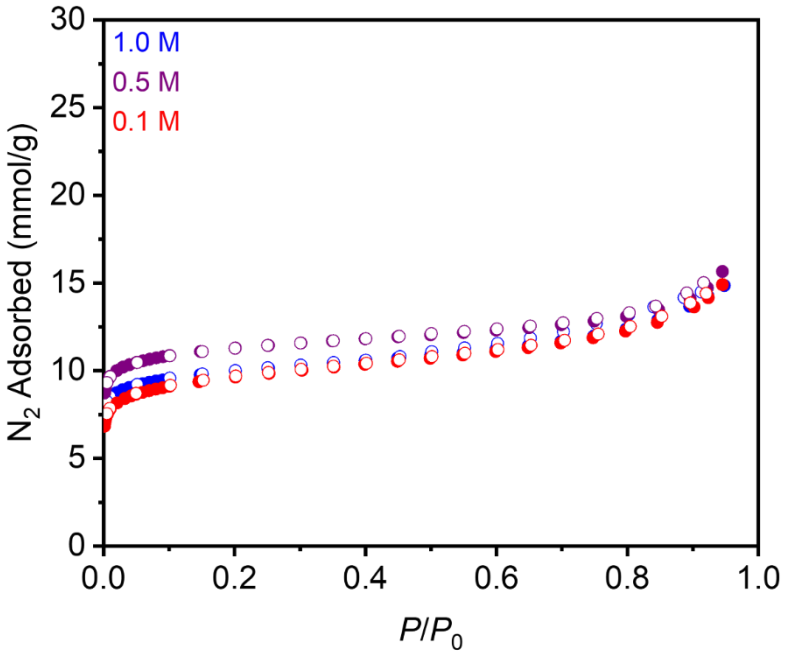

Figure S119. 77 K N_2 adsorption (filled circles) and desorption (open circles) isotherms of activated Ni_2(*m*-dobdc) at different concentrations after aqueous synthesis. BET surface areas determined from these data are 810 ± 1 m^2/g (0.1 M), 977 ± 1 m^2/g (0.5 M), and 854 ± 1 m^2/g (1.0 M). The Langmuir surface areas determined from these data are 1265 m^2/g (0.1 M), 1342 m^2/g (0.5 M), and 1268 m^2/g (1.0 M).

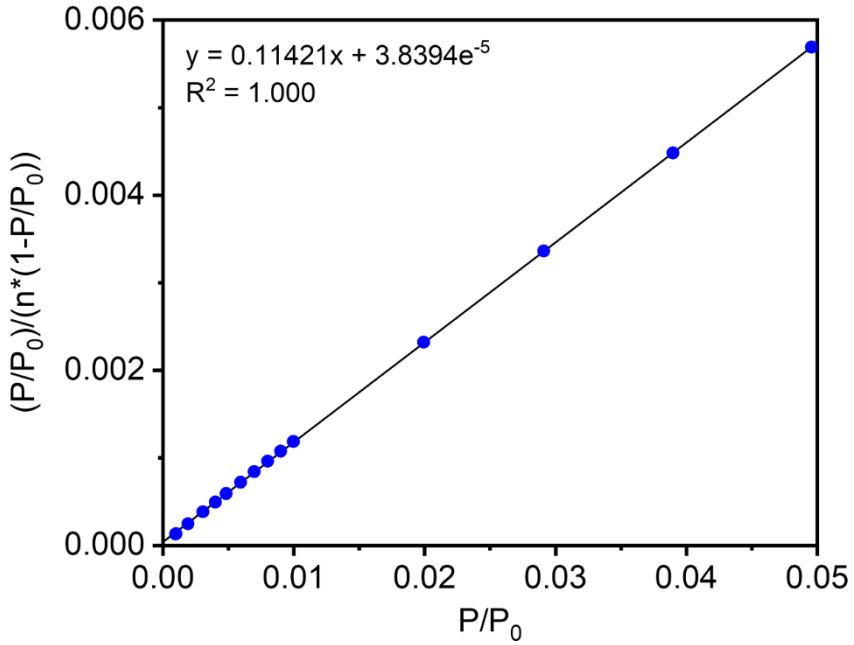

Figure S120. Linearized BET plot for the N_2 adsorption data of Ni_2(*m*-dobdc) synthesized at 1.0 M.

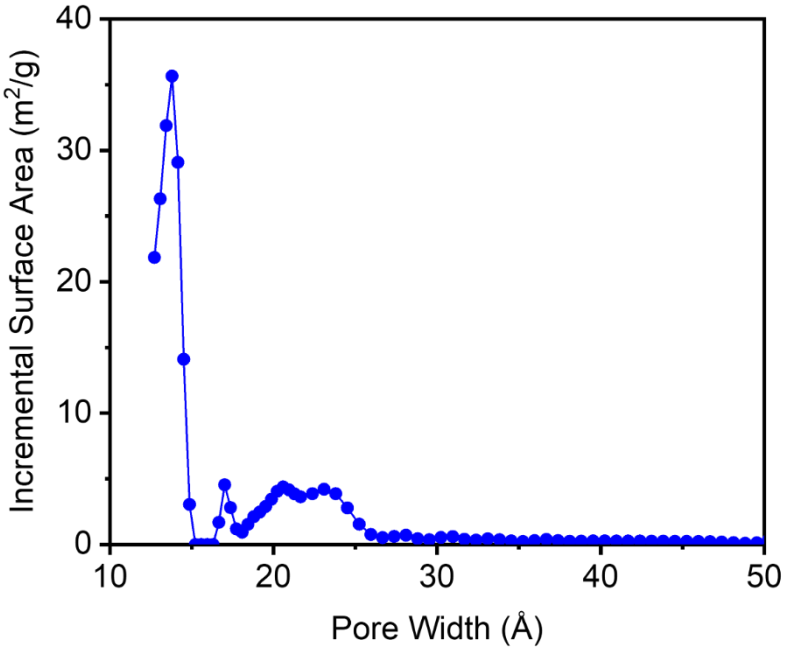

Figure S121. DFT-calculated pore size distribution for Ni_2(*m*-dobdc) synthesized at 1.0 M, assuming a cylindrical pore geometry.

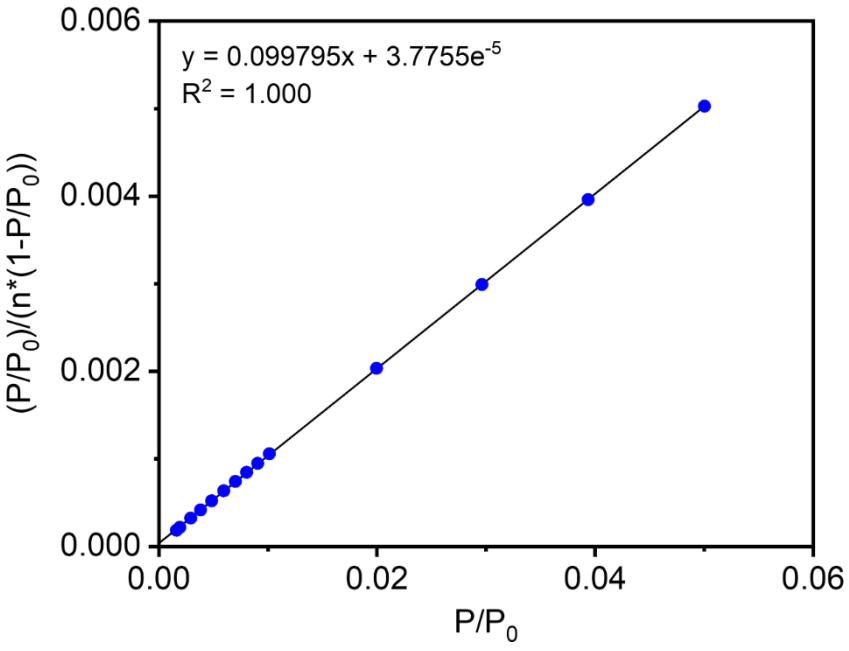

Figure S122. Linearized BET plot for the N_2 adsorption data of Ni_2(*m*-dobdc) synthesized at 0.5 M.

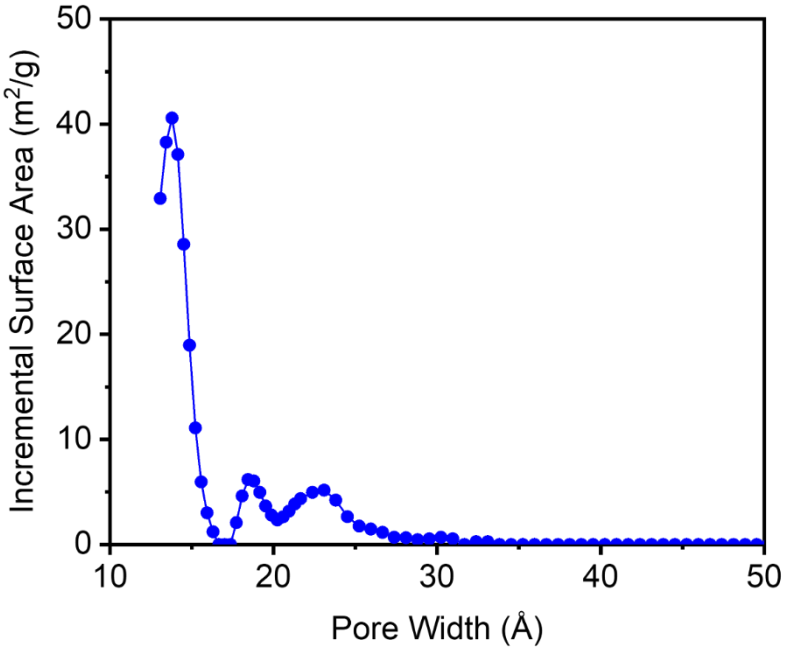

Figure S123. DFT-calculated pore size distribution for Ni_2(*m*-dobdc) synthesized at 0.5 M, assuming a cylindrical pore geometry.

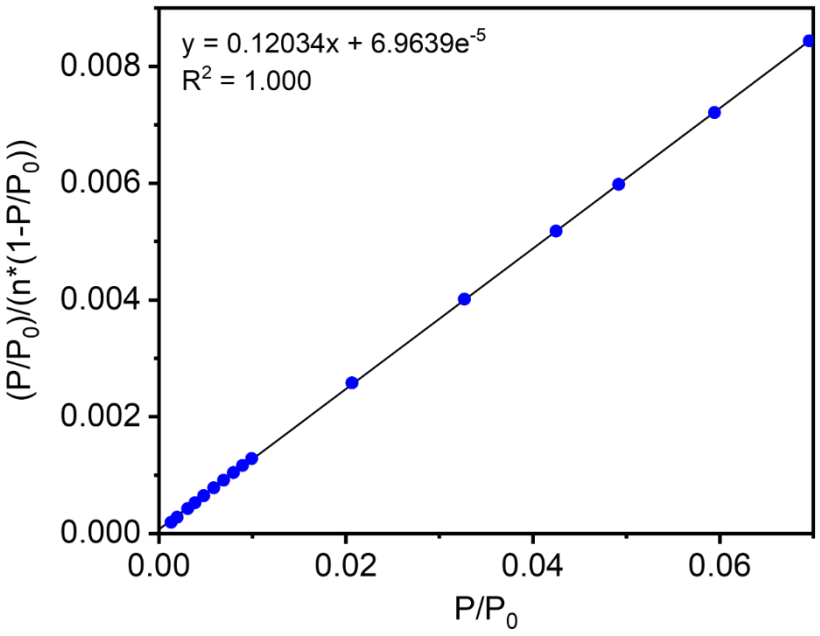

Figure S124. Linearized BET plot for the N_2 adsorption data of Ni_2(*m*-dobdc) synthesized at 0.1 M.

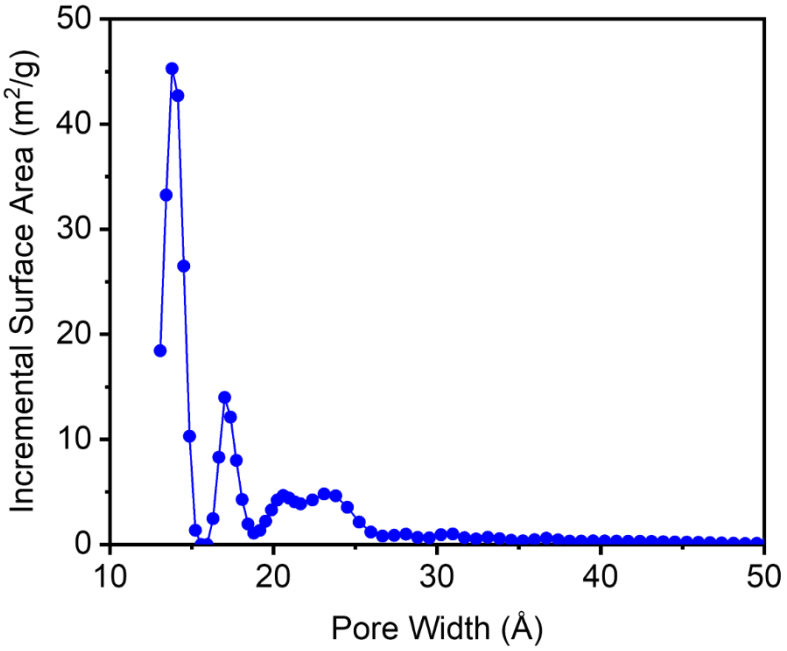

Figure S125. DFT-calculated pore size distribution for Ni_2(*m*-dobdc) synthesized at 0.1 M, assuming a cylindrical pore geometry.

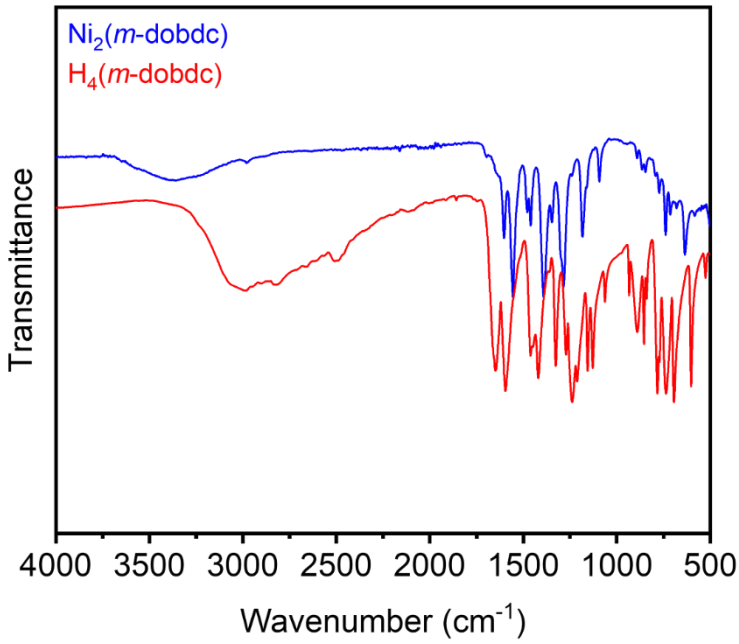

Figure S126. ATR-IR spectra of Ni_2(*m*-dobdc) synthesized at 0.5 M and the H_4(*m*-dobdc) linker.

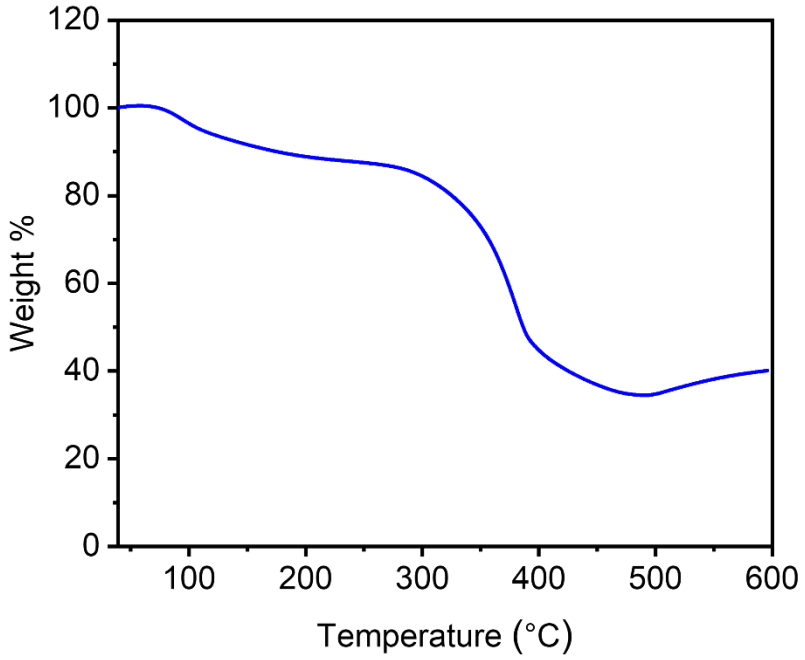

Figure S127. Thermogravimetric decomposition profile under N_2 of Ni_2(*m*-dobdc) synthesized at 0.5 M.

Table S12. Surface area data and yields for Ni_2(*m*-dobdc) at each synthesized concentration. Literature values for surface areas are included.

Concentration (M)	BET Surface Area (m^2/g)	Langmuir Surface Area (m^2/g)	Yield (%)
0.1	810 ± 1	1265	83.3
0.5	977 ± 1	1342	47.7
1.0	854 ± 1	1268	55.2
Literature	1321[16]	1592[16]	-

5.4. Zn_2(*m*-dobdc).

Prepared according to a modified literature procedure.[8] In a 20 mL scintillation vial, $Zn(NO_3)_2$•$6H_2O$ (372 mg, 1.25 mmol, 2.50 equiv.) was dissolved in H_2O (2.5 mL). In a separate 20 mL scintillation vial equipped with a stir bar, NaOH (80.0 mg, 2.00 mmol, 4.00 equiv.), H_4*m*-dobdc (99.0 mg, 0.50 mmol, 1.00 equiv.), and H_2O (2.5 mL) were combined. The $Zn(NO_3)_2$•H_2O solution was added all at once to the H_4*m*-dobdc solution via a plastic pipette. The mixture was stirred at room temperature for 1 h. The reaction mixture was vacuum-filtered, and the resulting solid was rinsed with MeOH (10–15 mL). The resulting beige solid was transferred to a new scintillation vial filled with MeOH (10–15 mL). The vial was transferred to an aluminum block on a hot plate that had been pre-heated to 60 °C and was allowed to stand at this temperature for at least 12 h. At this time, the heterogenous mixture was allowed to cool to room temperature, the solvent was decanted, and fresh MeOH (10–15 mL) was added. This process was repeated for a total of six MeOH soaks. After the final soak, the solvent was decanted, and the remaining solid was allowed to dry in air. The sample was then activated using supercritical CO_2 (See Section 1), yielding activated Zn_2(*m*-dobdc) (79.6% yield) that was immediately transferred to a glass adsorption tube equipped with a Micromeritics *CheckSeal*. The sample was activated on the SmartVac under high vacuum (<10 μbar), ramping the temperature slowly to 180 °C (0.1°C/min). The sample was allowed to stand at 180 °C under high vacuum (<10 μbar) for 12 h prior to gas adsorption analysis.

Attempted solvothermal syntheses.

Condition A: Attempted following a modified literature procedure for the synthesis of M_2(*m*-dobdc) materials.[16] In a 20 mL scintillation vial equipped with a stir bar, $Zn(NO_3)_2$•$6H_2O$ (134 mg, 0.45 mmol, 2.50 equiv.), H_4*m*-dobdc (35.6 mg, 0.18 mmol, 1.00 equiv.), DMF (0.78 mL), and MeOH (0.42 mL) (0.15 M 13:7 DMF:MeOH reaction mixture). The vial was sealed and transferred to an aluminum block that was heated to 120 °C. The reaction mixture was allowed to stir gently for 24 h at this temperature. The mixture was then allowed to cool to room temperature, filtered via vacuum filtration, and washed with DMF (10 mL). The collected solid was transferred to a new 20 mL scintillation vial filled with DMF (10–15 mL). The vial was transferred to an aluminum block on a hot plate that had been pre-heated to 120 °C and was allowed to stand at this temperature for at least 12 h. At this time, the heterogenous mixture was allowed to cool to room temperature, the solvent was decanted, and fresh DMF (10–15 mL) was added. This process was repeated for a total of three DMF soaks. After the final soak, the mixture was filtered via vacuum filtration and washed with MeOH (10 mL). The resulting solid was transferred to a new scintillation vial filled with MeOH (10–15 mL). The vial was transferred to an aluminum block on a hot plate that had been pre-heated to 60 °C and was allowed to stand at this temperature for at least 12 h. At this time, the heterogenous mixture was allowed to cool to room temperature, the solvent was decanted, and fresh MeOH (10–15 mL) was added. This process was repeated for a total of three MeOH

soaks. After the final soak, the solvent was decanted, and the remaining solid was allowed to dry in air. A PXRD measurement of the washed product was performed.

Condition B: Attempted following a modified literature procedure for the synthesis of M_2(*m*-dobdc) materials.[16] In a 20 mL scintillation vial equipped with a stir bar, $ZnCl_2$ (61.3 mg, 0.45 mmol, 2.50 equiv.), H_4*m*-dobdc (35.6 mg, 0.18 mmol, 1.00 equiv.), DMF (7.8 mL), and MeOH (4.2 mL) (0.015 M 13:7 DMF:MeOH reaction mixture). The vial was sealed and transferred to an aluminum block that was heated to 120 °C. The reaction mixture was allowed to stir gently for 24 h at this temperature. The mixture was then allowed to cool to room temperature, filtered via vacuum filtration, and washed with DMF (10 mL). The collected solid was transferred to a new 20 mL scintillation vial filled with DMF (10–15 mL). The vial was transferred to an aluminum block on a hot plate that had been pre-heated to 120 °C and was allowed to stand at this temperature for at least 12 h. At this time, the heterogenous mixture was allowed to cool to room temperature, the solvent was decanted, and fresh DMF (10–15 mL) was added. This process was repeated for a total of three DMF soaks. After the final soak, the mixture was filtered via vacuum filtration and washed with MeOH (10 mL). The resulting solid was transferred to a new scintillation vial filled with MeOH (10–15 mL). The vial was transferred to an aluminum block on a hot plate that had been pre-heated to 60 °C and was allowed to stand at this temperature for at least 12 h. At this time, the heterogenous mixture was allowed to cool to room temperature, the solvent was decanted, and fresh MeOH (10–15 mL) was added. This process was repeated for a total of three MeOH soaks. After the final soak, the solvent was decanted, and the remaining solid was allowed to dry in air. A PXRD measurement of the washed product was performed.

Condition C: Attempted following a modified literature procedure for the synthesis of M_2(*m*-dobdc) materials.[16] In a 20 mL scintillation vial equipped with a stir bar, $Zn(NO_3)_2$•$6H_2O$ (134 mg, 0.45 mmol, 2.50 equiv.), H_4*m*-dobdc (35.6 mg, 0.18 mmol, 1.00 equiv.), DMF (7.8 mL), and MeOH (4.2 mL) (0.015 M 13:7 DMF:MeOH reaction mixture). The vial was sealed and transferred to an aluminum block that was heated to 120 °C. The reaction mixture was allowed to stir gently for 24 h at this temperature. The mixture was then allowed to cool to room temperature, filtered via vacuum filtration, and washed with DMF (10 mL). The collected solid was transferred to a new 20 mL scintillation vial filled with DMF (10–15 mL). The vial was transferred to an aluminum block on a hot plate that had been pre-heated to 120 °C and was allowed to stand at this temperature for at least 12 h. At this time, the heterogenous mixture was allowed to cool to room temperature, the solvent was decanted, and fresh DMF (10–15 mL) was added. This process was repeated for a total of three DMF soaks. After the final soak, the mixture was filtered via vacuum filtration and washed with MeOH (10 mL). The resulting solid was transferred to a new scintillation vial filled with MeOH (10–15 mL). The vial was transferred to an aluminum block on a hot plate that had been pre-heated to 60 °C and was allowed to stand at this temperature for at least 12 h. At this time, the heterogenous mixture was allowed to cool to room temperature, the solvent was decanted, and fresh MeOH (10–15 mL) was added. This process was repeated for a total of three MeOH

soaks. After the final soak, the solvent was decanted, and the remaining solid was allowed to dry in air. A PXRD measurement of the washed product was performed.

Condition D: Attempted following a modified literature procedure for the synthesis of M_2(*m*-dobdc) materials.[16] In a 20 mL scintillation vial equipped with a stir bar, $ZnCl_2$ (61.3 mg, 0.45 mmol, 2.50 equiv.), H_4*m*-dobdc (35.6 mg, 0.18 mmol, 1.00 equiv.), DMF (0.78 mL), and MeOH (0.42 mL) (0.15 M 13:7 DMF:MeOH reaction mixture). The vial was sealed and transferred to an aluminum block that was heated to 120 °C. The reaction mixture was allowed to stir gently for 24 h at this temperature. The mixture was then allowed to cool to room temperature, filtered via vacuum filtration, and washed with DMF (10 mL). No solid was formed.

Condition E: Attempted following a modified literature procedure for the synthesis of M_2(dobdc) materials.[17] In a 20 mL scintillation vial equipped with a stir bar, $Zn(NO_3)_2$•$6H_2O$ (74.4 mg, 0.25 mmol, 2.50 equiv.), H_4*m*-dobdc (19.8 mg, 0.1 mmol, 1.00 equiv.), DMF (9 mL), EtOH (0.5 mL), and H_2O (0.5 mL) (0.01 M 18:1:1 DMF:EtOH:H_2O reaction mixture). The vial was sealed and transferred to an aluminum block that was heated to 120 °C. The reaction mixture was allowed to stir gently for 24 h at this temperature. The mixture was then allowed to cool to room temperature, filtered via vacuum filtration, and washed with DMF (10 mL). No solid was isolated.

Condition F: Attempted following a modified literature procedure for the synthesis of M_2(dobdc) materials.[17] In a 20 mL scintillation vial equipped with a stir bar, $ZnCl_2$ (34.1 mg, 0.25 mmol, 2.50 equiv.), H_4*m*-dobdc (19.8 mg, 0.1 mmol, 1.00 equiv.), DMF (9 mL), EtOH (0.5 mL), and H_2O (0.5 mL) (0.01 M 18:1:1 DMF:EtOH:H_2O reaction mixture). The vial was sealed and transferred to an aluminum block that was heated to 120 °C. The reaction mixture was allowed to stir gently for 24 h at this temperature. The mixture was then allowed to cool to room temperature, filtered via vacuum filtration, and washed with DMF (10 mL). No solid was isolated.

The PXRD patterns corresponding to the solids obtained under Conditions A–C are included in main text Figure 6A.

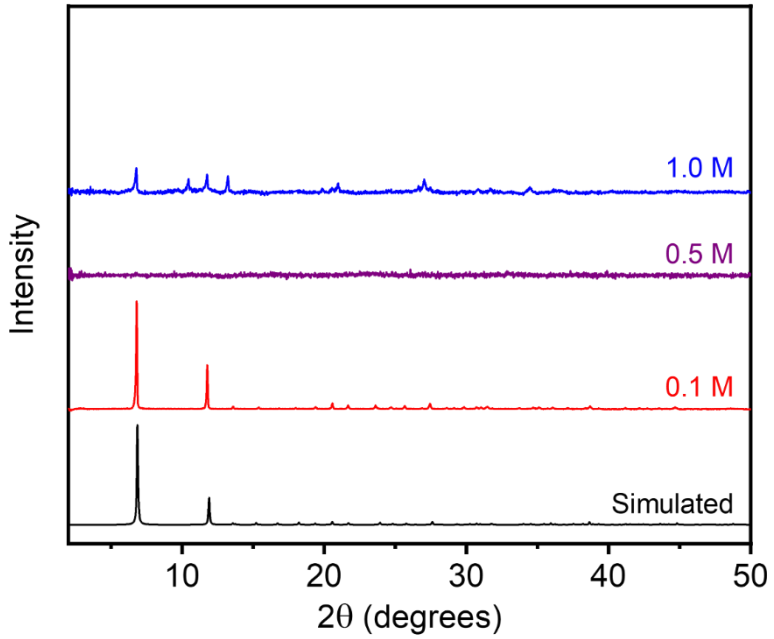

Figure S128. Baseline-corrected PXRD patterns (λ = 1.5406 Å) of MeOH-solvated Zn_2(*m*-dobdc) at different concentrations after aqueous synthesis. The simulated pattern based on the previously reported SCXRD structure of the isostructural framework Co_2(*m*-dobdc) is included for reference.[14] The Phase-pure MOF only formed at a concentration of 0.1 M.

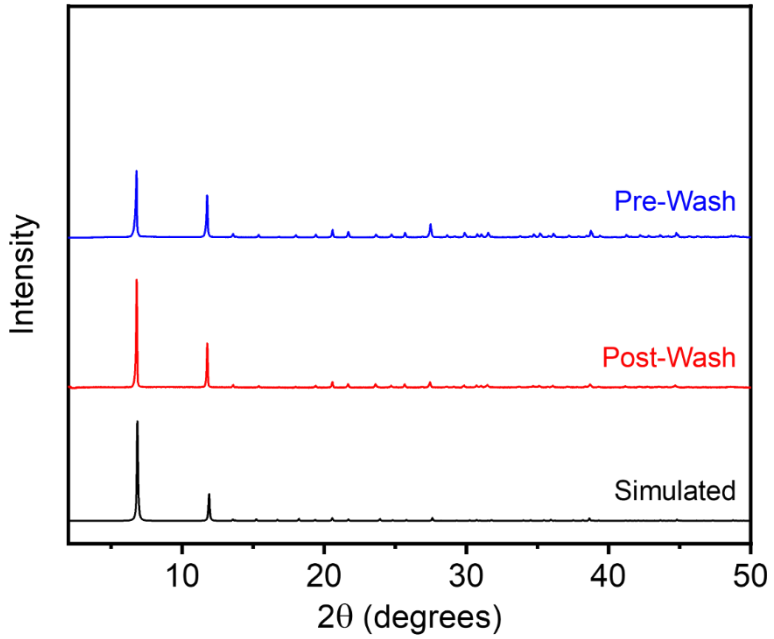

Figure S129. Baseline-corrected PXRD patterns (λ = 1.5406 Å) of MeOH-solvated Zn_2(*m*-dobdc) synthesized at 0.1 M before (pre-wash) and after (post-wash) soaking in MeOH. The simulated pattern based on the previously reported SCXRD structure of the isostructural framework Co_2(*m*-dobdc) is included for reference.[18] No significant change in the pattern was observed upon soaking the MOF in MeOH.

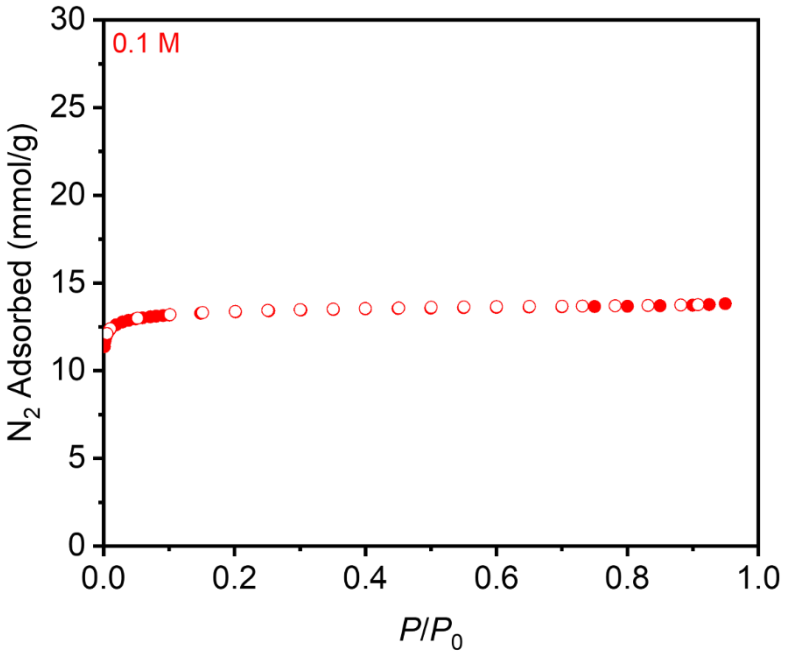

Figure S130. 77 K N_2 adsorption (filled circles) and desorption (open circles) isotherms of activated Zn_2(*m*-dobdc) after aqueous synthesis. BET surface area determined from this data is 1216 ± 1 m^2/g (0.1 M). The Langmuir surface area determined from this data is 1340 m^2/g (0.1 M).

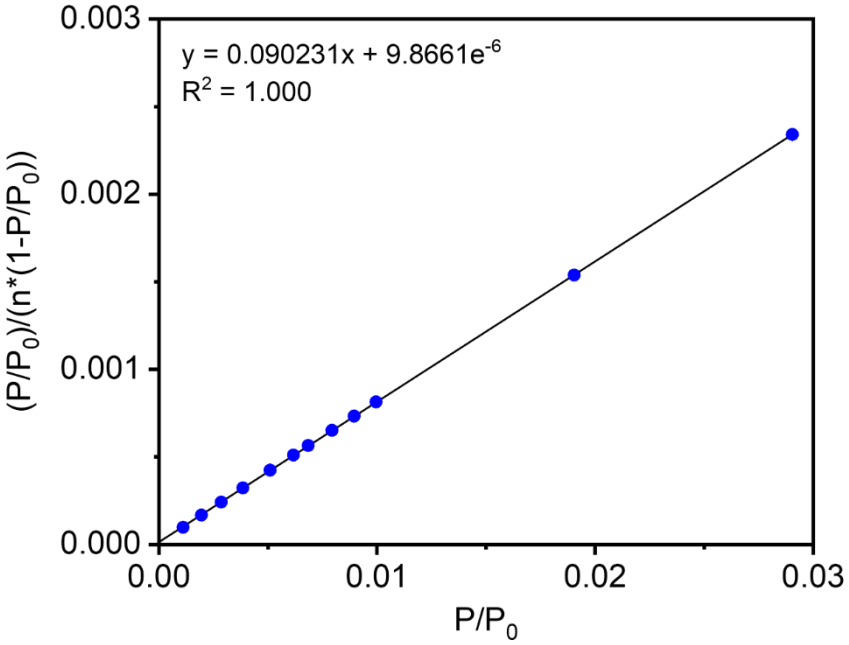

Figure S131. Linearized BET plot for the N_2 adsorption data of Zn_2(*m*-dobdc) synthesized at 0.1 M.

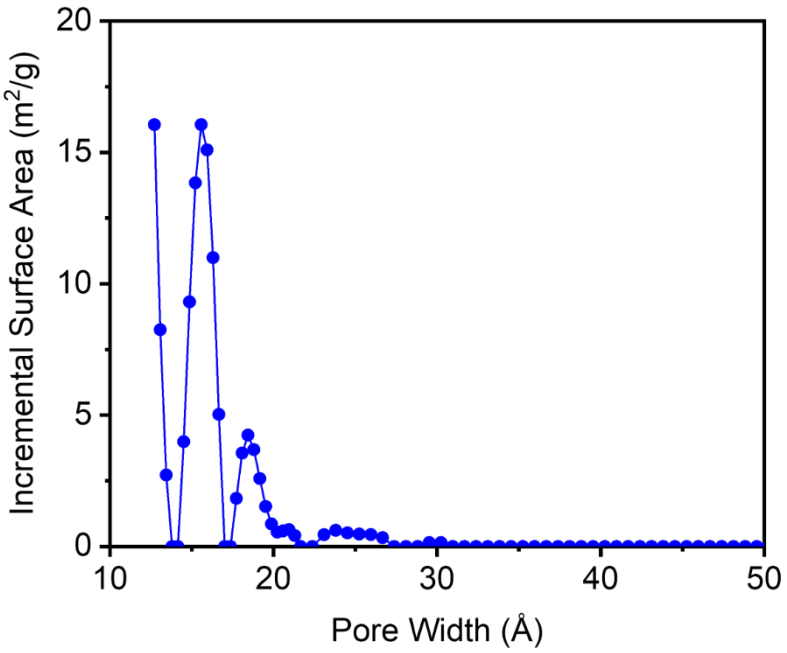

Figure S132. DFT-calculated pore size distribution for Zn_2(*m*-dobdc) synthesized at 0.1 M, assuming a cylindrical pore geometry. The primary pore size is below the lower limit of the measurement.

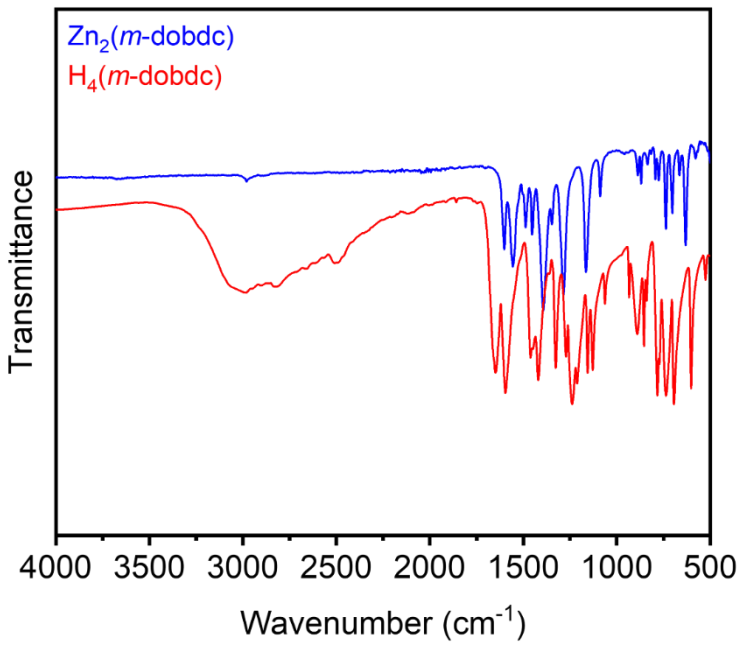

Figure S133. ATR-IR spectra of Zn_2(*m*-dobdc) synthesized at 0.1 M and the H_4(*m*-dobdc) linker.

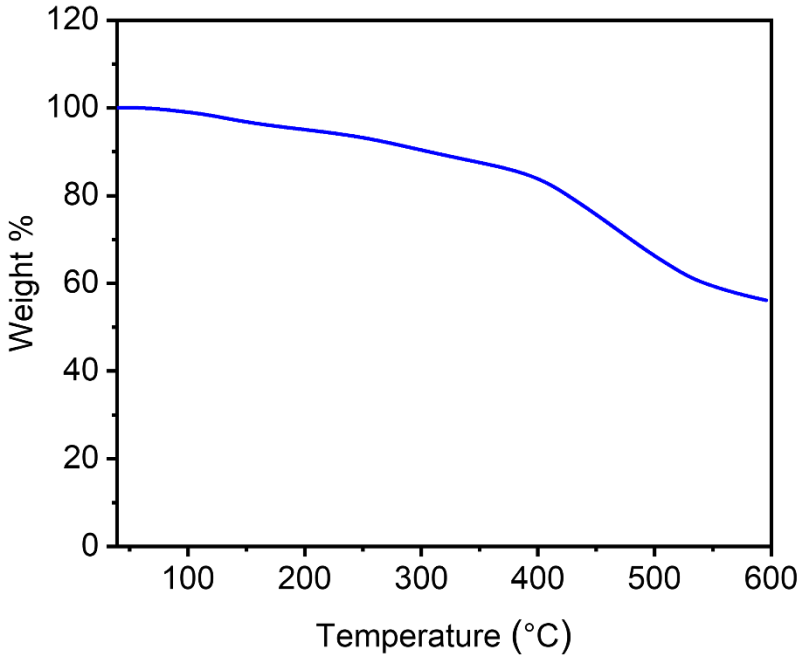

Figure S134. Thermogravimetric decomposition profile under N_2 of Zn_2(*m*-dobdc) synthesized at 0.1 M.

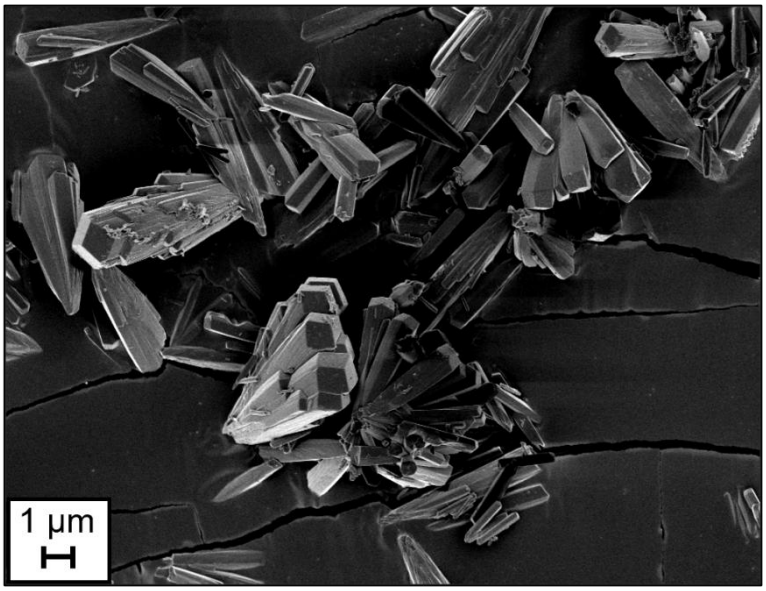

Figure S135. SEM image of Zn_2(*m*-dobdc).

6. Crystallographic Analysis.

PXRD measurements for crystalline domain size analysis. Volume-weighted average crystalline domain sizes (LVol-IB) of samples were determined through Pawley refinement of their PXRD (λ = 1.5418 Å) patterns. Space groups and preliminary unit cell parameters were obtained from the SCXRD structures of Zn_2(dobdc), Zn_2(dobpdc), and Co_2(*m*-dobdc), as appropriate.[9,14,19] Background coefficients (described by 5–10th order Chebyshev polynomials), zero-point error, unit cell, and peak profile (FP) parameters were freely refined. Crystallite size was modeled using Gaussian convolutions and freely refined. Strain was modeled using Gaussian and Lorentzian convolutions and freely refined.

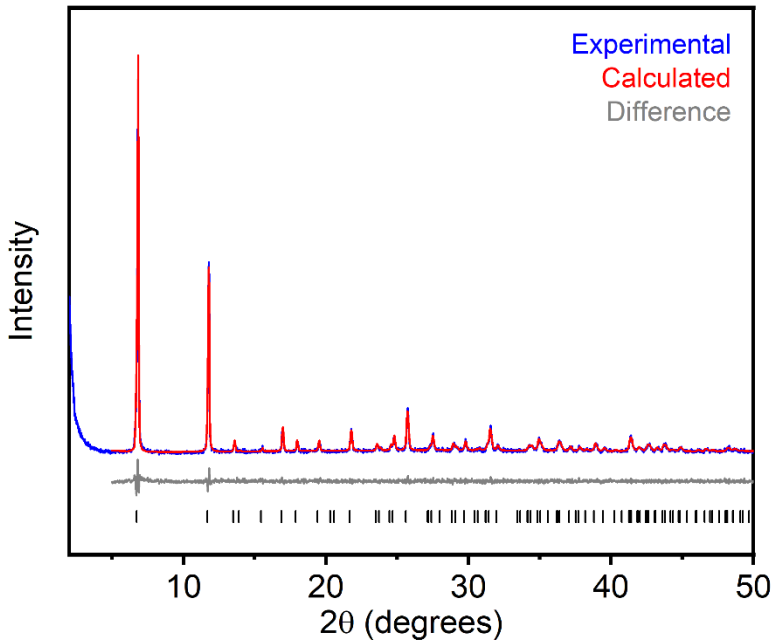

Figure S136. Representative Pawley refinement of the PXRD (λ = 1.54175 Å) pattern of a synthesized MOF to determine LVol-IB values. The analysis shown is of Zn_2(dobdc) synthesized at 0.5 M. Refined unit cell parameters: space group = $R\bar{3}$, a = 26.013(3) Å, c = 6.7786(13) Å. Black ticks correspond to calculated Bragg positions. Goodness of fit parameters: R_{wp} = 11.54%, R_p = 8.80%, R_{exp} = 25.53%, GoF = 0.45. LVol-IB: 145 ± 4.2 nm.

Table S13. Volume-weighted average crystalline domain sizes (LVol-IB) of synthesized salicylate-based frameworks and associated errors. The largest domain sizes are consistently observed for the Zn-based frameworks and the smallest for the Ni-based frameworks.

Sample	LVol-IB (nm)		
	0.1 M	**0.5 M**	**1.0 M**
Mg_2(dobdc)	195 ± 11	54 ± 3.4	42 ± 3.1
Co_2(dobdc)	56.3 ± 16	45.8 ± 12.8	63.2 ± 9.5
Ni_2(dobdc)	11.3 ± 0.6	10.4 ± 0.9	12.9 ± 0.8
Zn_2(dobdc)	773 ± 151	145 ± 4.2	289 ± 19
Mg_2(dobpdc)	10.5 ± 1.1	30 ± 3.6	15.7 ± 2.7
Co_2(dobpdc)	34.1 ± 4.6	43.3 ± 4.9	31.6 ± 9.6
Ni_2(dobpdc)	9 ± 0.2	9.7 ± 0.3	10.4 ± 0.8
Zn_2(dobpdc)	523 ± 68	157 ± 7.2	153 ± 9.8
Mg_2(*m*-dobdc)	67.8 ± 3.1	37 ± 2.5	59 ± 3
Co_2(*m*-dobdc)	156 ± 6.3	63.4 ± 7.7	116 ± 3
Ni_2(*m*-dobdc)	66 ± 0.7	46.5 ± 2.4	38.7 ± 2
Zn_2(*m*-dobdc)	330 ± 31	N/A	N/A

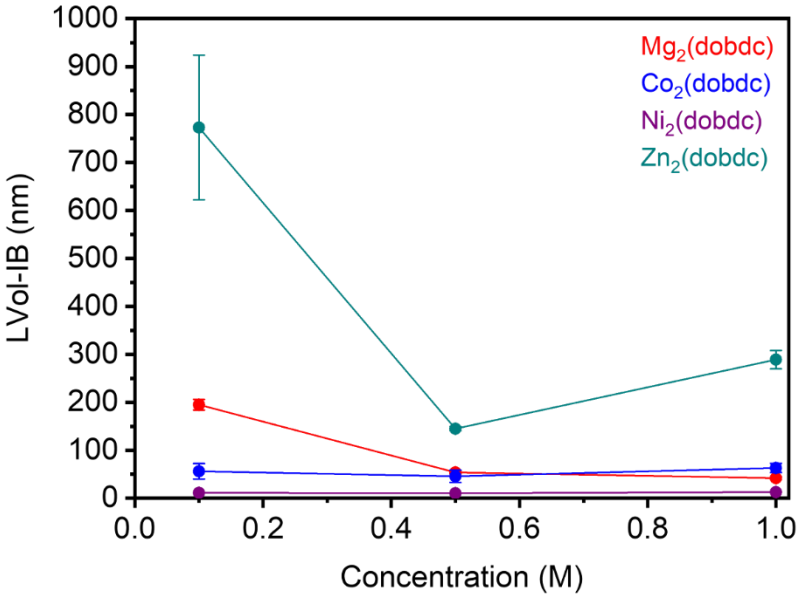

Figure S137. Concentration vs volume-weighted average crystalline domain sizes (LVol-IB) and associated errors of synthesized M_2(dobdc) samples. Some error bars are too small to see.

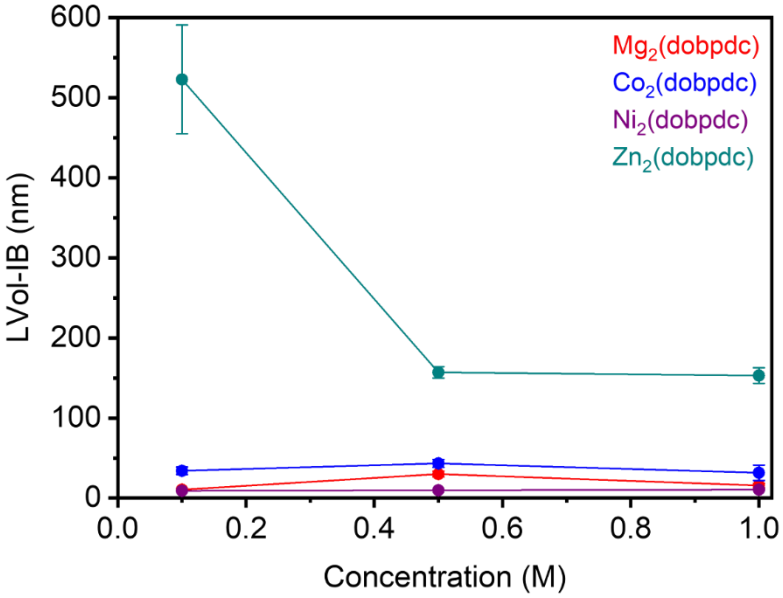

Figure S138. Concentration vs volume-weighted average crystalline domain sizes (LVol-IB) and associated errors of synthesized M_2(dobpdc) samples. Some error bars are too small to see.

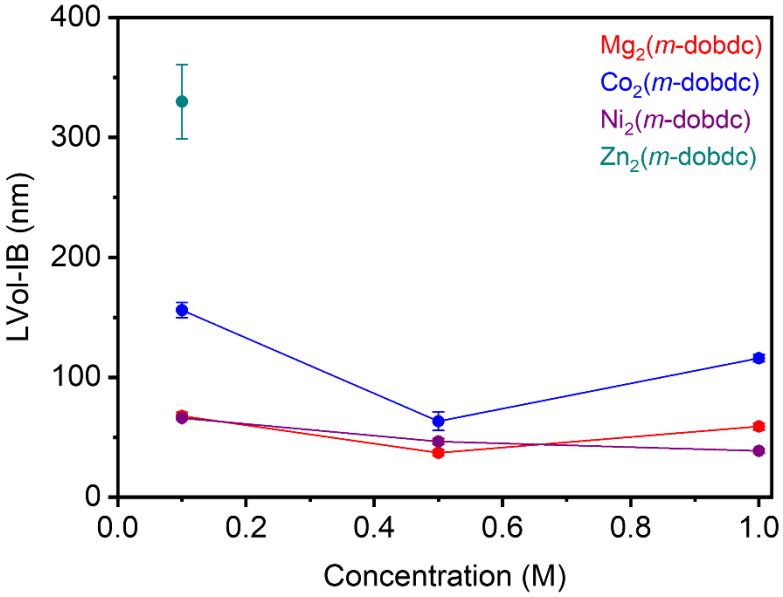

Figure S139. Concentration vs volume-weighted average crystalline domain sizes (LVol-IB) and associated errors of synthesized M_2(*m*-dobdc) samples. Some error bars are too small to see.

PXRD measurements for Rietveld refinement. Samples for Rietveld refinement were loosely packed into glass capillaries (1.0 mm OD, approximately 10 mg) in an N_2-filled glovebox, then sealed under N_2 with capillary wax and mounted using a capillary spin attachment head. Samples were spun at a rate of 1 rotation per step during data collection with a 0.01 ° step size at a minimum scan rate of 0.1 °/min. Data were collected in transmission mode and Debye-Sherrer geometry at 298 K using a Rigaku Smartlab SE Multipurpose diffractometer equipped with Cu Kα radiation (λ = 1.5418 Å), a Göbel mirror, a scattered radiation protector, a D/teX Ultra 250 detector, and mounting the following optics: incident Soller slits (2.5°), length-limiting slit (10 mm), incident slit (1.0 mm), receiving slit 1 (16 mm), receiving slit 2 (open), parallel slit analyzer (open), and receiving Soller slits (2.5°). The generator was set at 40 kV and 45 mA.

Analysis of the PXRD data of Zn_2(*m*-dobdc) was performed using TOPAS V6. A structureless Pawley refinement of the PXRD pattern of Zn_2(*m*-dobdc) based on the unit cell and space group of the isostructural MOF Co_2(*m*-dobdc)[14] effectively modeled the observed (93) reflections, providing initial unit cell and space group parameters, as well as a background model used in the subsequent Rietveld refinement of Zn_2(*m*-dobdc). An initial structural model of Zn_2(*m*-dobdc) was generated in the Materials Studio software package based on these parameters and used for Rietveld refinement. During the Rietveld refinement, the positions of C and O atoms of the carboxylate groups were refined but O–C–O bond angles were constrained to approximately 124°, and constraints were added to flatten the carboxylates. The hydroxyl O atoms and Zn atoms were freely refined. A rigid, idealized model was employed for aromatic carbon atoms of the linker based on their positions in Co_2(*m*-dobdc).[14] Hydrogen atoms were placed at ideal positions and C–H bond lengths were fixed at 0.95 Å. The occupancies of all atoms were fixed at unity. A single

refined isotropic thermal parameter was assigned to each C, O, and H atom. The isotropic thermal parameter of Zn was freely refined. Unit cell parameters were freely refined. The sample background was modeled by an 8th order Chebyshev polynomial and fixed at values determined through Pawley refinement. Gaussian and Lorentzian convolutions were used to model crystallite size and strain, respectively. Minor preferred orientation not eliminated by spinning the sample was modeled with a one-directional March-Dollase correction (2 -1 0). The calculated diffraction pattern for the final structural model of Zn_2(*m*-dobdc) is in excellent agreement with the experimental diffraction pattern (main text Figure 6B). CCDC deposition number: 2461999.

Table S14. Fractional atomic coordinates and displacement parameters in Zn_2(*m*-dobdc). CCDC deposition number: 2461999. Values in parenthesis indicate one standard deviation from the parameter value.

Atom	*x*	*y*	*z*	Multiplicity	Occupancy	B_{eq} (Å^2)
Zn1	0.6568(2)	0.61971(14)	0.4608(17)	18	1	2.19(10)
O1	0.5881(5)	0.5909(5)	0.652(3)	18	1	2.7(2)
O2	0.6160(6)	0.5616(6)	1.250(3)	18	1	2.7(2)
O3	0.6442(5)	0.6292(7)	1.019(3)	18	1	2.7(2)
C1	0.6134(10)	0.5775(9)	1.081(3)	18	1	2.7(2)
C2	0.5513	0.5441	0.7562	18	1	2.7(2)
C3	0.5605	0.534	0.9559	18	1	2.7(2)
C4	0.5178	0.4822	1.0494	9	1	2.7(2)
C5	0.5	0.5	0.6666667	9	1	2.7(2)
H1	0.49376	0.50624	0.53296	9	1	2.7(2)
H2	0.52435	0.47565	1.18202	9	1	2.7(2)

Table S15. Bond angles and bond lengths in Zn_2(*m*-dobdc). Values in parenthesis indicate one standard deviation from the parameter value.

Bond	Angle (°)	Bond	Angle (°)	Bond	Distance (Å)
O3–Zn1–O2	99.7(9)	Zn1–O3–C1	132.0(15)	Zn1–O2	1.960(19)
O1–Zn1–O3	97.2(8)	C1–O3–Zn1	121.6(6)	Zn1–O3	2.007(14)
O1–Zn1–O2	98.5(7)	O3–C1–O2	124.5(18)	Zn1–O1	2.020(19)
O3–Zn1–O1	83.3(8)	C3–C1–O3	117.5(19)	Zn1–O3	2.11(2)
O3–Zn1–O3	81.8(3)	C3–C1–O2	116.8(15)	Zn1–O1	2.148(16)
O3–Zn1–O2	177.4(6)	O3–C1–C3	139.6(16)	O1–C2	1.312(14)
O1–Zn1–O3	82.5(7)	C5–C2–O1	118.5(9)	O2–C1	1.23(3)
O1–Zn1–O1	165.7(11)	C3–C2–C5	116.4939(7)	O3–C1	1.24(2)
O1–Zn1–O3	82.6(7)	C3–C2–O1	125.0(9)	C1–C3	1.52(2)
O1–Zn1–O2	95.6(8)	C2–C3–C4	119.0714(7)	C2–C5	1.38550(2)
Zn1–O1–C2	141.8(11)	C1–C3–C2	124.5(8)	C2–C3	1.42330(4)
Zn1–O1–Zn1	90.8(4)	C1–C3–C4	116.3(8)	C3–C4	1.39285(2)
Zn1–O1–C2	117.9(14)	C3–C4–H2	118.6024(7)	C4–H2	0.94712(2)
Zn1–O2–C1	121.4(14)	C3–C4–C3	122.7947(15)	H1–C5	0.94995(2)
Zn1–O3–C1	134.1(17)	C2–C5–H1	116.9755(7)		
Zn1–O3–Zn1	92.4(7)	C2–C5–C2	126.0038(14)		

Indexing and unit cell refinement of the PXRD patterns of unknown phases. All apparent reflections in the PXRD pattern of the unknown Mg-based sample synthesized using H_4dobdc at 0.1 M were identified by visual inspection (58 total) and indexed using TOPAS V6. Its unit cell was suggested with high figures of merit (space group = *P*21/c, a = 6.8794 Å, b = 8.2287 Å, c = 16.9392 Å, β = 79.7980°, GoF = 3.79). A Pawley refinement based on this solution was performed to obtain precise unit cell parameters (Figure S140). Other unidentified crystalline products of Zn_2(dobpdc) and Mg_2(*m*-dobdc) syntheses could not be definitively indexed, precluding unit cell determination in those cases.

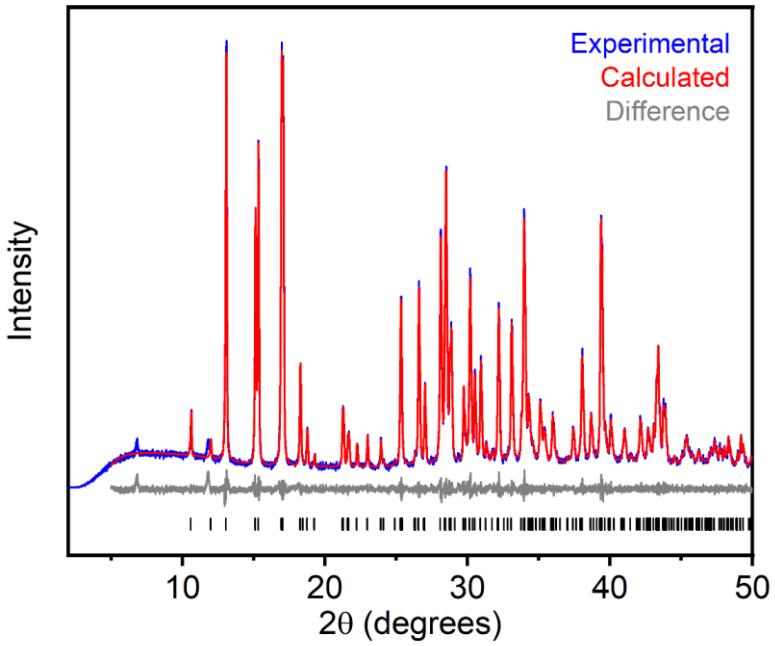

Figure S140. Pawley refinement of the PXRD (λ = 1.54175 Å) pattern of the Mg-based sample synthesized using H_4dobdc at 0.1 M. The minor peaks at approx. 6.8° and 11.8° are attributed to a small amount of Mg_2(dobdc). Refined unit cell parameters: space group = *P*21/c, *a* = 6.88228(16) Å, *b* = 8.22969(19) Å, *c* = 16.9478(4) Å, *β* = 79.8280(14)°. Black ticks correspond to calculated Bragg positions. Goodness of fit parameters: R_{wp} = 5.48%, R_p = 3.96%, R_{exp} = 4.69%, GoF = 1.17.

7. CO_2/N_2 Selectivity Calculations.

CO_2 and N_2 adsorption data were fit using the dual-site Langmuir model (eq. S1), where $Q(P)$ is the predicted uptake Q at pressure P in mmol/g, Q_{sati} is the saturation pressure of binding site i in mmol/g, b_i is the Langmuir parameter of site i, v_i is the Freundlich parameter of site i, $-S_i$ is the entropy of binding site i in J/mol•K, R is the ideal gas constant, E_i is the enthalpy of adsorption for binding site i in kJ/mol, and T is the temperature in K. The isotherms were fit with v_1 and v_2 set as 1. Fits were obtained using Solver in Microsoft Excel.

$$Q(P) = \frac{Q_{sat1} b_1 P^{v_1}}{1+b_1 P^{v_1}} + \frac{Q_{sat1} b_2 P^{v_2}}{1+b_2 P^{v_2}};\ b_i = e^{\left(\frac{-S_i}{R}\right)\left(\frac{1000 \cdot E_i}{RT}\right)} \qquad \text{eq. S1}$$

Ideal Adsorbed Solution Theory (IAST) was used to calculate adsorption selectivities from the single-component adsorption isotherms.[20,21] This approach solves for the spreading pressure and subsequently the composition of the adsorbed phase for each mixture. The IAST selectivity (S) was determined using eq. S2, where x_i is the mole fraction in the adsorbed phase and y_i is the mole fraction in the gas phase of component i. The IAST selectivities for various mixtures were determined using Mathematica.

$$S = \frac{x_{CO_2}/x_{N_2}}{y_{CO_2}/y_{N_2}} \qquad \text{eq. S2}$$

Table S16. Langmuir fit parameters determined for fits to the dual-site Langmuir model for the isotherms shown in main text Figure 6C.

	Zn2(dobdc)		**Zn2(*m*-dobdc)**	
Parameter	**CO_2**	**N_2**	**CO_2**	**N_2**
$Q_{sat}1$ (mmol/g)	8.29	0.00	7.50	1.2×10^{-4}
S1 (in multiples of R)	0.215	0.396	0.197	0.100
E1 (kJ/mol)	1.37	0.019	2.66	0.00
V1	1.00	1.00	1.00	1.00
$Q_{sat}2$ (mmol/g)	0.00	6.55	0.00	4.60
S2 (in multiples of R)	2.25	3.24	2.25	2.61
E2 (kJ/mol)	0.507	0.181	0.507	0.197
V2	1.00	1.00	1.00	1.00

8. Solvothermal Synthesis of Salicylate MOFs.

General Procedure. In a 250 mL Pyrex jar, $M(NO_3)_2$•$6H_2O$ (25 mmol or 2.5 mmol for 0.1 M and 0.01 M synthesis, respectively, 2.50 equiv.) and linker (10 mmol or 1 mmol for 0.1 M and 0.01 M synthesis, respectively, 1.00 eq) were dissolved in solvent (100 mL). Solvent mixtures were selected based on literature conditions. For M_2(dobpdc) materials, the synthesis was only conducted at a concentration of 0.01 M. The mixture was sonicated until all of the solids dissolved. The jar was placed in an oven that was preheated at 120 °C and kept at this temperature for 24 h. At this time, the heterogenous mixture was allowed to cool to room temperature, the solvent was decanted, and fresh MeOH (50 mL) was added. The mixture was allowed to stand at 60 °C for 18 h. At this time, the MeOH was decanted and replaced with fresh MeOH (50 mL). This process was repeated for a total of six hot MeOH soaks. After the final soak, the solvent was decanted, and the remaining solid was allowed to dry in air. The sample was activated under high vacuum (<10 μbar), ramping the temperature slowly to 180 °C (0.1°C/min). The sample was allowed to stand at 180 °C under high vacuum (<10 μbar) for 12 h prior to gas adsorption analysis.

Table S17. Solvothermal syntheses of salicylate MOFs.

Sample	Linker	Solvent Ratio	Yield (%)		BET Surface Area (m^2/g)	
			0.1 M	0.01 M	0.1 M	0.01 M
Mg_2(dobdc)	H_4dobdc	18:1:1 DMF:EtOH:H_2O[22]	N/a	81	no MOF	1506 ± 1
Co_2(dobdc)	H_4dobdc	1:1:1 DMF:EtOH:H_2O[22]	43	59	472 ± 1	1092 ± 2
Ni_2(dobdc)	H_4dobdc	8:1 DMF:MeOH[22]	98	60	1154 ± 1	1383 ± 1
Zn_2(dobdc)	H_4dobdc	1:1 DMF:EtOH[22]	89	60	354 ± 1	1200 ± 1
Mg_2(dobpdc)	H_4dobpdc	1:1 DMF:MeOH[23]	-	90	-	2850 ± 84
Co_2(dobpdc)	H_4dobpdc	1:1:1 DMF:EtOH:H_2O[23]	-	43	-	3250 ± 87
Ni_2(dobpdc)	H_4dobpdc	1:1:1 DMF:EtOH:H_2O[23]	-	76	-	3240 ± 87
Zn_2(dobpdc)	H_4dobpdc	1:1 DMF:EtOH[23]	-	N/a	-	no MOF
Mg_2(*m*-dobdc)	H_4*m*-dobdc	1:1 DMF:MeOH[15]	30	46	791 ± 1	1404 ± 2
Co_2(*m*-dobdc)	H_4*m*-dobdc	1:1 DMF:MeOH[16]	38	63	1107 ± 1	1166 ± 1
Ni_2(*m*-dobdc)	H_4*m*-dobdc	2:1 DMF:MeOH[16]	85	83	1009 ± 1	1080 ± 1

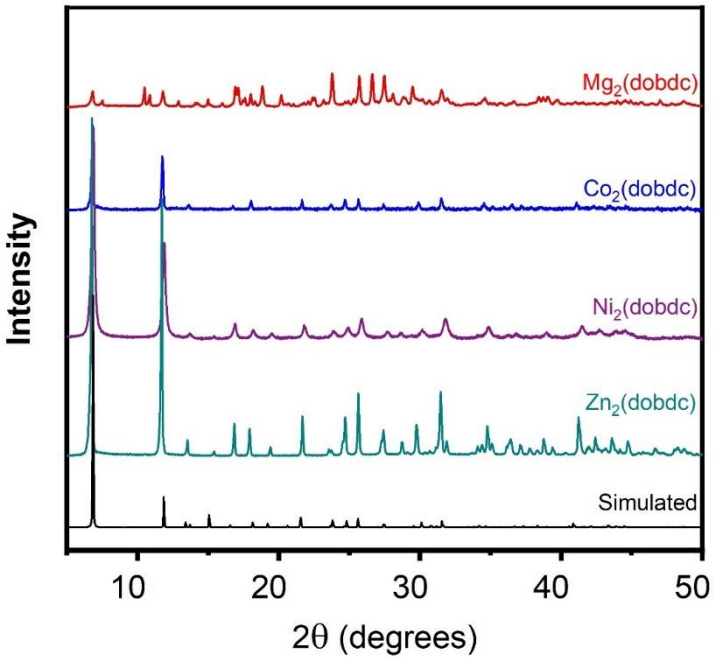

Figure S141. PXRD patterns of MeOH-solvated M_2(dobdc) after 0.1 M solvothermal synthesis. The simulated pattern based on the previously reported SCXRD structure of Zn_2(dobdc) is included for reference.[9] Phase-pure Mg_2(dobdc) was not obtained under these conditions, as expected.[24,25]

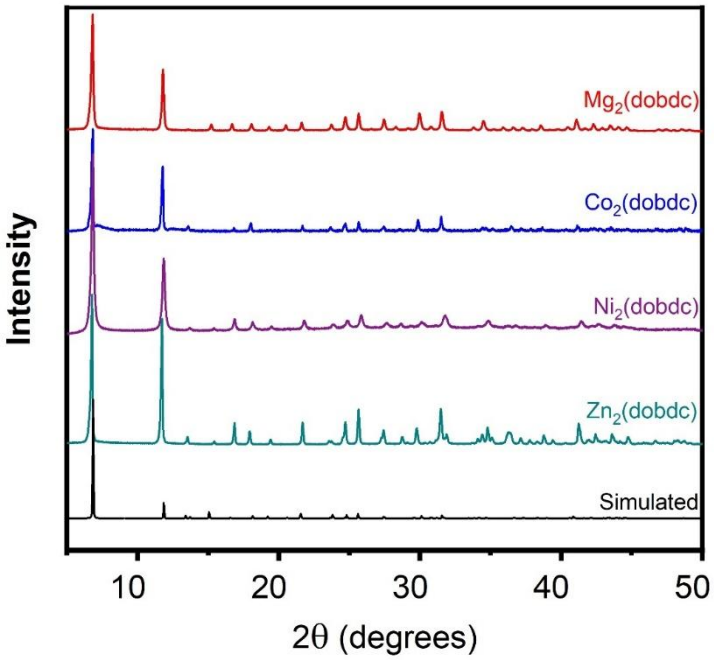

Figure S142. PXRD patterns of MeOH-solvated M_2(dobdc) after 0.01 M solvothermal synthesis. The simulated pattern based on the previously reported SCXRD structure of Zn_2(dobdc) is included for reference.[9]

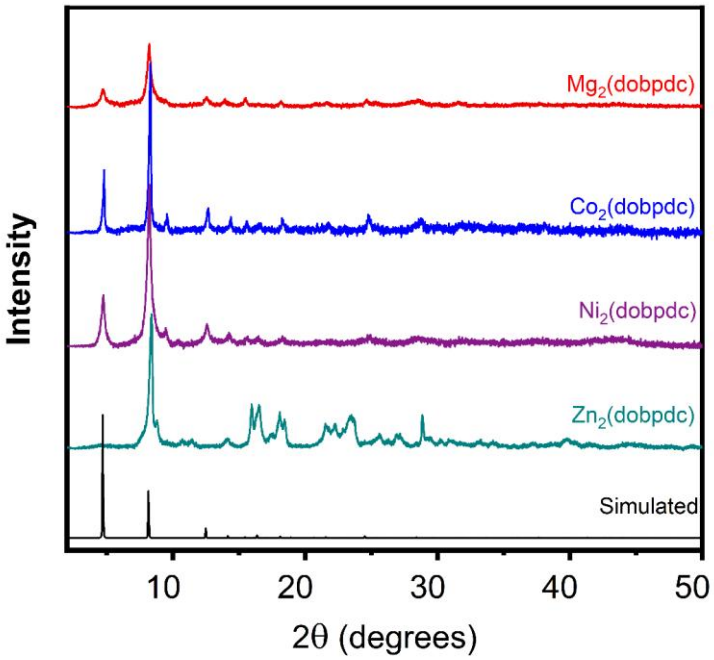

Figure S143. PXRD patterns of MeOH-solvated M_2(dobpdc) after 0.01 M solvothermal synthesis. The simulated pattern based on the previously reported SCXRD structure of Zn_2(dobpdc) is included for reference.[13] Zn_2(dobpdc) was not obtained under these conditions.

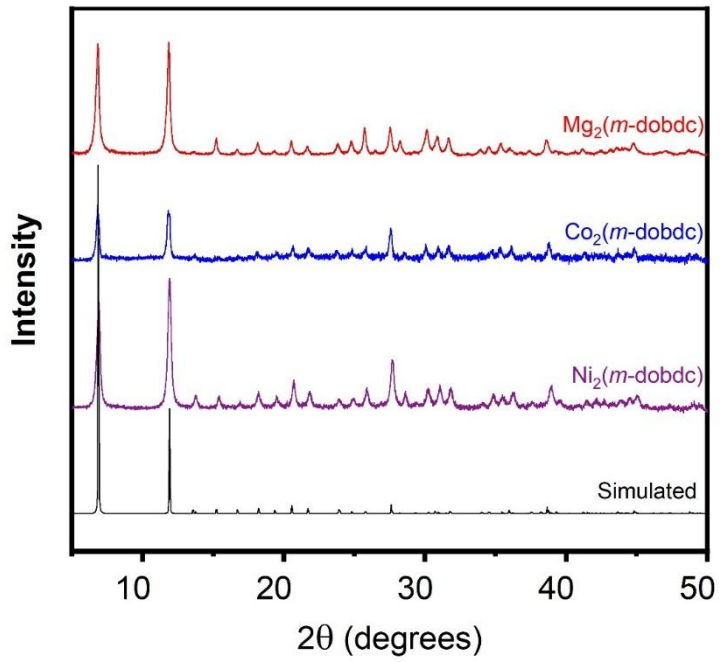

Figure S144. PXRD patterns of MeOH-solvated M_2(*m*-dobdc) after 0.1 M solvothermal synthesis. The simulated pattern based on the previously reported SCXRD structure of Co_2(*m*-dobdc) is included for reference.[14]

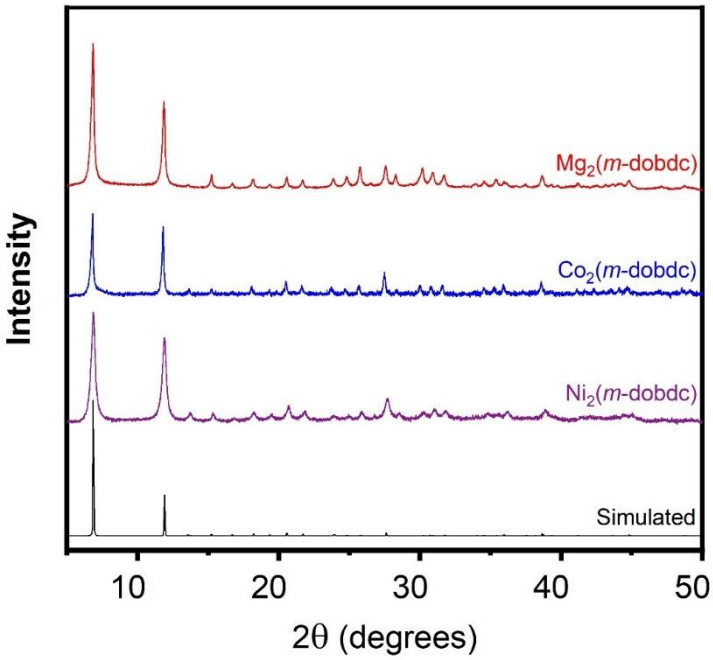

Figure S145. PXRD patterns of MeOH-solvated M_2(*m*-dobdc) after 0.01 M solvothermal synthesis. The simulated pattern based on the previously reported SCXRD structure of Co_2(*m*-dobdc) is included for reference.[14]

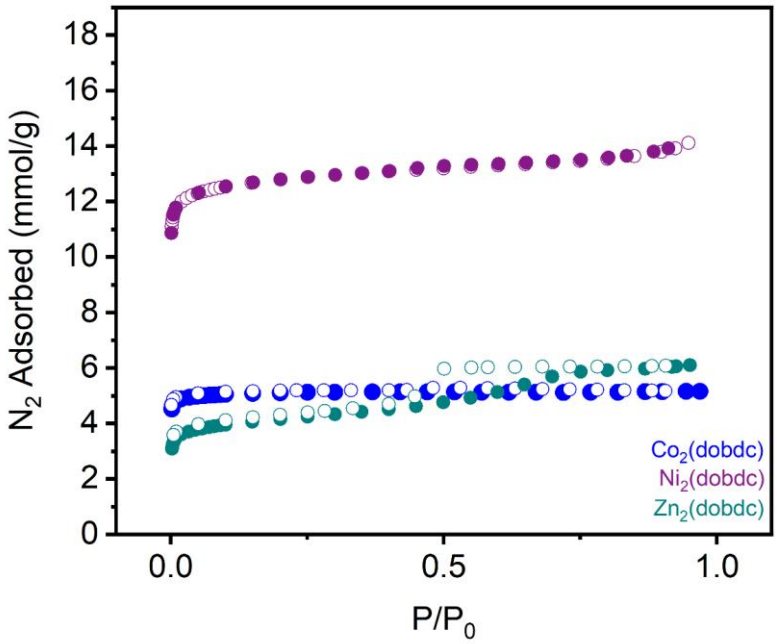

Figure S146. 77 K N_2 adsorption (filled circles) and desorption (open circles) isotherms of activated M_2(dobdc) synthesized at 0.1 M. The BET surface areas determined from these data are 472 ± 1 m^2/g (Co_2(dobdc)), 1154 ± 1 m^2/g (Ni_2(dobdc)) and 354 ± 1 m^2/g (Zn_2(dobdc)). The Langmuir surface areas determined from these data are 502 ± 0.3 m^2/g (Co_2(dobdc)), 1338 ± 7 m^2/g (Ni_2(dobdc)), and 580 ± 14 m^2/g (Zn_2(dobdc)).

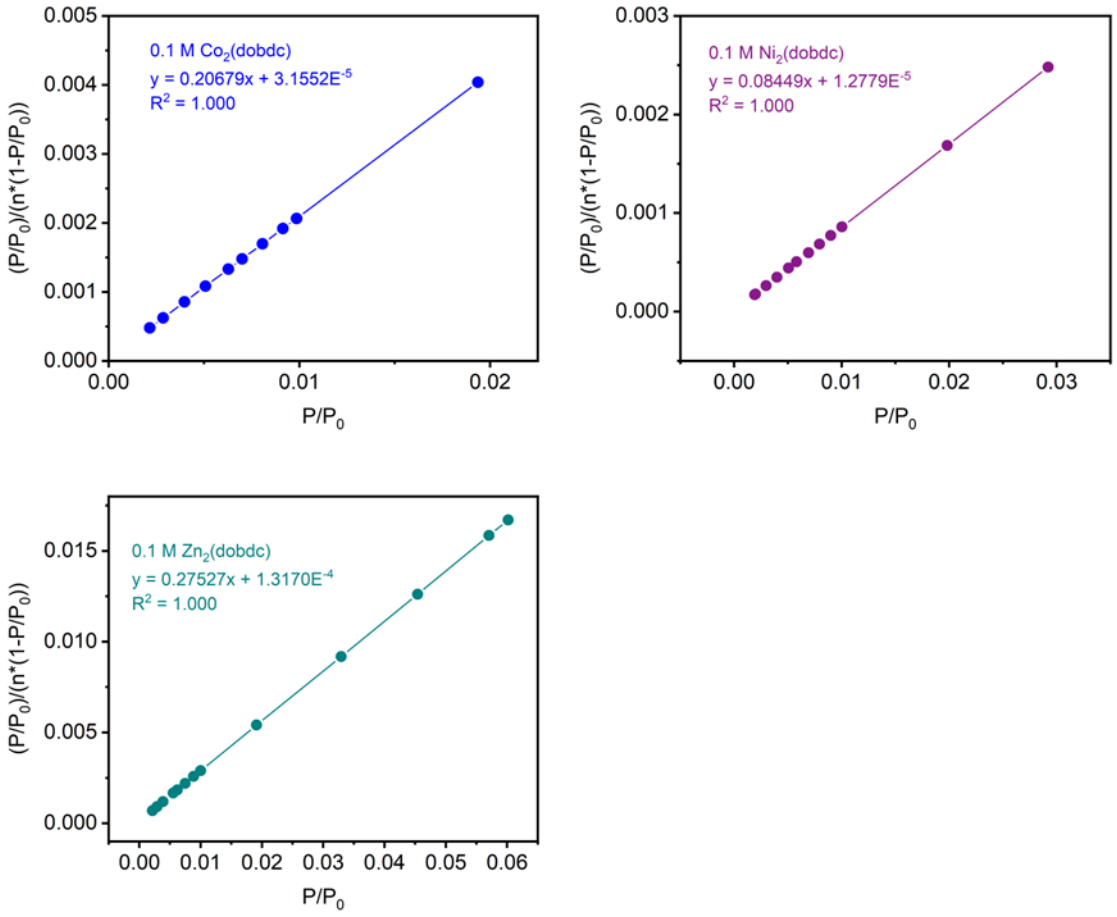

Figure S147. Linearized BET plots for the N_2 adsorption data of M_2(dobdc) synthesized at 0.1 M.

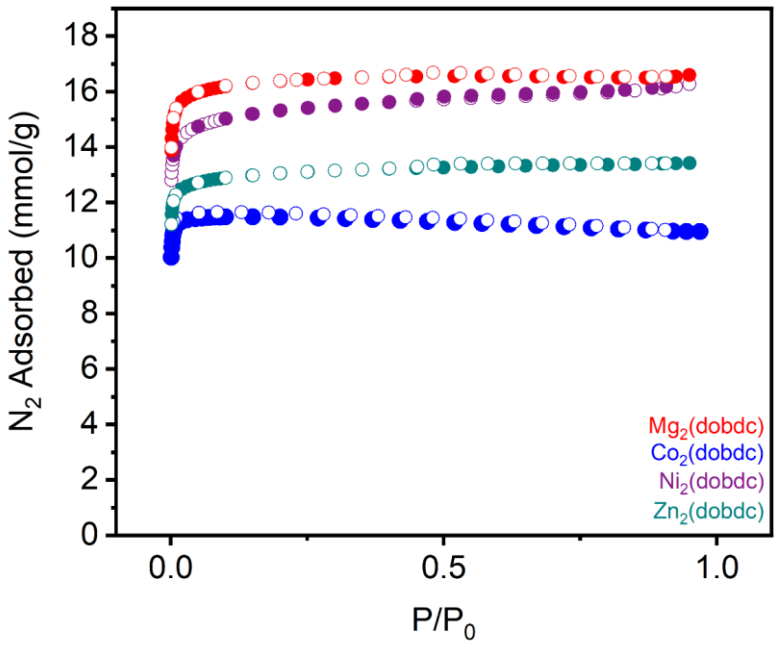

Figure S148. 77 K N_2 adsorption (filled circles) and desorption (open circles) isotherms of activated M_2(dobdc) synthesized at 0.01 M. The BET surface areas determined from these data are 1506 ± 1 m^2/g (Mg_2(dobdc)), 1092 ± 2 m^2/g (Co_2(dobdc)), 1383 ± 1 m^2/g (Ni_2(dobdc)) and 1200 ± 0.5 m^2/g (Zn_2(dobdc)). The Langmuir surface areas determined from these data are 1615 ± 1 m^2/g (Mg_2(dobdc)), 1077 ± 3 m^2/g (Co_2(dobdc)), 1569 ± 4 m^2/g (Ni_2(dobdc)) and 1307 ± 1 m^2/g (Zn_2(dobdc)).

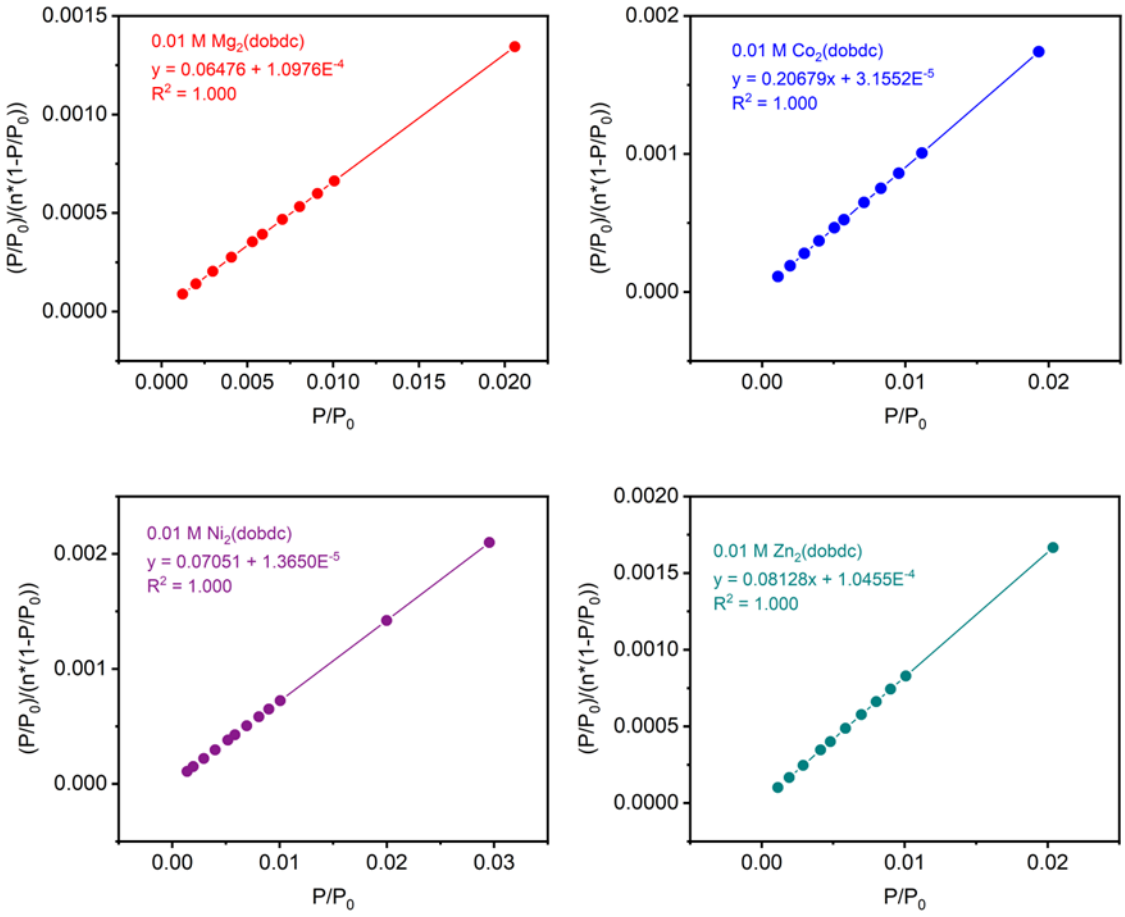

Figure S149. Linearized BET plots for the N_2 adsorption data of M_2(dobdc) synthesized at 0.01 M.

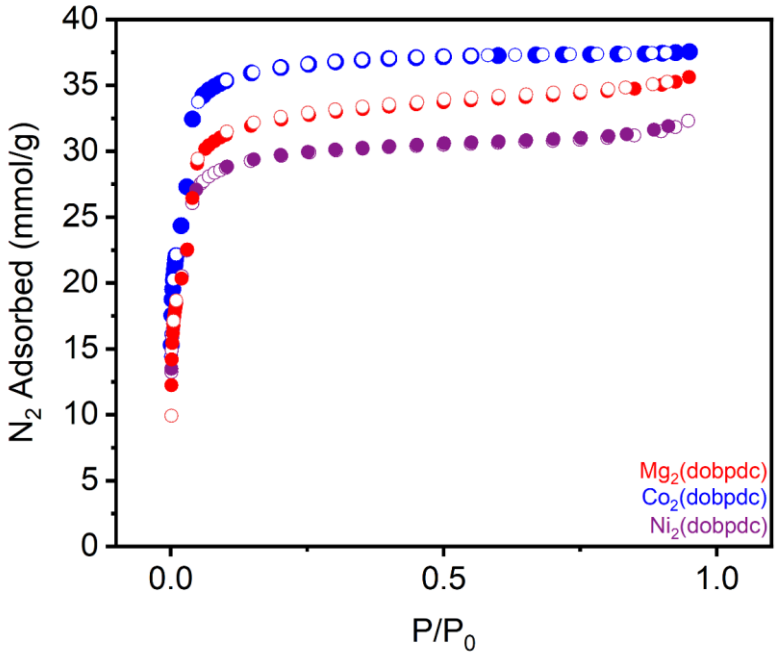

Figure S150. 77 K N_2 adsorption (filled circles) and desorption (open circles) isotherms of activated M_2(dobpdc) synthesized at 0.01 M. The BET surface areas determined from these data are 2850 ± 84 m²/g (Mg_2(dobpdc)), 3250 ± 87 m²/g (Co_2(dobpdc)), and 3240 ± 87 m²/g (Ni_2(dobpdc)). The Langmuir surface areas determined from these data are 3427 ± 14 m²/g (Mg_2(dobpdc)), 3674 ± 4 m²/g (Co_2(dobpdc)), and 3080 ± 13 m²/g (Ni_2(dobpdc)).

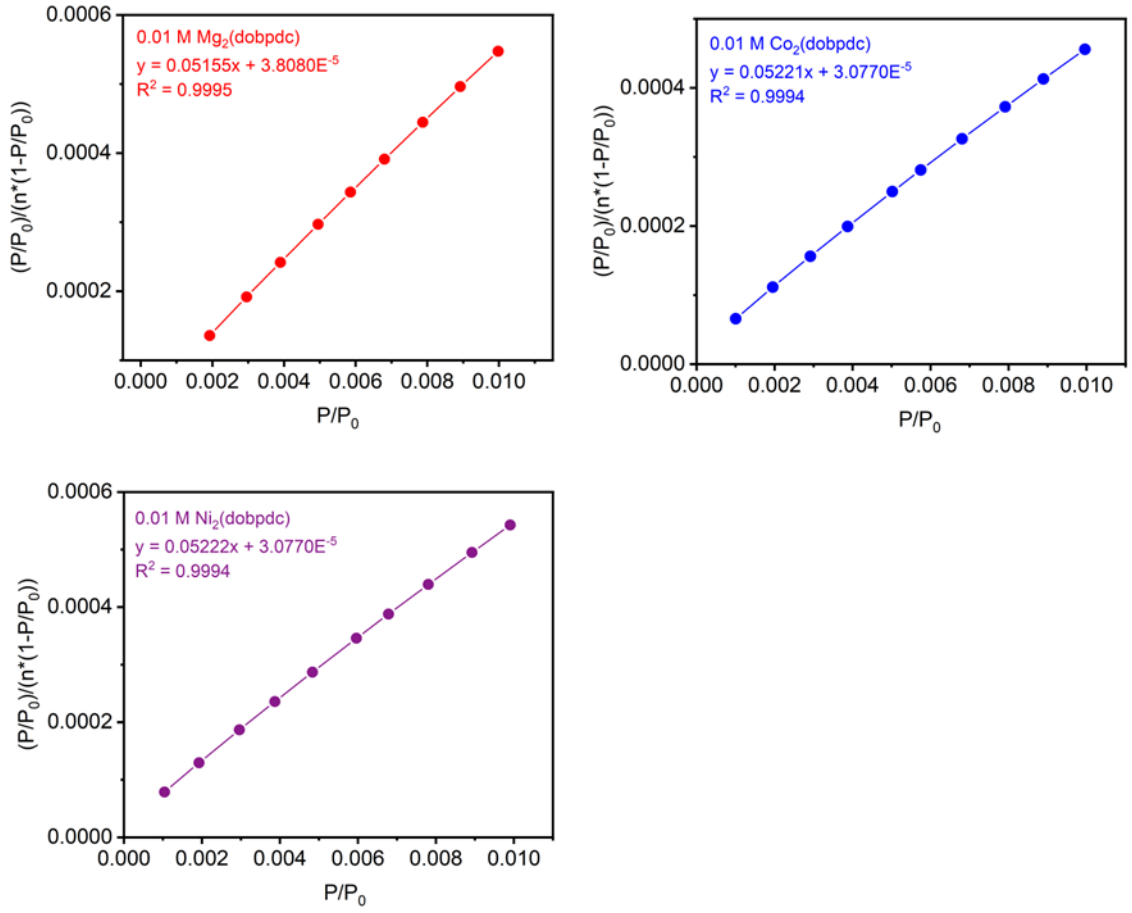

Figure S151. Linearized BET plots for the N_2 adsorption data of M_2(dobpdc) synthesized at 0.01 M.

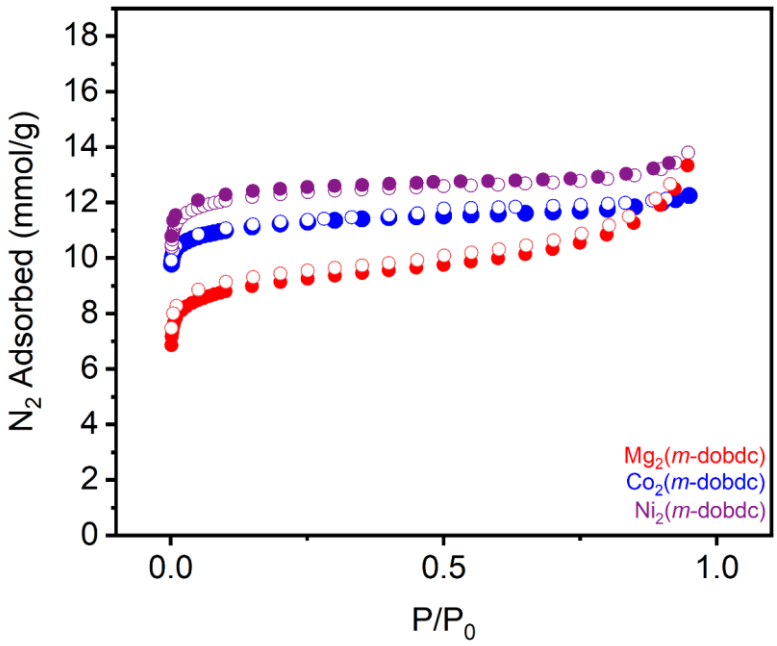

Figure S152. 77 K N_2 adsorption (filled circles) and desorption (open circles) isotherms of activated M_2(*m*-dobdc) synthesized at 0.1 M. The BET surface areas determined from these data are 791 ± 1 m^2/g (Mg_2(*m*-dobdc)), 1107 ± 1 m^2/g (Co_2(*m*-dobdc)), and 1009 ± 1 m^2/g (Ni_2(*m*-dobdc)). The Langmuir surface areas determined from these data are 1120 ± 27 m^2/g (Mg_2(*m*-dobdc)), 1163 ± 6 m^2/g (Co_2(*m*-dobdc)), and 1281 ± 9 m^2/g (Ni_2(*m*-dobdc)).

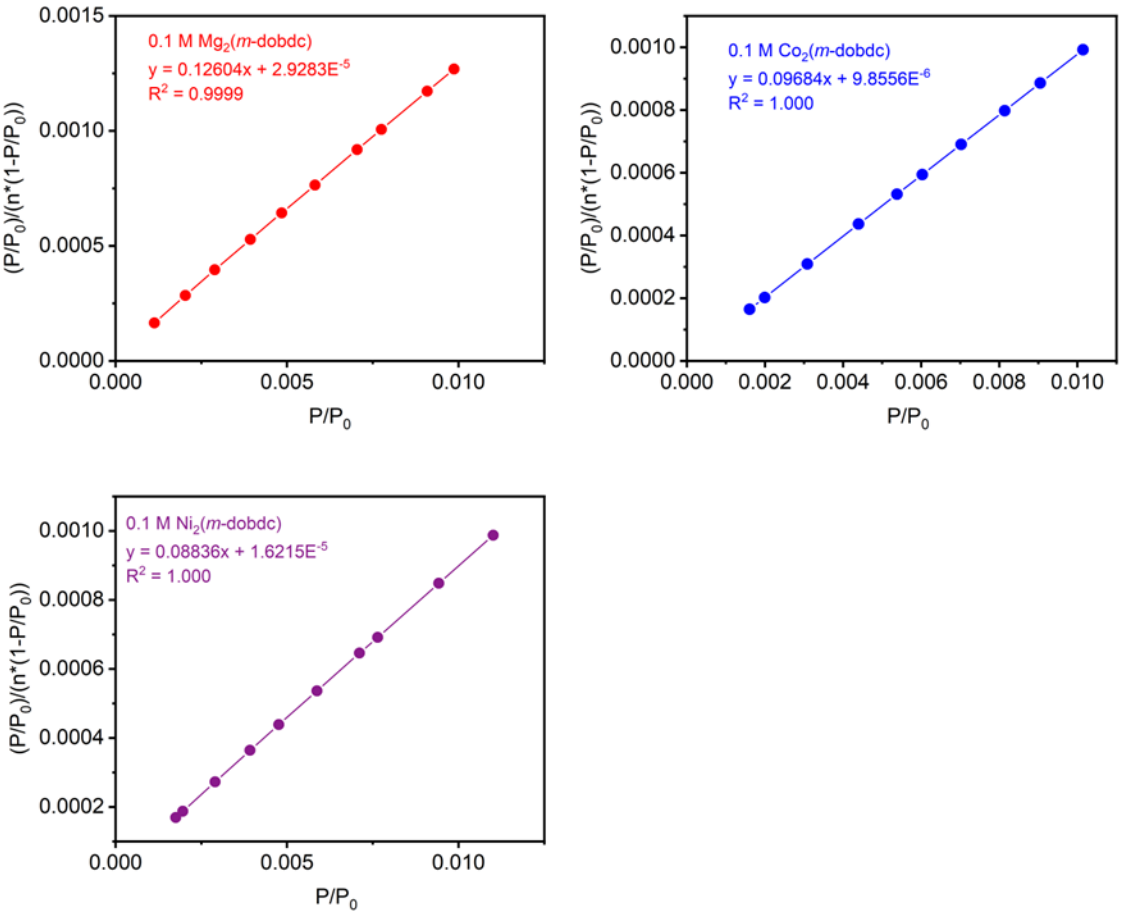

Figure S153. Linearized BET plots for the N_2 adsorption data of M_2(*m*-dobdc) synthesized at 0.1 M.

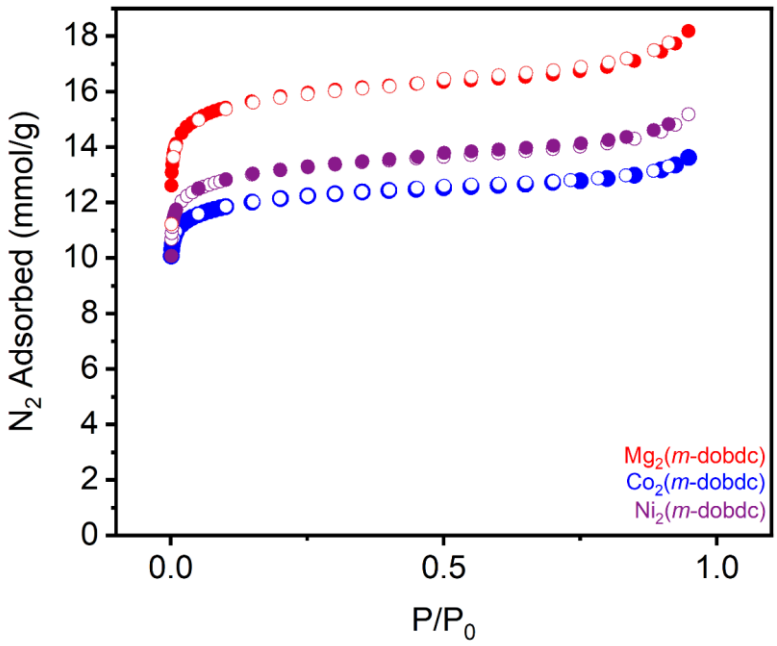

Figure S154. 77 K N_2 adsorption (filled circles) and desorption (open circles) isotherms of activated M_2(*m*-dobdc) synthesized at 0.1 M. The BET surface areas determined from these data are 1404 ± 2 m²/g (Mg_2(*m*-dobdc)), 1166 ± 1 m²/g (Co_2(*m*-dobdc)), and 1080 ± 1 m²/g (Ni_2(*m*-dobdc)). The Langmuir surface areas determined from these data are 1690 ± 14 m²/g (Mg_2(*m*-dobdc)), 1278 ± 8 m²/g (Co_2(*m*-dobdc)), and 1410 ± 11 m²/g (Ni_2(*m*-dobdc)).

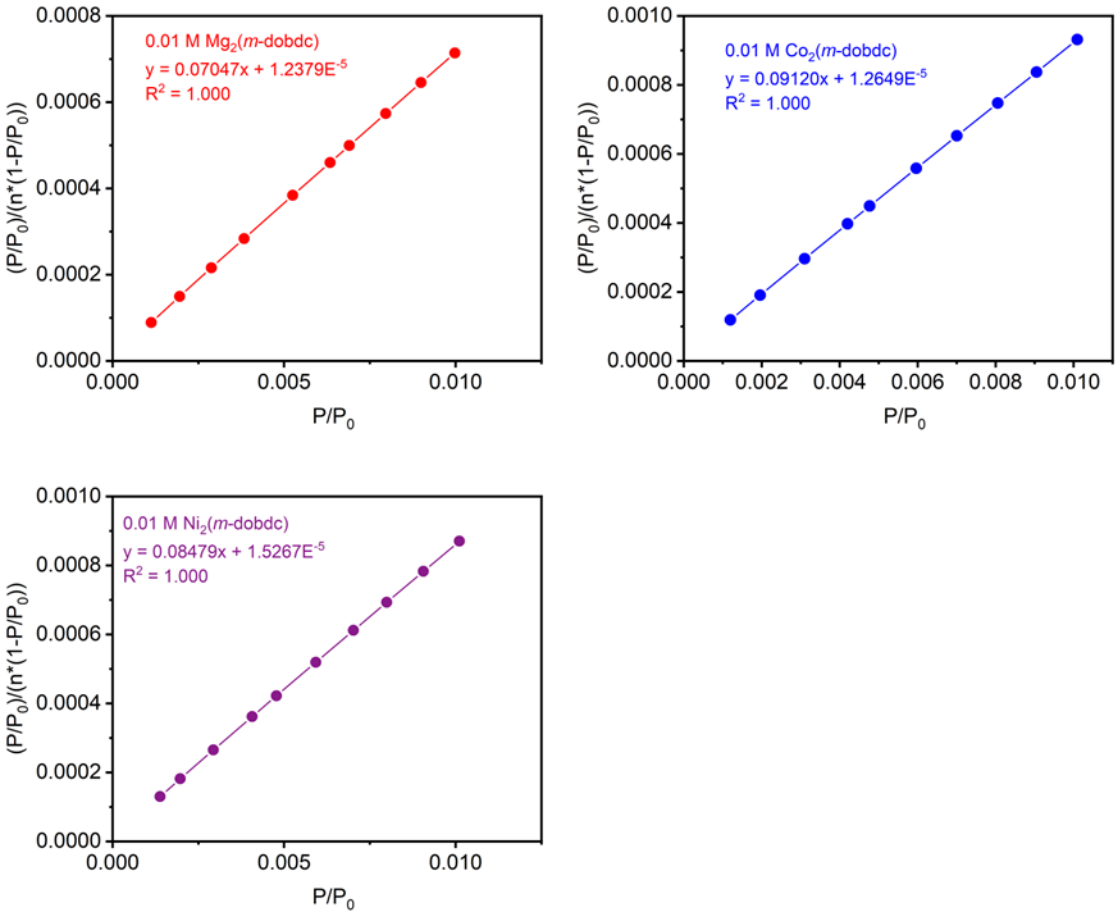

Figure S155. Linearized BET plots for the N_2 adsorption data of M_2(*m*-dobdc) synthesized at 0.01 M.

9. Large-Scale Synthesis of Zn_2(*m*-dobdc).

In a 250 mL Pyrex jar, $Zn(NO_3)_2$•$6H_2O$ (3.72 g, 12.5 mmol, 2.50 equiv.) was dissolved in H_2O (25 mL). In a separate 100 mL round-bottom flask equipped with a stir bar, NaOH (800 mg, 20.0 mmol, 4.00 equiv.), H_4*m*-dobdc (1.0 g, 5.00 mmol, 1.00 equiv.), and H_2O (25 mL) were combined. The $Zn(NO_3)_2$•H_2O solution was added all at once to the H_4*m*-dobdc solution. The mixture was stirred at room temperature for 1 h. The reaction mixture was vacuum-filtered, and the resulting solid was rinsed with MeOH (100 mL). The resulting beige solid was transferred to a new jar filled with MeOH (100 mL). The vial was transferred to an oven that had been pre-heated to 60 °C and was allowed to stand at this temperature for at least 12 h. At this time, the heterogenous mixture was allowed to cool to room temperature, the solvent was decanted, and fresh MeOH (100 mL) was added. This process was repeated for a total of six MeOH soaks. After the final soak, the solvent was decanted, and the remaining solid was allowed to dry in air. The sample was activated under high vacuum (<10 μbar), ramping the temperature slowly to 180 °C (0.1°C/min). The sample was allowed to stand at 180 °C under high vacuum (<10 μbar) for 12 h prior to gas adsorption analysis. Activated Zn_2(*m*-dobdc) was obtained in 40% yield.

The high BET surface area obtained for this material confirms that activation using supercritical CO_2 is unnecessary.

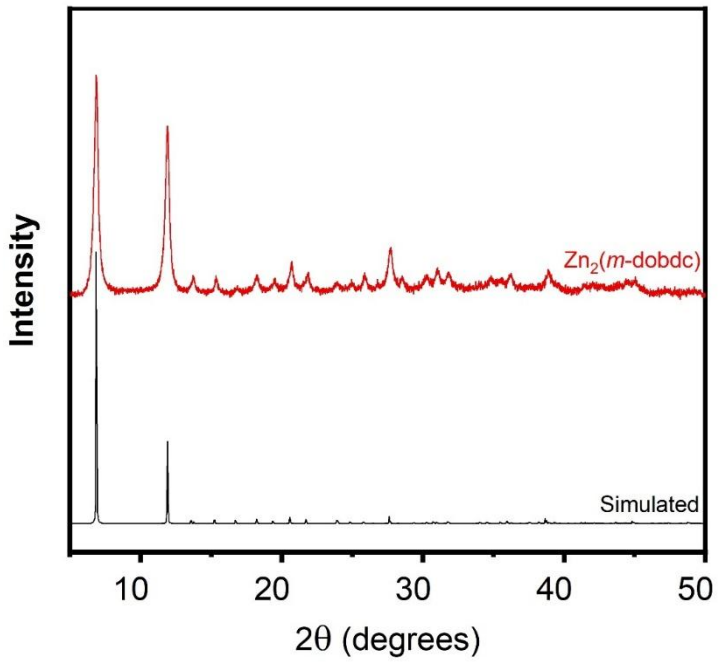

Figure S156. PXRD pattern of MeOH-solvated Zn_2(*m*-dobdc) after large-scale synthesis. The simulated pattern based on the previously reported SCXRD structure of the isostructural framework Co_2(*m*-dobdc) is included for reference.[14]

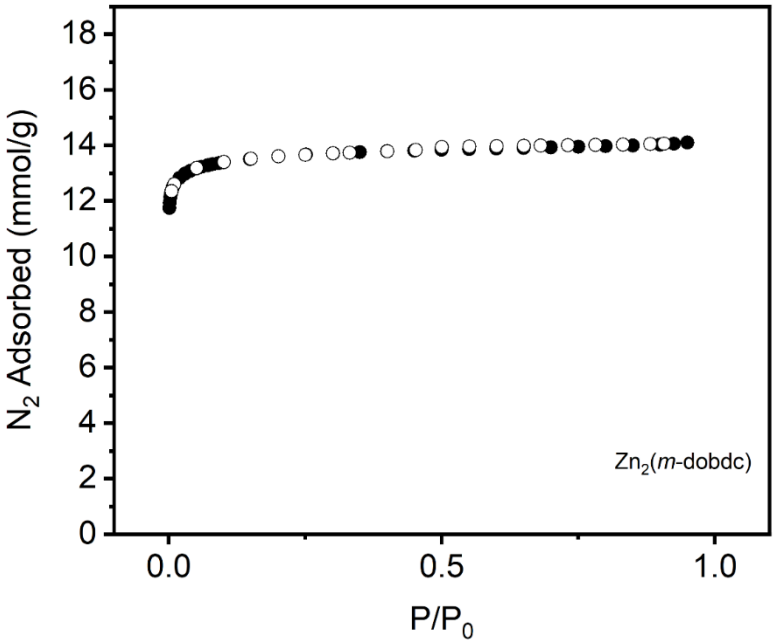

Figure S157. 77 K N_2 adsorption (filled circles) and desorption (open circles) isotherms of activated Zn_2(*m*-dobdc) after large-scale synthesis. The BET surface area determined from these data is 1228 ± 1 m^2/g, comparable to that obtained on a small scale (1216 ± 1 m^2/g). The Langmuir surface area determined from these data is 1368 ± 2 m^2/g.

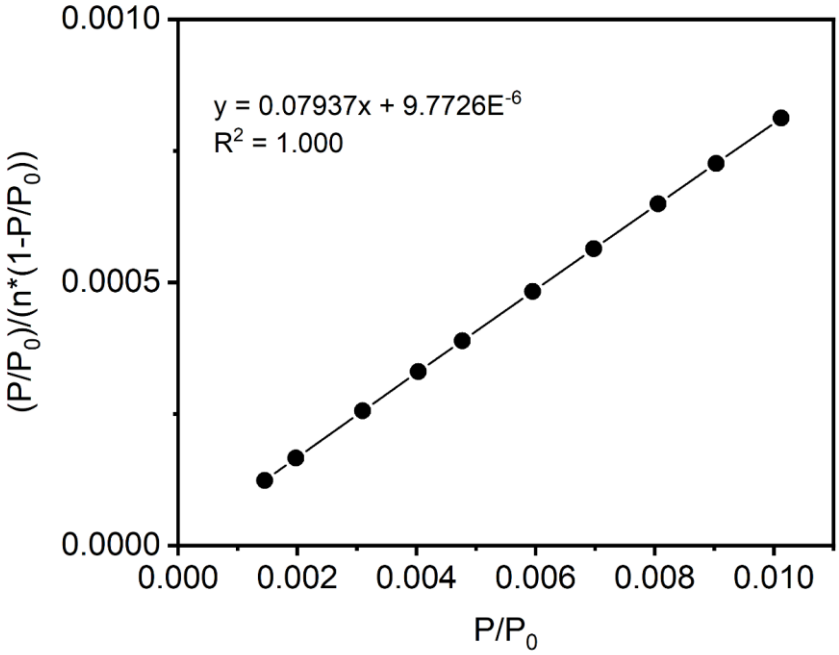

Figure S158. Linearized BET plot for the N_2 adsorption data of Zn_2(*m*-dobdc after large-scale synthesis.

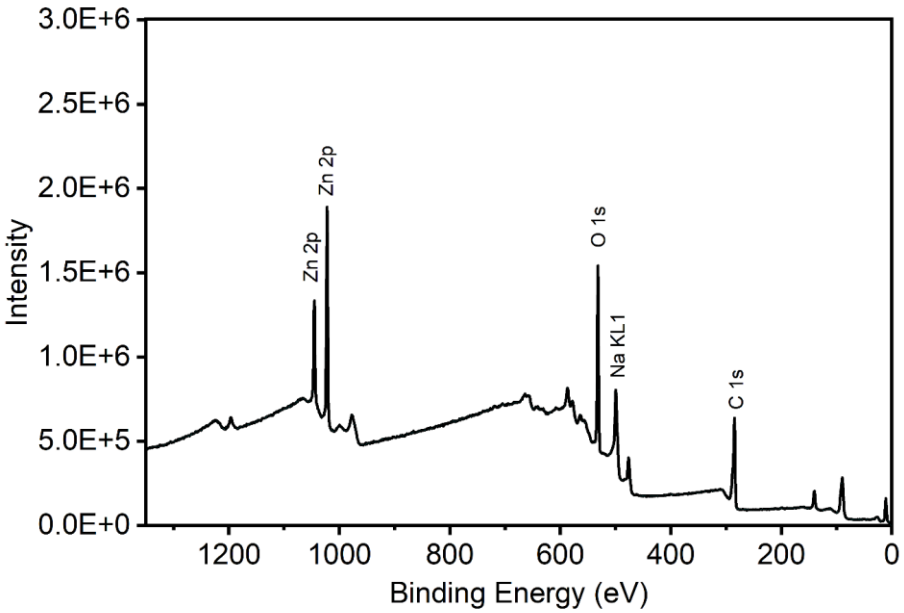

Figure S159. XPS survey scan of Zn_2(*m*-dobdc) after large-scale synthesis. The material consists largely of Zn, O, and C, as expected. A small amount of Na was also detected, likely left over from the NaOH used during MOF synthesis.

10. References.

(1) Bruno, N. C.; Tudge, M. T.; Buchwald, S. L. Design and Preparation of New Palladium Precatalysts for C–C and C–N Cross-Coupling Reactions. *Chem. Sci.* **2013**, *4* (3), 916–920. https://doi.org/10.1039/C2SC20903A.

(2) Nelson, A. P.; Farha, O. K.; Mulfort, K. L.; Hupp, J. T. Supercritical Processing as a Route to High Internal Surface Areas and Permanent Microporosity in Metal−Organic Framework Materials. *J. Am. Chem. Soc.* **2009**, *131* (2), 458–460. https://doi.org/10.1021/ja808853q.

(3) Gonzalez, M. I.; Kapelewski, M. T.; Bloch, E. D.; Milner, P. J.; Reed, D. A.; Hudson, M. R.; Mason, J. A.; Barin, G.; Brown, C. M.; Long, J. R. Separation of Xylene Isomers through Multiple Metal Site Interactions in Metal–Organic Frameworks. *J. Am. Chem. Soc.* **2018**, *140* (9), 3412–3422. https://doi.org/10.1021/jacs.7b13825.

(4) Wang, Z.; Bilegsaikhan, A.; Jerozal, R. T.; Pitt, T. A.; Milner, P. J. Evaluating the Robustness of Metal–Organic Frameworks for Synthetic Chemistry. *ACS Appl. Mater. Interfaces* **2021**, *13* (15), 17517–17531. https://doi.org/10.1021/acsami.1c01329.

(5) Xiao, D. J.; Oktawiec, J.; Milner, P. J.; Long, J. R. Pore Environment Effects on Catalytic Cyclohexane Oxidation in Expanded Fe_2(dobdc) Analogues. *J. Am. Chem. Soc.* **2016**, *138* (43), 14371–14379. https://doi.org/10.1021/jacs.6b08417.

(6) Lundvall, F.; Vajeeston, P.; Wragg, D. S.; Dietzel, P. D. C.; Fjellvåg, H. Two New Series of Coordination Polymers and Evaluation of Their Properties by Density Functional Theory. *Cryst. Growth Des.* **2016**, *16* (1), 339–346. https://doi.org/10.1021/acs.cgd.5b01302.

(7) Gygi, D.; Bloch, E. D.; Mason, J. A.; Hudson, M. R.; Gonzalez, M. I.; Siegelman, R. L.; Darwish, T. A.; Queen, W. L.; Brown, C. M.; Long, J. R. Hydrogen Storage in the Expanded Pore Metal–Organic Frameworks M_2(dobpdc) (M = Mg, Mn, Fe, Co, Ni, Zn). *Chem. Mater.* **2016**, *28* (4), 1128–1138. https://doi.org/10.1021/acs.chemmater.5b04538.

(8) Keasler, K. T.; Zick, M. E.; Stacy, E. E.; Kim, J.; Lee, J.-H.; Aeindartehran, L.; Runčevski, T.; Milner, P. J. Handling Fluorinated Gases as Solid Reagents Using Metal-Organic Frameworks. *Science* **2023**, *381* (6665), 1455–1461. https://doi.org/10.1126/science.adg8835.

(9) Dietzel, P. D. C.; Johnsen, R. E.; Blom, R.; Fjellvåg, H. Structural Changes and Coordinatively Unsaturated Metal Atoms on Dehydration of Honeycomb Analogous Microporous Metal–Organic Frameworks. *Chem. Eur. J.* **2008**, *14* (8), 2389–2397. https://doi.org/10.1002/chem.200701370.

(10) Sumida, K.; Brown, C. M.; Herm, Z. R.; Chavan, S.; Bordiga, S.; Long, J. R. Hydrogen Storage Properties and Neutron Scattering Studies of Mg_2(dobdc)—a Metal–Organic Framework with Open Mg^{2+} Adsorption Sites. *Chem. Commun.* **2011**, *47* (4), 1157–1159. https://doi.org/10.1039/C0CC03453C.

(11) Sánchez-Sánchez, M.; Getachew, N.; Díaz, K.; Díaz-García, M.; Chebude, Y.; Díaz, I. Synthesis of Metal–Organic Frameworks in Water at Room Temperature: Salts as Linker Sources. *Green Chem.* **2015**, *17* (3), 1500–1509. https://doi.org/10.1039/C4GC01861C.

(12) Kim, H.; Hong, C. S. MOF-74-Type Frameworks: Tunable Pore Environment and Functionality through Metal and Ligand Modification. *CrystEngComm* **2021**, *23* (6), 1377–1387. https://doi.org/10.1039/D0CE01870H.

(13) Siegelman, R. L.; McDonald, T. M.; Gonzalez, M. I.; Martell, J. D.; Milner, P. J.; Mason, J. A.; Berger, A. H.; Bhown, A. S.; Long, J. R. Controlling Cooperative CO_2 Adsorption in Diamine-Appended Mg_2(dobpdc) Metal–Organic Frameworks. *J. Am. Chem. Soc.* **2017**, *139* (30), 10526–10538. https://doi.org/10.1021/jacs.7b05858.

(14) Bachman, J. E.; Kapelewski, M. T.; Reed, D. A.; Gonzalez, M. I.; Long, J. R. M_2(*m*-dobdc) (M = Mn, Fe, Co, Ni) Metal–Organic Frameworks as Highly Selective, High-Capacity Adsorbents for Olefin/Paraffin Separations. *J. Am. Chem. Soc.* **2017**, *139* (43), 15363–15370. https://doi.org/10.1021/jacs.7b06397.

(15) Chen, E. Y.; Mandel, R. M.; Milner, P. J. Evaluating Solvothermal and Mechanochemical Routes towards the Metal–Organic Framework Mg_2(*m*-dobdc). *CrystEngComm* **2022**, *24* (41), 7292–7297. https://doi.org/10.1039/D2CE00739H.

(16) Kapelewski, M. T.; Geier, S. J.; Hudson, M. R.; Stück, D.; Mason, J. A.; Nelson, J. N.; Xiao, D. J.; Hulvey, Z.; Gilmour, E.; FitzGerald, S. A.; Head-Gordon, M.; Brown, C. M.; Long, J. R. M_2(*m*-dobdc) (M = Mg, Mn, Fe, Co, Ni) Metal–Organic Frameworks Exhibiting Increased Charge Density and Enhanced H_2 Binding at the Open Metal Sites. *J. Am. Chem. Soc.* **2014**, *136* (34), 12119–12129. https://doi.org/10.1021/ja506230r.

(17) Caskey, S. R.; Wong-Foy, A. G.; Matzger, A. J. Dramatic Tuning of Carbon Dioxide Uptake via Metal Substitution in a Coordination Polymer with Cylindrical Pores. *J. Am. Chem. Soc.* **2008**, *130* (33), 10870–10871. https://doi.org/10.1021/ja8036096.

(18) Forse, A. C.; Colwell, K. A.; Gonzalez, M. I.; Benders, S.; Torres-Gavosto, R. M.; Blümich, B.; Reimer, J. A.; Long, J. R. Influence of Pore Size on Carbon Dioxide Diffusion in Two Isoreticular Metal–Organic Frameworks. *Chem. Mater.* **2020**, *32* (8), 3570–3576. https://doi.org/10.1021/acs.chemmater.0c00745.

(19) Forse, A. C.; Gonzalez, M. I.; Siegelman, R. L.; Witherspoon, V. J.; Jawahery, S.; Mercado, R.; Milner, P. J.; Martell, J. D.; Smit, B.; Blümich, B.; Long, J. R.; Reimer, J. A. Unexpected Diffusion Anisotropy of Carbon Dioxide in the Metal–Organic Framework Zn_2(dobpdc). *J. Am. Chem. Soc.* **2018**, *140* (5), 1663–1673. https://doi.org/10.1021/jacs.7b09453.

(20) Myers, A. L.; Prausnitz, J. M. Thermodynamics of Mixed-Gas Adsorption. *AIChE J.* **1965**, *11* (1), 121–127. https://doi.org/10.1002/aic.690110125.

(21) Jerozal, R. T.; Kim, J.; Ma, C.; Pitt, T. A.; Lee, J.-H.; Milner, P. J. Enhancing Selective Hydrofluorocarbon Greenhouse Gas Capture via Halogenation of Metal–Organic Frameworks. *J. Am. Chem. Soc.* **2025**, *147* (8), 7127–7136. https://doi.org/10.1021/jacs.5c00393.

(22) Zick, M. E.; Lee, J.-H.; Gonzalez, M. I.; Velasquez, E. O.; Uliana, A. A.; Kim, J.; Long, J. R.; Milner, P. J. Fluoroarene Separations in Metal–Organic Frameworks with Two Proximal Mg^{2+} Coordination Sites. *J. Am. Chem. Soc.* **2021**, *143* (4), 1948–1958. https://doi.org/10.1021/jacs.0c11530.

(23) McDonald, T. M.; Mason, J. A.; Kong, X.; Bloch, E. D.; Gygi, D.; Dani, A.; Crocellà, V.; Giordanino, F.; Odoh, S. O.; Drisdell, W. S.; Vlaisavljevich, B.; Dzubak, A. L.; Poloni, R.; Schnell, S. K.; Planas, N.; Lee, K.; Pascal, T.; Wan, L. F.; Prendergast, D.; Neaton, J. B.; Smit, B.; Kortright, J. B.; Gagliardi, L.; Bordiga, S.; Reimer, J. A.; Long, J. R. Cooperative Insertion of CO_2 in Diamine-Appended Metal-Organic Frameworks. *Nature* **2015**, *519* (7543), 303–308. https://doi.org/10.1038/nature14327.

(24) Halder, A.; Bain, D. C.; Pitt, T. A.; Shi, Z.; Oktawiec, J.; Lee, J.-H.; Tsangari, S.; Ng, M.; Fuentes-Rivera, J. J.; Forse, A. C.; Runcevski, T.; Muller, D. A.; Musser, A. J.; Milner, P. J. Kinetic Trapping of Photoluminescent Frameworks During High-Concentration Synthesis of Nonemissive Metal–Organic Frameworks. *Chem. Mater.* **2023**, *35* (23), 10086–10098. https://doi.org/10.1021/acs.chemmater.3c02121.

(25) Pitt, T. A.; Bain, D. C.; Del Campo, M.; Musser, A. J.; Milner, P. J. Controlled Growth and Interconversion of Photoluminescent Metal-Organic Frameworks under High-Concentration Conditions. *Chem. Mater.* **2025**, *37* (8), 2964–2975. https://doi.org/10.1021/acs.chemmater.5c00355.